

Wayne State University Dissertations


---

1-1-2018

## Synthesis Of Volatile And Thermally Stable Aluminum Hydride Complexes And Their Use In Atomic Layer Deposition Of Metal Thin Films

Kyle Blakeney  
Wayne State University, kylejblakeney@gmail.com

Follow this and additional works at: [https://digitalcommons.wayne.edu/oa\\_dissertations](https://digitalcommons.wayne.edu/oa_dissertations)

 Part of the [Inorganic Chemistry Commons](#), and the [Materials Science and Engineering Commons](#)

---

### Recommended Citation

Blakeney, Kyle, "Synthesis Of Volatile And Thermally Stable Aluminum Hydride Complexes And Their Use In Atomic Layer Deposition Of Metal Thin Films" (2018). *Wayne State University Dissertations*. 2091.  
[https://digitalcommons.wayne.edu/oa\\_dissertations/2091](https://digitalcommons.wayne.edu/oa_dissertations/2091)

This Open Access Dissertation is brought to you for free and open access by DigitalCommons@WayneState. It has been accepted for inclusion in Wayne State University Dissertations by an authorized administrator of DigitalCommons@WayneState.

**SYNTHESIS OF VOLATILE AND THERMALLY STABLE ALUMINUM HYDRIDE  
COMPLEXES AND THEIR USE IN ATOMIC LAYER DEPOSITION OF METAL THIN  
FILMS**

by

**KYLE JORDAN BLAKENEY**

**DISSERTATION**

Submitted to the Graduate School

of Wayne State University,

Detroit, Michigan

in partial fulfillment of the requirements

for the degree of

**DOCTOR OF PHILOSOPHY**

2018

MAJOR: CHEMISTRY (Inorganic)

Approved By:

---

Advisor

Date

---

---

---

---

**© COPYRIGHT BY**  
**KYLE JORDAN BLAKENEY**  
**2018**  
**All Rights Reserved**

## DEDICATION

*To my parents and my teachers.*

*“We know very little, and yet it is astonishing that we know so much, and still more astonishing that so little knowledge can give us so much power.”*

- Bertrand Russell

*“The fact that we live at the bottom of a deep gravity well, on the surface of a gas covered planet going around a nuclear fireball 90 million miles away and think this to be normal is obviously some indication of how skewed our perspective tends to be.”*

- Douglas Adams

## ACKNOWLEDGEMENTS

This dissertation would not have been possible without the support of many people. First, I would like to thank my advisor, Professor Charles H. Winter, for teaching me to be an independent scientist and to always think “outside of the known universe.” Professor Winter has been a wonderful professional role model who has taught me to handle complicated scientific, business, and intellectual property issues with honesty and integrity.

I thank my dissertation committee, Professor Matthew J. Allen, Professor Thomas H. Linz, and Dr. Nicole M. Grynawski, for their comments and advice. BASF Corporation is acknowledged for generous financial support of this project. Special thanks are given to my collaborators at BASF Corporation in Ludwigshafen, Germany: Dr. Lukas Mayr, Dr. Hagen Wilmer, Dr. David Schweinfurth, Dr. Daniel Löffler, Dr. Daniel Waldmann, Dr. Sinja Verena Klenk, and Dr. Kerstin Schierle-Arndt, for their support and advocacy for this project and for many hours of discussions over the past three years. Dr. Joseph Klesko and Dr. Thomas Knisley are gratefully acknowledged for their willingness to share their time and expertise with me. Thank you to my fellow Winter group members past and present. For technical assistance with instruments, materials characterization, and crystal structure determination, I would like to thank Dr. Kai Sun and Dr. Haiping Sun at the University of Michigan, Dr. Mike Mei, Dr. Cassandra Ward and Dr. Phil Martin at Wayne State University. Thank you to the Science Stores and Hazardous Materials Shipping staff for invaluable help with shipping and receiving chemicals and equipment, especially Jason Parizon for continually going above and beyond to help me. Thank you to Jackie Baldyga, Melissa Barton, and the administrative staff for so much help, especially as I was wrapping up. Thank you to Jeff and Whitney and all my friends for helping to make grad school bearable.

My career in chemistry began during my Junior year at Iowa State University when I asked Professor Javier Vela if I could join his group as an undergraduate researcher. I found that I enjoyed doing chemistry research and Prof. Vela and Dr. Michelle Thompson were wonderful mentors. I would not have decided to pursue my Ph.D. without their influence.

To my Grandma Mary, your memory continues to inspire me. I wish you would have been able to help me edit this dissertation. Most importantly, thank you to my parents, John and Shelley, my brother, Aaron, Grandma Mary Nell, and Grandma Ilene, for their love and encouragement.

## TABLE OF CONTENTS

DEDICATION .....	ii
ACKNOWLEDGEMENTS .....	iii
LIST OF TABLES .....	vi
LIST OF FIGURES .....	vii
LIST OF SCHEMES.....	xi
LIST OF ABBREVIATIONS.....	xii
CHAPTER 1 Introduction.....	1
CHAPTER 2 Atomic Layer Deposition of Aluminum Metal Films Using a Thermally Stable Aluminum Hydride Reducing Agent .....	25
CHAPTER 3 Aluminum Dihydride Complexes and their Unexpected Application in Atomic Layer Deposition of Titanium Carbonitride Films .....	42
CHAPTER 4 Thermal Atomic Layer Deposition of Tungsten Carbide Films from $WCl_6$ and $AlMe_3$ .....	64
CHAPTER 5 Atomic Layer Deposition of Tungsten-Rich Tungsten Carbide Films using $WCl_6$ and $AlH_2(tBuNCH_2CH_2NMe_2)$ as Precursors.....	76
CHAPTER 6 A Volatile Dialane Complex from Ring-Expansion of a Saturated N-Heterocyclic Carbene and its Use in Atomic Layer Deposition of Aluminum Metal Films .....	91
CHAPTER 7 Conclusions.....	110
APPENDIX Permission/License Agreements for Copyrighted Material.....	113
REFERENCES .....	116
ABSTRACT .....	133
AUTOBIOGRAPHICAL STATEMENT.....	135

## LIST OF TABLES

Table 1.	Selected standard reduction potentials for metal ions and applications of the metals in microelectronics devices. ....	23
Table 2.	Physical properties of <b>1-4</b> . ....	47
Table 3.	Selected bond lengths (Å) and angles (°) for <b>4</b> . ....	49
Table 4.	Film compositions from XPS using TiCl <sub>4</sub> and <b>1</b> . ....	56



## LIST OF FIGURES

Figure 1.	Simplified schematic representation of one ALD cycle of Al <sub>2</sub> O <sub>3</sub> deposition from trimethylaluminum (Al(CH <sub>3</sub> ) <sub>3</sub> ) and water. ....	4
Figure 2.	Example saturation curve showing a self-limiting film growth process.....	5
Figure 3.	Example ALD window plot showing different growth regimes.....	6
Figure 4.	List of reducing co-reactants that have been reported in thermal ALD growth of metal films. ....	9
Figure 5.	Structures of Cu(dmap) <sub>2</sub> and transition metal di- <i>tert</i> -butyl diazadienyl complexes...	14
Figure 6.	Structures of the novel ALD reducing agents 1-methyl-2,5-bis(trimethylsilyl)-2,5-cyclohexadiene (CHD) and 1,4-bis(trimethylsilyl)-1,4-dihydropyrazine (DHP). ....	15
Figure 7.	Selected precursors for aluminum metal CVD. ....	17
Figure 8.	Synthesis of a hydride-rich Mg cluster from treatment of a NHC-Mg amide precursor with triphenylsilane.....	19
Figure 9.	TGA curve of <b>1</b> . ....	28
Figure 10.	Growth rate versus precursor pulse length after 200 cycles at 140 °C for (a) <b>1</b> and (b) AlCl <sub>3</sub> . ....	31
Figure 11.	(a) Growth rate and sheet resistivity versus temperature after 200 cycles. (b) Film thickness and sheet resistivity versus number of cycles at 140 °C. ....	32
Figure 12.	Plane-view scanning electron microscopy images after different numbers of cycles at 140 °C on TiN.....	33
Figure 13.	AFM micrographs. (Left) 72.8 nm thick Al film deposited after 200 cycles at 140 °C, Rms roughness = 17.1 nm. (Right) 101.5 nm thick Al film deposited after 300 cycles at 140 °C, Rms roughness = 19.0 nm. ....	34
Figure 14.	GIXRD patterns after 200 cycles at different temperatures on TiN. ....	35
Figure 15.	(a) XPS depth profile, (b) survey scan, and (c) high-resolution Al 2p core level scan of a 120 nm thick film (300 cycles) deposited at 100 °C after Ar ion sputtering. ....	36
Figure 16.	Reducing Agents for ALD.....	43
Figure 17.	Structure of previously reported dimeric Al dihydride complexes coordinated by a methyl or ethyl-substituted amido-amine ligand. ....	46

Figure 18. Perspective view of <b>2</b> with thermal ellipsoids at the 50% level. Hydrogen atoms are omitted for clarity. ....	49
Figure 19. TGA curves for <b>1-4</b> . ....	51
Figure 20. A) Growth rate and bulk resistivity versus pulse length of <b>1</b> . B) Growth rate and resistivity versus pulse length of $\text{TiCl}_4$ . ....	53
Figure 21. A) Growth rate and resistivity versus temperature. B) Film thickness versus number of cycles. ....	54
Figure 22. A) XPS survey spectrum after Ar ion sputtering of a film deposited at 300 C after 250 cycles using $\text{TiCl}_4$ and <b>1</b> . High-resolution core level scans of B) Ti 2p, C) N 1s, and D) C 1s regions. ....	55
Figure 23. A) GIXRD patterns of $\text{TiC}_x\text{N}_y$ films deposited at 280 °C (red, bottom) and 400 °C (blue, top). B) AFM micrograph of a $\text{TiC}_x\text{N}_y$ film deposited at 300 °C for 250 cycles. ....	57
Figure 24. Comparison of growth rates using Al dihydride complexes <b>1</b> and <b>3</b> . ....	58
Figure 25. Plots of growth rate versus precursor pulse length of (a) $\text{WCl}_6$ and (b) $\text{AlMe}_3$ after 500 cycles at 325 °C. ....	67
Figure 26. Plot of growth rate versus substrate temperature after 500 cycles using $\text{WCl}_6$ and $\text{AlMe}_3$ . ....	68
Figure 27. (a) Plot of film thickness versus number of cycles at 325 °C. (b) Plot of growth rate versus number of cycles at 325 °C. ....	69
Figure 28. (a) XPS survey scan of a $\text{WC}_x$ film deposited at 300 °C after Ar ion sputtering to remove adventitious carbon and oxygen. High resolution XPS (b) W 4f and (c) Al 2p core level scans of a $\text{WC}_x$ film deposited at 300 °C after Ar ion sputtering to remove adventitious carbon and oxygen. ....	70
Figure 29. AFM micrographs of films deposited from $\text{WCl}_6$ and $\text{AlMe}_3$ at (a) 300 °C and (b) 375 °C after 500 cycles on $\text{SiO}_2$ substrates. ....	72
Figure 30. Possible mechanism of $\text{WC}_x$ formation. ....	74
Figure 31. Structure of the co-reactant <b>1</b> . ....	77
Figure 32. TGA and DTG (first derivative) curves for $\text{WCl}_6$ . A small amount of tungsten oxychloride is present due to brief air exposure during sample loading. ....	80
Figure 33. Growth rate versus precursor pulse length for (a) <b>1</b> and (b) $\text{WCl}_6$ at 300 °C. ....	82
Figure 34. Growth rate versus temperature after 300 ALD cycles. ....	83

Figure 35. Film thickness versus number of ALD cycles at 300 °C.....	84
Figure 36. XRR analysis for films deposited on Si using WCl <sub>6</sub> and <b>1</b> at 300 °C after 65 (top), 100 (middle), and 400 (bottom) cycles.....	85
Figure 37. GIXRD patterns of a film deposited from WCl <sub>6</sub> and <b>1</b> at 300 °C after 300 cycles. Reference patterns are included for W metal (blue lines, PDF#04-0806) and WC <sub>1-x</sub> (green lines, PDF#20-1316). Weak reflections at 2θ = 21° and 54° were indexed to WO <sub>3</sub> (reference not included for clarity). .....	86
Figure 38. (Left) XPS depth profile of a film deposited from WCl <sub>6</sub> and <b>1</b> after 250 cycles at 300 °C. (Right) High resolution XPS scans of W 4f, C 1s, N 1s, and Al 2p regions after sputtering.....	88
Figure 39. Possible mechanism for carbon incorporation by ligand transfer from <b>1</b> to the growth surface and subsequent decomposition and carbide formation.....	89
Figure 40. Aluminum hydride promoted NHC ring expansion reactions. A) using β-diketiminato aluminum dihydride complexes, B) using NHC-AlH <sub>3</sub> complexes, and C) this work. 92	
Figure 41. Structures of NHC-AlH <sub>3</sub> complexes <b>7-9</b> .....	97
Figure 42. POV-Ray rendered ORTEP plot of the structure of <b>5</b> . Hydrogen atoms not bonded to Al are omitted for clarity. Selected bond distances (Å) and angles (°): Al(1)-N(1) 1.971(2), Al(1)-C(7) 2.012(3), Al(2)-N(1) 1.932(2), Al(2)-N(2) 1.971(2), Al(1)-H(B) 1.53(4), Al(1)-H(C) 1.53(3), Al(2)-H 1.50(3), Al(2)-H(A) 1.49(3), N(1)-Al(1)-C(7) 90.49(10), N(1)-Al(2)-N(2) 85.55(9).....	99
Figure 43. TGA curves of <b>5</b> , <b>8</b> , and <b>9</b> .....	100
Figure 44. POV-Ray rendered ORTEP structure of <b>6</b> . Hydrogen atoms not bonded to Al are omitted for clarity. Selected bond distances (Å) and angles (°): Al(1)-N(1) 2.081(3), Al(1)-C(11) 2.006(40), Al(1)-Cl(1) 2.1823(12), Al(1)-H(A) 1.75(5), Al(1)-H(B) 1.63(4), Ti(1)-H(A) 1.79(4), Ti(1)-H(B) 1.88(6), Al(2)-N(1) 1.917(3), Al(2)-N(2) 1.965(3), Al(2)-Cl(2) 2.1379(13), Al(2)-H 1.78(2), N(1)-Al(1)-C(11) 100.34(9), N(1)-Al(1)-Cl(1) 88.50(12), C(11)-Al(1)-Cl(1) 108.80(10), N(1)-Al(2)-N(2) 87.08(12), N(1)-Al(2)-Cl(2) 113.82(10), N(2)-Al(2)-Cl(2) 113.06(9).....	101
Figure 45. Growth rate versus temperature after 100 cycles of AlCl <sub>3</sub> and <b>5</b> on TiN.....	102
Figure 46. Growth rate versus precursor pulse length for (a) AlCl <sub>3</sub> and (b) <b>5</b> after 100 cycles at 140 °C. ....	103
Figure 47. Film thickness versus number of cycles at 140 °C on TiN.....	104
Figure 48. Top-view SEM images of Al metal films grown on TiN substrates at 140 °C after 100 cycles (top) or 300 cycles (bottom) using AlCl <sub>3</sub> and <b>5</b> .....	106

Figure 49. XPS core level scans after Ar ion sputtering of the Al 2p, C 1s, N 1s, and Cl 2p regions of an Al film deposited at 140 °C after 300 cycles. .... 108

## LIST OF SCHEMES

Scheme 1. Design and synthesis of the thermally stable Al hydride complex <b>1</b> .....	27
Scheme 2. Proposed reaction between AlCl <sub>3</sub> and <b>1</b> leading to Al metal film growth with formation of H <sub>2</sub> and <b>2</b> as by-products. ....	29

## LIST OF ABBREVIATIONS

°C	Degrees Celsius
$\delta$	Chemical shift (NMR)
Å	Angström
Acac	Acetylacetonate
AFM	Atomic Force Microscopy
ALD	Atomic Layer Deposition
at.%	Atomic Percent
CHD	2-Methyl-1,4-bis(trimethylsilyl)-2,5-cyclohexadiene
Cp	Cyclopentadienyl
CVD	Chemical Vapor Deposition
$\Delta H$	Reaction Enthalpy
DHP	1,4-Bis(trimethylsilyl)-1,4-dihydropyrazine
EDS	Energy Dispersive X-ray Spectroscopy
Et	Ethyl (C <sub>2</sub> H <sub>5</sub> )
GIXRD	Grazing Incidence X-ray Diffraction
HR ESI-MS	High Resolution Electrospray Ionization Mass Spectrometry
IR	Infrared Spectroscopy
iPr	Isopropyl (C <sub>3</sub> H <sub>7</sub> )
Me	Methyl (CH <sub>3</sub> )
Mp	Melting Point
NHC	N-Heterocyclic Carbene
NMR	Nuclear Magnetic Resonance Spectroscopy

PEALD.....	Plasma-Enhanced Atomic Layer Deposition
pK <sub>a</sub> .....	Acid Dissociation Constant
PVD.....	Physical Vapor Deposition
RCA .....	Radio Corporation of America
RMS .....	Root Mean Square
SEM .....	Scanning Electron Microscopy
<i>t</i> Bu.....	<i>tert</i> -Butyl (C <sub>4</sub> H <sub>9</sub> )
TGA .....	Thermogravimetric Analysis
XPS .....	X-ray Photoelectron Spectroscopy
XRD .....	X-ray Diffraction
XRR .....	X-ray Reflectivity

# CHAPTER 1

## INTRODUCTION

### 1.1 Metallic Thin Films

Thin films are layers of materials that range in thickness between approximately 1 nm to several micrometers. Metal thin films have been heavily studied due their high electrical conductivity, magnetic properties, high reflectivity, high hardness, low gas permeability, and their applications in energy generation (solar cells) and storage (batteries). Metal thin films and conductive metallic compounds such as metal nitrides, carbides, and carbonitrides have wide-ranging applications in microelectronic devices, but fabrication of these metallic films has many challenges and has been the subject of intense study for decades.<sup>1</sup> The co-founder of Intel, Gordon Moore, predicted in 1965 that the number of transistors in each device would double about every 18 months.<sup>2</sup> Moore's Law has since become the driving force for miniaturization in the microelectronics industry.<sup>3</sup> The miniaturization demands of Moore's Law call for deposition of thin metallic films in nanoscale high aspect ratio features.<sup>3</sup> So-called metallization is a critical step throughout the manufacturing of integrated circuits in applications such as interconnects, vias, gate electrodes, and diffusion barriers.<sup>4</sup> This dissertation presents the results of a research project broadly aimed towards the deposition of metallic thin films by a technique called Atomic Layer Deposition.

### 1.2 Thin Film Deposition by Chemical Vapor Deposition (CVD) and Atomic Layer Deposition (ALD)

CVD and ALD are advanced thin film deposition techniques which possess significant advantages over traditional physical vapor deposition (PVD) techniques such as sputtering and evaporation in terms of film conformality and selectivity.<sup>5-7</sup> CVD has roots tracing back at least as far as the late 19<sup>th</sup> century with the development of the Mond process for nickel purification



by CVD of volatile  $\text{Ni}(\text{CO})_4$ .<sup>5</sup> More recently, metal CVD of tungsten and aluminum found early applications in microelectronics.<sup>8</sup> Significant experimental and theoretical knowledge of CVD growth processes has been developed.<sup>9,10</sup> A great deal of research into CVD processes and chemistry can be applied for developing new ALD processes. Selective metallization by CVD has been studied for over 30 years, which is potentially highly relevant to the recent emergence of selective deposition as a vital technology for advanced semiconductor fabrication.<sup>11,12</sup> Although there are very sophisticated techniques and results showing that CVD can conformally coat high aspect ratio structures, true CVD is inherently limited in terms of conformality compared to ALD. Thus, ALD chemistry and film growth results will be the focus of this dissertation.

ALD was developed independently in the 1960's in the Soviet Union and in the 1970's in Finland.<sup>13</sup> ALD has significant advantages over CVD in that ALD processes can produce films with inherently perfect conformality and that are substantially void-free and dense. Layer-by-layer thickness control is also obtained with ALD. Originally called Molecular Layering by the Soviets and Atomic Layer Epitaxy by the West, ALD eventually became the standard term for this technique.<sup>14</sup> A team led by Tuomo Suntola in Finland developed this technique to manufacture large electroluminescent flat panel displays.<sup>15</sup> A recent detailed bibliometric, social network, and text analysis study of the ALD field showed that it is rapidly increasing in size with a high degree of collaboration.<sup>16</sup> ALD is now the major technique for depositing thin films in high aspect ratio features, especially in the microelectronics industry.<sup>17</sup>

The utility of ALD is due to sequential, *self-limiting* surface reactions between two or more precursors which are separated in time by purge periods. The purge periods ensure that no gas-phase reactions occur and film growth proceeds only by surface chemistry. A schematic of

one ALD cycle of aluminum oxide ( $\text{Al}_2\text{O}_3$ ) deposited from trimethylaluminum and water is shown in Figure 1.<sup>18</sup> In the first step in this example (a) trimethylaluminum molecules react with a hydroxyl-terminated surface, such as silicon with native oxide. The Al-CH<sub>3</sub> bonds in trimethylaluminum are very basic ( $\text{pK}_a$  of CH<sub>4</sub> = 48) and are rapidly protonated by the surface hydroxyl groups ( $\text{pK}_a$  of surface Si-OH groups = 7.1)<sup>19</sup> to form CH<sub>4</sub> and strong Al-O bonds. This acid-base reaction continues until all of the hydroxyl groups have reacted, forming one monolayer of deposited material. Excess trimethylaluminum does not react with the Al-Me-terminated surface, which results in a *self-limited* surface reaction. Self-limiting surface chemistry is the hallmark of ALD and is the source of its inherently perfect conformality and high degree of thickness control and uniformity. In the second step (b) the excess trimethylaluminum precursor and reaction byproducts (CH<sub>4</sub>) are purged from the system which leaves an Al-CH<sub>3</sub> terminated surface. The third step (c) is exposure of the second precursor, water ( $\text{pK}_a = 15.7$ ), which reacts with the Al-CH<sub>3</sub> terminated surface. Once again, this reaction is self-limiting and excess water does not react with the surface once all of the reactive sites are used up. Excess water and the reaction byproducts (CH<sub>4</sub>) are purged from the system in step 4 (d), which regenerates the hydroxyl-terminated surface. This completes one full ALD cycle with deposition of one monolayer of  $\text{Al}_2\text{O}_3$ .

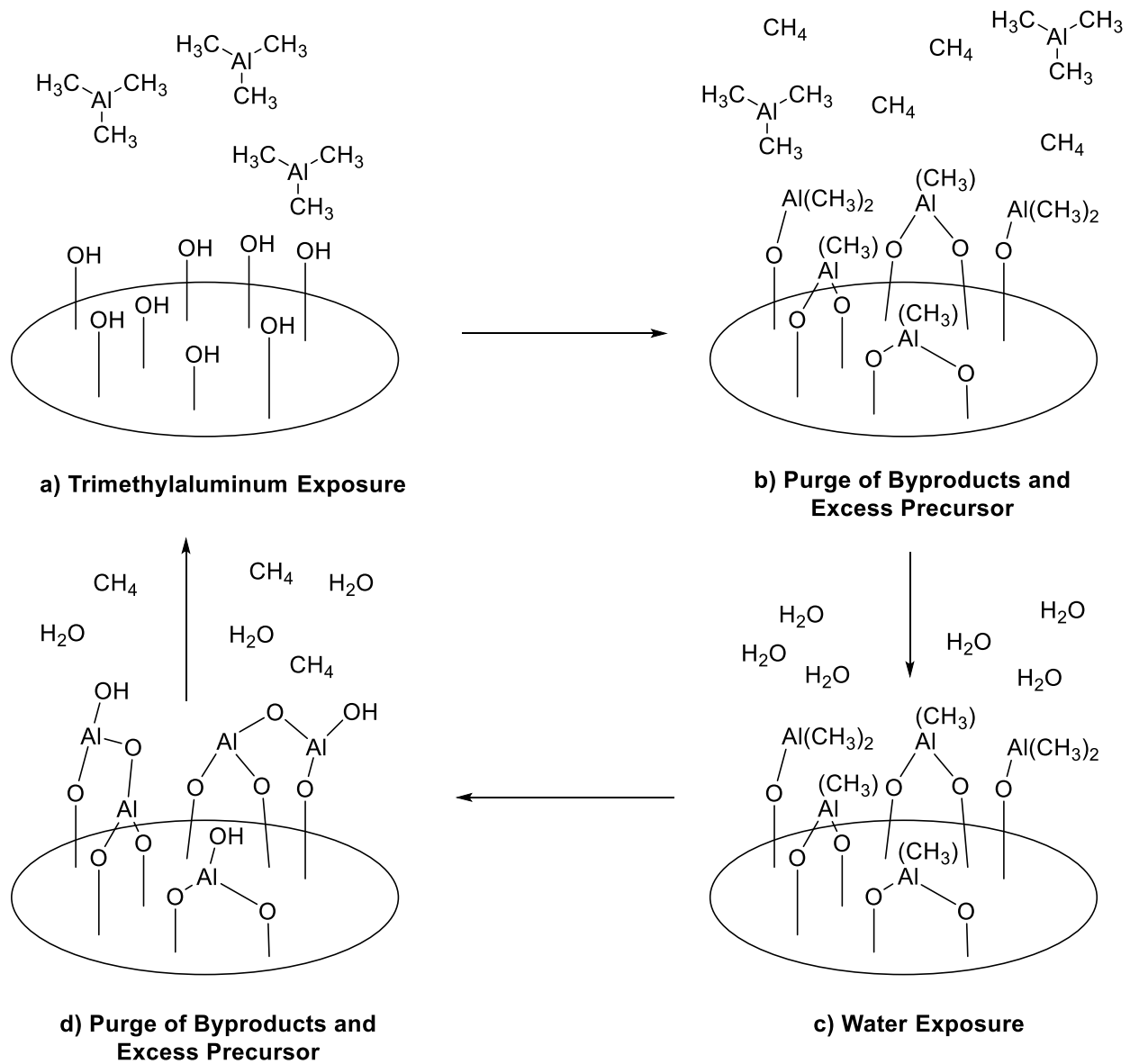


Figure 1. Simplified schematic representation of one ALD cycle of  $\text{Al}_2\text{O}_3$  deposition from trimethylaluminum ( $\text{Al}(\text{CH}_3)_3$ ) and water.

To verify if self-limiting growth is occurring in an ALD process, the pulse lengths (exposure times) of each precursor can be varied and the growth rate is measured while keeping all other parameters constant. If the precursor exposure is self-limiting, then excess precursor will not contribute to the film growth rate, which will plateau at a constant value (Figure 2). This

is due to two separate, critical factors: (1) the precursor reacting with all available surface reactive sites and (2) the precursor being sufficiently thermally stable not to undergo self-decomposition at the surface temperature.

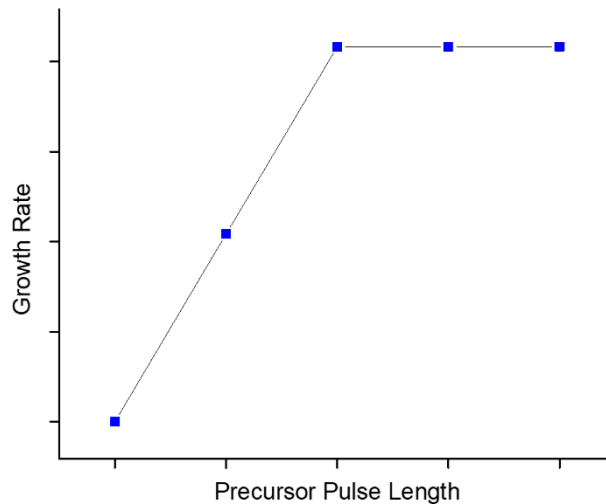


Figure 2. Example saturation curve showing a self-limiting film growth process.

Once sufficient doses of both precursors are confirmed to be delivered, the growth temperature can be varied to determine the temperature region where the best film properties are obtained. Although not required for self-limiting ALD growth, very often there will be a temperature region where the growth rate is constant. This is termed the “ALD window” (Figure 3). The best film properties are not necessarily obtained within the ALD window but operating within this window will tend to guarantee self-limiting surface reactions for a given ALD process. Outside of the ALD window, the cause of the change in growth rate can be due to a variety of factors. At temperatures below the ALD window, the growth rate can be (1) higher, which may be due to precursor condensation and formation of more than one monolayer, or (2) lower, due to insufficient thermal energy to drive the reaction between the precursor and the

growth surface or the reaction of the second precursor with the monolayer of the first precursor. Above the ALD window, the growth rate can be (3) higher due to precursor self-decomposition and CVD-type growth, which would also likely reduce the conformality of the deposited film, or (4) lower due to desorption of the precursors from the growth surface. Also possible is dehydration leading to loss of surface reactive sites, decomposition of the first precursor on the surface which modifies its reactive functional groups in such a way as to render the surface unreactive toward the second precursor, or decomposition of the second precursor in the gas-phase which prevents it from reacting with the first precursor but does not lead to CVD-type film growth. Precursor chemistry is clearly the central concept in true self-limiting ALD thin film growth.

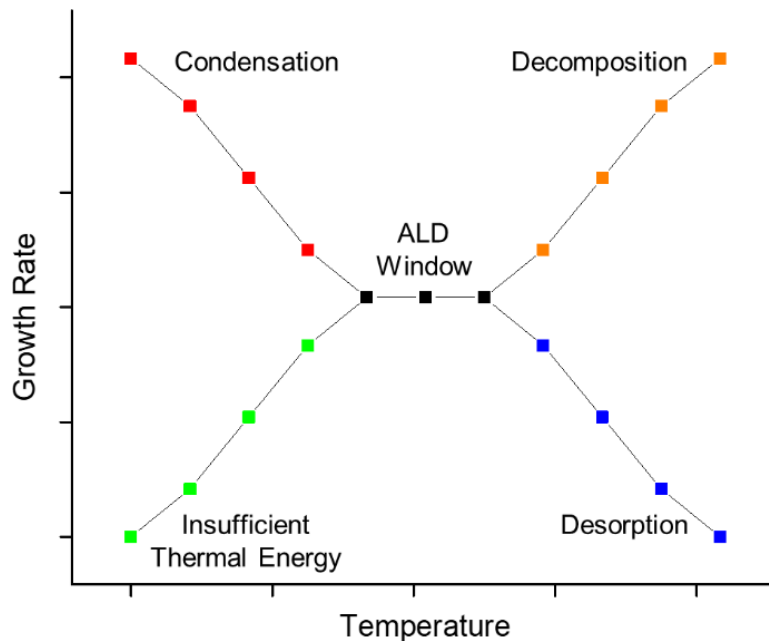


Figure 3. Example ALD window plot showing different growth regimes.

### 1.3 ALD Chemistry for Metal Films

ALD chemistry can be divided into two classes, thermal and plasma-enhanced. This dissertation is focused on the chemistry of thermal ALD, but plasma-enhanced ALD (PEALD) can deposit many metals and materials which are difficult to deposit by purely thermal ALD at present.<sup>20</sup> In many cases this is due to the use of a hydrogen plasma which generates atomic hydrogen. Atomic hydrogen is a very powerful reducing agent and has been demonstrated to be able to deposit such difficult metals as titanium and tantalum by ALD from the metal halide precursors.<sup>21-23</sup> Thermal ALD is desirable over plasma-based processes due to improved conformality and substrate damage from energetic plasma species.<sup>24</sup> Purely thermal ALD chemistry for metal films presents difficult chemical challenges.<sup>25</sup> Serious research efforts have been focused on development of ALD precursors over the last 15-20 years.<sup>6,26-28</sup> Design of a thermal ALD process for metal film growth entails designing a chemical reaction where the *product* of the reaction is a zerovalent metal. To date, far less research has been carried out exploring the reducing co-reactant as opposed to the metal precursor. Volatile and thermally stable precursors exist for nearly every element and multiple different classes of precursors have been developed for many elements. The reducing co-reactant must react with the metal precursor, remove any metal precursor ligands, reduce the metal ion to the zerovalent state, and leave the growth surface as volatile byproducts which do not incorporate into the film.<sup>29</sup> Thus, there is a great need for novel chemical approaches to thin film growth by ALD.

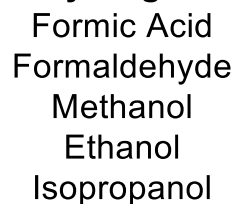
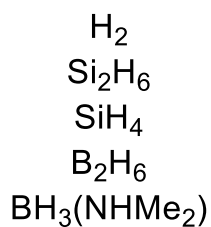
ALD of pure metal films is difficult and very metal-dependent. Noble metals like Ru, Os, Rh, Ir, Pd, Pt, and Au can be deposited from the corresponding metal precursor and oxidants such as O<sub>2</sub> or O<sub>3</sub>, which combusts the precursor ligands and forms a metal oxide film which decomposes to give a metal film.<sup>30</sup> Oxidative combustion for noble metal ALD will not be

discussed in this dissertation. Electropositive metals require a reducing agent that meets the strict requirements for volatility and thermal stability imposed by ALD. An early ALD reducing agent was zinc metal. For ALD processes above 400 °C, addition of a zinc pulse improved resistivities for TiN and TaN films.<sup>31,32</sup> Zinc as an ALD precursor is far from ideal due to its low vapor pressure and its tendency to alloy with the growing film which leads to a loss of self-limiting growth.<sup>33</sup>

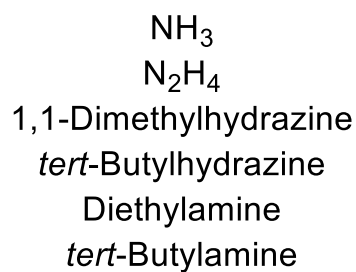
A list of all reducing co-reactants which have been reported in thermal ALD growth of metal films is given in Figure 4. Hydrogen has been the most common reducing agent for metal ALD, but molecular hydrogen exhibits low reactivity toward most metal precursors in the desired ALD film growth temperature region (<400 °C). An early report used hydrogen with metal acetylacetonate precursors (Ni, Cu, Pt) at 250 °C.<sup>34</sup> Metallic film growth was observed on metal substrates (Ti and Al), but not on hydrogen-terminated Si or glass. A second method, reduction of NiO by hydrogen was tested by first deposited an ALD NiO film from Ni(acac)<sub>2</sub> and O<sub>3</sub> on glass and then treating the film with forming gas (5% H<sub>2</sub> in Ar) at temperatures as low as 230 °C. Thermal ALD of first row transition metals iron, cobalt, nickel, and copper using amidinate precursors and hydrogen was reported.<sup>35</sup> Growth rates were low (< 0.5 Å/cycle for Cu, < 0.12 Å/cycle for Co) and the growth temperatures were generally high (225-375 °C) due to the low reactivity of molecular hydrogen. To increase the reactivity of hydrogen, precursors containing hydrogen bonded to a different element are commonly employed. Silanes and boranes are more reactive hydride donors and have been used in several ALD processes (*vide infra*). Unfortunately, these heteroatoms can contaminate the growing metal film and form carbides, nitrides, silicides, borides, or oxides. As long as the desired metal film does not form stable

compounds with this heteroatom, it will be possible to deposit a high purity metal film using an H-X containing co-reactant, e.g. noble metals + oxygen-containing co-reactants.

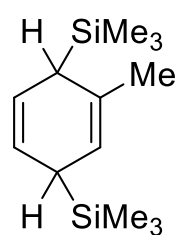
**Si-H/B-H Hydrogen Sources      O-H/C-H Hydrogen Sources**



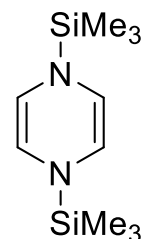
**N-H Hydrogen Sources**



**Electron Sources**

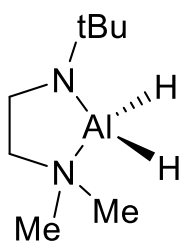


CHD

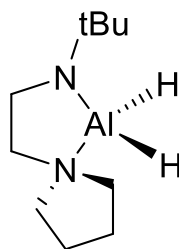


DHP

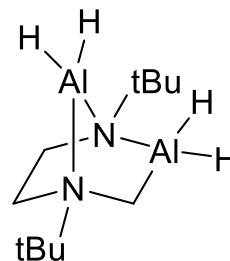
**Al-H Sources (This Work)**



1



3



5

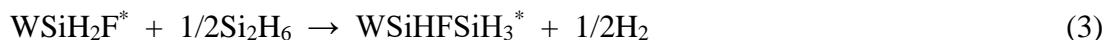
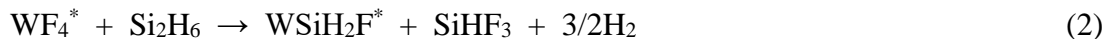
Figure 4. List of reducing co-reactants that have been reported in thermal ALD growth of metal films.



## 1.4 Selected Metal CVD/ALD Processes

### 1.4.1 Tungsten Metal

Tungsten metal ALD is arguably the most successful metal ALD process to date and is heavily used in the microelectronics industry. The initial report from George used  $\text{WF}_6 + \text{Si}_2\text{H}_6$  and deposited tungsten metal films with a growth rate of  $2.5 \text{ \AA}/\text{cycle}$  between  $150\text{-}325 \text{ }^\circ\text{C}$ .<sup>36</sup> The growth rate for this process corresponds to approximately one monolayer of tungsten metal deposited with each cycle. This is higher than most ALD processes such as  $\text{Al}_2\text{O}_3$  ALD from trimethylaluminum and water, which has a growth rate of  $0.9 \text{ \AA}/\text{cycle}$ , or approximately 1/3 of an  $\text{Al}_2\text{O}_3$  monolayer. Detailed mechanistic studies based on gas phase reaction products and quartz crystal microbalance measurements of this tungsten ALD process followed<sup>37,38</sup> and determined the growth proceeds according to the following self-limited surface reactions:



The surface chemical reactions proposed in (1)-(3) are quite complex, but the main message which relates to the growth rate is the insertion of multiple silyl groups into the W-Si surface bond in (2), essentially generating more than one monolayer of silane. The incoming  $\text{WF}_6$  exposure then reacts with the multiple silyl groups to deposit a larger amount of W atoms than would be possible with only one surface W-silyl group. Tungsten metal can also be deposited by ALD using  $\text{B}_2\text{H}_6$  or  $\text{SiH}_4$  as the reducing agent.<sup>39,40</sup> Mo metal can also be deposited by thermal ALD using  $\text{MoF}_6$  and  $\text{Si}_2\text{H}_6$  as precursors.<sup>41</sup> Use of  $\text{Si}_2\text{H}_6$  as a reducing agent in

tantalum metal ALD was attempted, but this resulted in TaSi<sub>x</sub> films.<sup>42,43</sup> A detailed study of the reaction in solution of silanes with titanium, zirconium, and hafnium amido complexes found the reactions are facile at room temperature and produce H<sub>2</sub> and aminosilanes,<sup>44</sup> but ALD results using this precursor combination have not been reported.

### 1.4.2 Tungsten Carbide

Tungsten carbide is found in two major phases: the stoichiometric WC and the tungsten-rich W<sub>2</sub>C. These materials are characterized by very high hardnesses, low resistivities, and chemical and oxidation resistance.<sup>45</sup> Tungsten carbides are also important materials for hard coatings and for their catalytic properties which can be similar to noble metals like platinum.<sup>46-48</sup> WF<sub>6</sub> is by far the most common industrial tungsten precursor. Tungsten carbide can be deposited by CVD using WF<sub>6</sub> or WCl<sub>6</sub> + C<sub>3</sub>H<sub>8</sub> + H<sub>2</sub> at temperatures greater than 650 °C for WF<sub>6</sub> and greater than 750 °C for WCl<sub>6</sub>.<sup>49,50</sup> Tungsten carbide CVD can be achieved at much lower temperatures using W(CO)<sub>6</sub> + C<sub>2</sub>H<sub>4</sub> between 250-450 °C.<sup>51</sup> Single-source organometallic precursors to tungsten carbide films at low temperatures include tris(neopentyl)neopentylidyne tungsten<sup>52</sup> and alkenyl tungsten carbonyl precursors such as *cis*-(1,3-butadiene)<sub>2</sub>W(CO)<sub>2</sub>.<sup>53</sup> There are few reports of thermal ALD of tungsten carbide films. Brief mentions of high quality tungsten carbide films deposited by thermal ALD were contained in two recent review articles.<sup>17,24</sup> As with most tungsten film deposition reports, this process used WF<sub>6</sub> as the tungsten precursor. The co-reactant was diethylsilane (SiH<sub>2</sub>Et<sub>2</sub>) which enabled deposition of tungsten carbide films between 150-300 °C with low resistivities between 400-500 μΩ·cm. An alternative tungsten precursor, WCl<sub>6</sub>, was reported in the thermal ALD of tungsten carbide films using AlMe<sub>3</sub> as the co-reactant.<sup>54</sup> These results are presented in Chapter 4.

### 1.4.3 Titanium Nitride/Titanium Carbide

Titanium nitride (TiN) and titanium carbide (TiC) films are quite similar in structure and properties and are characterized by very high hardness, good chemical and oxidation resistance, and low resistivity. TiN, which is a gold-colored material, has lower resistivity than titanium metal, higher hardness than sapphire ( $\text{Al}_2\text{O}_3$ ), and melts at  $2930\text{ }^\circ\text{C}$ .<sup>55</sup> The related material TiC has the same cubic rock salt crystal structure, but is not gold-colored and has a higher melting point of  $3160\text{ }^\circ\text{C}$ . TiN can be deposited by CVD using  $\text{TiCl}_4$  and a mixture of nitrogen and hydrogen gases at  $900\text{-}1200\text{ }^\circ\text{C}$  or a mixture of ammonia and hydrogen gases at  $575\text{-}700\text{ }^\circ\text{C}$ .<sup>55</sup> Single-source precursors to TiN films have been reported such as  $[\text{TiCl}_2(\text{NH}t\text{Bu})_2(\text{NH}_2t\text{Bu})_2]_2$ .<sup>56</sup> Most microelectronic devices require much lower growth temperatures. TiN is commonly used in microelectronics as a barrier layer, adhesion layer, diffusion barrier, and as a work function metal.<sup>1,24</sup> TiN is one of the most studied ALD processes and was first reported in 1987, where  $\text{TiCl}_4$  and  $\text{NH}_3$  were used as precursors.<sup>31,57</sup> Perfect conformality of the TiN films was demonstrated using trenched substrates.<sup>58</sup> The films are deposited with a growth rate of  $\sim 0.2\text{ \AA/cycle}$ , resistivities are  $\sim 250\text{ }\mu\Omega\cdot\text{cm}$ , and temperatures above  $350\text{ }^\circ\text{C}$  must be used to minimize formation of nonvolatile  $\text{NH}_4\text{Cl}$ . Halide impurities from the  $\text{TiCl}_4$  precursor can be detrimental to devices and the byproduct HCl is corrosive to the chips and processing equipment. ALD of TiN using the metalorganic precursor  $\text{Ti}(\text{NMe}_2)_4$  has been attempted using ammonia as the co-reactant.<sup>1,24,55,59</sup>  $\text{Ti}(\text{NMe}_2)_4$  has poor thermal stability and it was found that  $\text{Ti}(\text{NMe}_2)_4$  does not adsorb onto the growth surface in a self-limiting fashion and the growth rate increased significantly with larger precursor doses. The resulting films have low densities, poor stability in air, and high resistivities ( $> 10^4\text{ }\mu\Omega\cdot\text{cm}$ ).

Incorporation of aluminum into TiN leads to increased oxidation resistance and, for semiconductor applications, lowers the work function of the material.<sup>60</sup> Ti(Al)(C)N films were deposited by a three-step thermal ALD process using  $\text{TiCl}_4 + \text{AlMe}_3 + \text{NH}_3$ .<sup>61</sup> Trimethylaluminum was employed as an added reducing agent in an attempt to improve the film quality and lower the deposition temperature from the binary  $\text{TiCl}_4 + \text{NH}_3$  process. The resulting films had Al and C contents between 3-15 at.% and 6-16 at.%, respectively. TiAlN has also been deposited by PEALD using  $\text{Ti}(\text{NMe}_2)_4 + \text{NH}_3$  plasma and  $\text{AlMe}_3 + \text{H}_2$  plasma.<sup>62</sup>

Titanium carbide can be deposited by CVD at high temperatures using  $\text{TiCl}_4$ ,  $\text{CH}_4$ , and hydrogen above 1000 °C. A much lower temperature CVD processes for TiC was developed using tetrakis(neopentyl)titanium which deposits TiC films at 150 °C.<sup>63,64</sup> Ti(Al)C films have been deposited by ALD and tested as a work function metal using  $\text{TiCl}_4$  and  $\text{AlMe}_3$ .<sup>65</sup>

Titanium carbonitride (TiCN) films can have properties superior to the binary TiN or TiC phases.<sup>66,67</sup> CVD of TiCN was reported using metalorganic titanium guanidinate complexes.<sup>68</sup> TiCN has been investigated as a work function metal.<sup>69</sup> Chapter 3 presents the results of a thermal ALD study where TiCN films were deposited by from  $\text{TiCl}_4$  and an aluminum dihydride precursor.<sup>70</sup>

#### 1.4.4 First Row Transition Metals

Copper metal ALD is now well developed. Arguably, a new era of advanced ALD chemistries began with the 2009 report of copper metal ALD using  $\text{Cu}(\text{dmap})_2 + \text{diethylzinc}$  as the reducing agent (Figure 5).<sup>71</sup> Unfortunately, diethylzinc has poor thermal stability and zinc impurities were found in the copper films at all deposition temperatures. Zinc contamination has significant deleterious effects in integrated circuits, so this process cannot be used in microelectronics devices. Solution chemistry for Cu ALD using similar copper precursors with

diethylzinc and other similar reducing agents was studied in detail.<sup>72</sup> These results were then tested in ALD Cu metal film growth.<sup>73</sup> A three-step process using  $\text{Cu}(\text{dmap})_2$  + formic acid + hydrazine gave high purity, low resistivity copper metal films.<sup>74,75</sup>  $\text{Cu}(\text{dmap})_2$  was also used with the novel reducing agent  $\text{BH}_3(\text{NHMe}_2)$  to deposit Cu metal and Cu-Mn alloy films.<sup>76,77</sup> An alternative method for metal ALD has been to first deposit a metal oxide film and then reduce it to the metal in a subsequent step. This allowed deposition of very thin smooth Cu metal films.<sup>78</sup> A two-step process using  $\text{Cu}(\text{dmap})_2$  and *tert*-butylhydrazine produced very high purity and low resistivity Cu metal films.<sup>79</sup> A major challenge is obtaining smooth films at very small thickness. This was studied in detail which found that the major factor is not necessarily growth temperature but can be more heavily influenced by the choice of substrate material.<sup>80</sup>

First row transition metal diazadienyl precursors were synthesized and subsequently used in low temperature, selective ALD of Co and Ni films using formic acid or alkylamines such as *tert*-butylamine as co-reactants (Figure 5).<sup>81-85</sup> Ni metal and  $\text{Ni}_3\text{C}$  films have been deposited from  $\text{Ni}(\text{acac})_2$  and short-chain alcohols.<sup>86</sup>

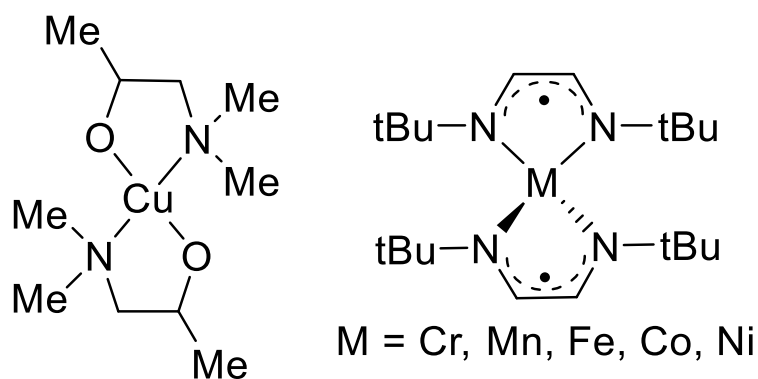


Figure 5. Structures of  $\text{Cu}(\text{dmap})_2$  and transition metal di-*tert*-butyl diazadienyl complexes.

ALD reducing agents based on reductively silylated 6-membered rings were recently reported (Figure 6).<sup>87,88</sup> The application of these reagents was inspired by recent work from Mashima using similar compounds as soluble and salt-free reducing agents for generation of low-valent metal species in solution with applications in catalysis.<sup>89-93</sup> The precursors 1-methyl-2,5-bis(trimethylsilyl)-2,5-cyclohexadiene (CHD) and 1,4-bis(trimethylsilyl)-1,4-dihydropyrazine (DHP) were first reported in thermal ALD of titanium films with  $\text{TiCl}_4$ .<sup>87</sup> DHP was also reported in three-step ALD processes where cobalt or nickel bis(1,4-di-*tert*-butyl-1,3-diazabutadienyl) precursors + formic acid + DHP yielded high purity cobalt and nickel metal films at 180 °C.<sup>82</sup>

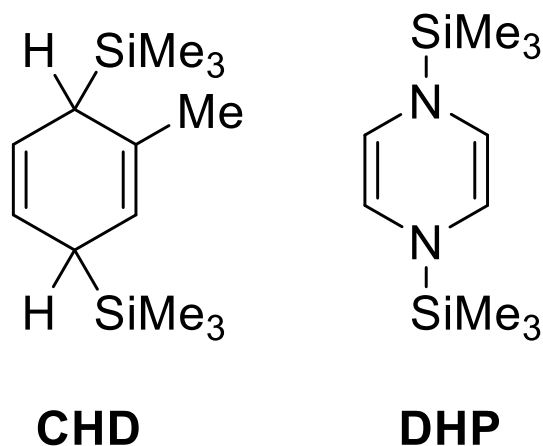


Figure 6. Structures of the novel ALD reducing agents 1-methyl-2,5-bis(trimethylsilyl)-2,5-cyclohexadiene (CHD) and 1,4-bis(trimethylsilyl)-1,4-dihydropyrazine (DHP).

#### 1.4.5 Aluminum Metal

Aluminum is the most abundant metal in the Earth's crust, nearly 2000 times more abundant than copper, and is the fourth-most conductive metal behind silver, copper, and gold with a room temperature bulk resistivity of  $2.65 \mu\Omega \cdot \text{cm}$ .<sup>94</sup> Aluminum thin films are commonly

used for metallization of polymers (e.g. potato chip bags) and for household mirrors due to its low gas permeability and high reflectivity. Aluminum has advantages in plasmonics over traditional plasmonic metals such as silver and gold due to its low cost and ability to be used over a wider spectral range including ultraviolet wavelengths.<sup>95</sup> Aluminum is also a popular component of thermite-based thin film energetic materials.<sup>96–98</sup>

CVD of aluminum metal is a mature subject where many different precursors have been developed which can produce high purity films. A great deal of information has been discovered about the surface chemistry of these precursors.<sup>99</sup> Selected precursor structures for aluminum metal CVD are shown in Figure 7. Trimethylaluminum, which exists as the dimer  $\text{Al}_2\text{Me}_6$ , is a poor CVD precursor to aluminum metal since there is no low energy pathway to cleave the Al-C bonds. Film growth proceeds only at high temperatures ( $> 350\text{ }^\circ\text{C}$ ) and the films have significant carbon contamination. Dimethylaluminum hydride and triisobutylaluminum produce significantly more pure aluminum metal films at lower temperatures ( $<250\text{ }^\circ\text{C}$ ) than trimethylaluminum and were the first commercially successful aluminum CVD precursors.<sup>8,100–103</sup> Even lower deposition temperatures ( $<100\text{ }^\circ\text{C}$ ) and carbon contamination have resulted from alkylamine-alane adducts which contain no Al-C bonds such as trimethylamine alane, N-methylpyrrolidine alane, and trimethylamine alane borane.<sup>104–107</sup>

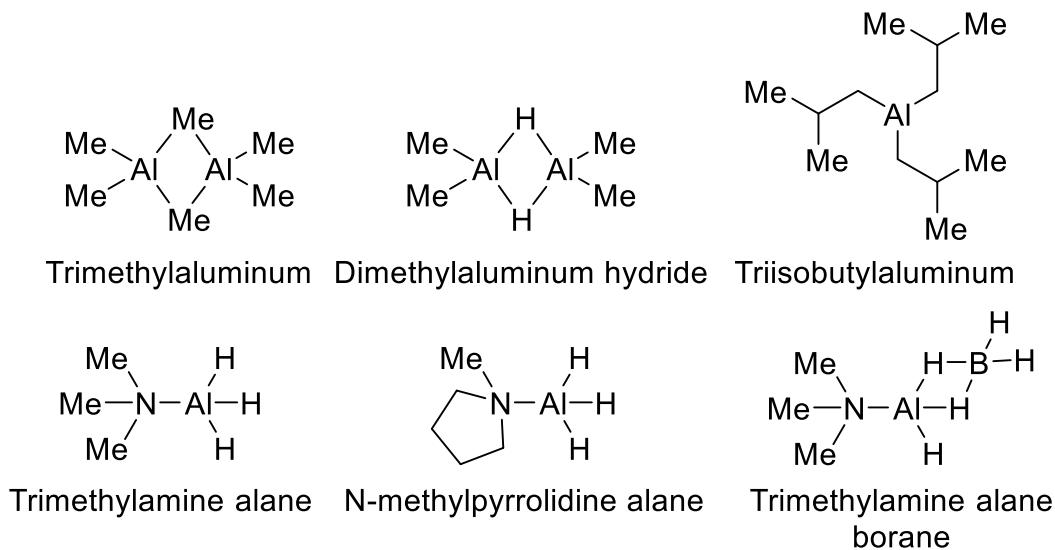


Figure 7. Selected precursors for aluminum metal CVD.

The low cost of aluminum, its low resistivity, and the availability of CVD processes to produce high purity films led to its widespread use. Aluminum was the standard conductive material in integrated circuits until recently when it has been largely replaced by copper over the last 10-15 years. Unfortunately, aluminum suffers from significant electromigration issues which can lead to voids and short circuits in the interconnect wiring. Alloying with copper can improve the electromigration properties of aluminum and the copper-rich intermetallic phase  $\text{Cu}_9\text{Al}_4$  has been investigated as a metallization material.<sup>108,109</sup> Nevertheless, aluminum still has significant applications in microelectronic devices such as a component of the work function metal in the gate electrode.<sup>60,110–113</sup>

Although CVD of aluminum metal films is successful and quite well understood, continued miniaturization following Moore's Law demands metal film deposition in increasingly high aspect ratio structures. The conformality of CVD is inherently limited compared to ALD, but ALD of aluminum and other electropositive metals is extremely difficult due to stringent



demands of precursor stability and self-limiting growth. Prior to the work presented in this dissertation, there was only one reported process for aluminum metal ALD. This was a plasma-based process which used trimethylaluminum and hydrogen plasma at 250 °C and deposited aluminum metal films with a growth rate of 1.5 Å/cycle.<sup>114,115</sup> New processes for aluminum metal ALD are presented in Chapters 2 and 6.

### 1.5 Metal Hydride Chemistry

Metal hydride chemistry is synthetically challenging but exceedingly useful in diverse research areas from catalysis to materials science to energy. Metal hydride species are key players in biological NH<sub>3</sub> synthesis by nitrogenase enzymes.<sup>116-119</sup> Metal hydride catalyst surfaces are thought to play a key role in the Haber-Bosch process for industrial NH<sub>3</sub> synthesis from N<sub>2</sub> and H<sub>2</sub>.<sup>120</sup> Molecular transition metal hydride complexes have recently generated interest for their reactivity with the generally inert N<sub>2</sub> molecule.<sup>120,121</sup> The hydride ligands can function as both a source of electrons and protons, so N<sub>2</sub> activation can be done in the absence of external reducing agents or proton source.<sup>120</sup> The electronegativity difference between hydrogen (2.20) and metals (generally <2 for non-noble metals), often produces complexes where the hydrogen atom ligand can be thought of as anionic H<sup>-</sup> and displays nucleophilic characteristics, though this is not always the case.<sup>122</sup>

Main group metal hydrides are reviewed here because of their potential applications as vapor-phase reducing agents for metal thin film growth. The high reactivity of most main group metal hydrides is promising for this application. In particular, the low molecular weights of Mg, Al, and Zn hydrides are promising for generating volatile complexes. Molecular hydride complexes of the group 1 and 2 metals are challenging to prepare because of the very high lattice energies of the solids and the high polarity of the metal-hydride bonds.<sup>123</sup> Main group metal

hydrides are currently heavily investigated in renewable energy fields for their applications as catalyst intermediates and hydrogen storage materials.<sup>123–126</sup>  $\text{MgH}_2$  and  $\text{ZnH}_2$  are mostly insoluble polymeric solids which decompose at approximately 300 and 100 °C, respectively. The synthesis of these compounds can be achieved by treatment of a magnesium or zinc alkyl, such as dibutylmagnesium or diethylzinc, with  $\text{LiAlH}_4$ . The insoluble hydride products can be collected by filtration. The reaction of these main group hydrides with pyridine was studied in the early 1980's.<sup>127–130</sup> Complexes of Mg and Zn with 1,4-dihydropyridyl ligands were formed and their application as soluble reducing agents for carbonyl functional groups was studied.<sup>129</sup>

Metal hydride complexes with N-heterocyclic carbenes (NHCs) have been appearing with increasing frequency.<sup>131–133</sup> NHCs are neutral, strongly coordinating ligands which can stabilize a variety of unusual molecular structures, such as the NHC adduct of  $\text{Al}_2\text{H}_4$  reported by Jones from reduction of the NHC- $\text{AlH}_3$  complex with a Mg(I) dimer.<sup>134</sup> Hill explored NHC-Mg complexes which were expected to enable the preparation of a tractable Mg hydride complex.<sup>135</sup> Treatment of an NHC-Mg amide precursor with the simple hydride source phenylsilane ( $\text{PhSiH}_3$ ) lead to a hydride-rich Mg cluster (Figure 8).<sup>135</sup> The Mg:H ratio of 1:1.5 is higher than any known molecular Mg hydride complex reported to date.

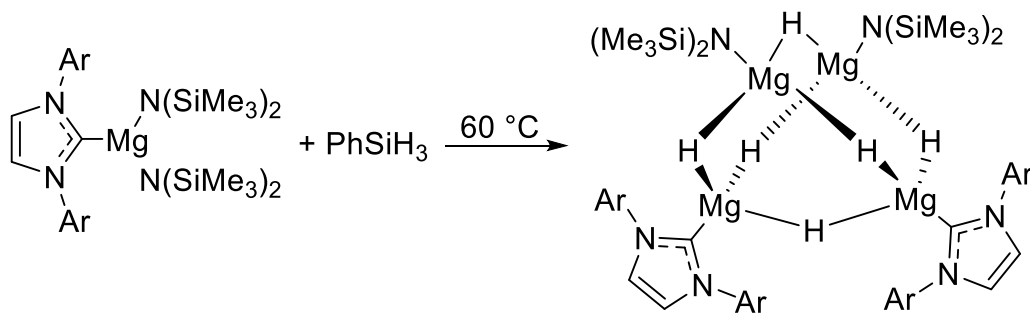


Figure 8. Synthesis of a hydride-rich Mg cluster from treatment of a NHC-Mg amide precursor with triphenylsilane.

## 1.6 Volatile Aluminum Hydride Complexes

Aluminum hydride complexes have found great use in vapor phase thin film growth due to their low molecular weight/high volatility and high reactivity.<sup>136,137</sup> The straightforward synthesis of  $\text{AlH}_3(\text{NMe}_3)$  from  $\text{LiAlH}_4$  and trimethylammonium chloride was first reported in 1960.<sup>138</sup>  $\text{AlH}_3$  can form both 1:1 and 1:2 adducts with  $\text{NMe}_3$  and both are volatile colorless crystalline solids.  $\text{AlH}_3(\text{NMe}_3)_2$  has a slightly higher vapor pressure of 1.8 Torr at 25 °C than the 1:1 adduct, but dissociates to the 1:1 adduct in the gas phase above 80 °C.<sup>104</sup> Replacing trimethylamine for dimethylethylamine or triethylamine produces liquid precursors with similarly high vapor pressures.<sup>139,140</sup> Reducing the cone angle of the trialkylamine leads to increased Lewis basicity and a corresponding increase in stability of the  $\text{AlH}_3$  complex, as in N-methylpyrrolidine alane and quinuclidine alane.<sup>106,141</sup> Quinuclidine alane is the most thermally stable of the trialkylamine-alane adducts with a solid state thermal decomposition point of ~190 °C, however its higher melting point and lower vapor pressure (sublimation at 120 °C) limits its applications in vapor phase film growth.

Aluminum dihydride complexes coordinated by simple monoanionic amido-amine ligands were reported by Beachley in 1976.<sup>142</sup> Although these complexes were found to be dimeric according to solution molecular weight measurements, they sublimed at low temperatures (50 °C). The dimeric structures of these complexes were later confirmed by X-ray crystallography.<sup>143</sup> These complexes have also been used as CVD precursors to aluminum metal films.<sup>144</sup> The new aluminum dihydride complexes presented in Chapters 2 and 3 are based on subtle but important modifications of these complexes which resulted in dramatic changes in thermal stability and film growth properties.

Al hydrides are powerful reducing agents due to the highly polarized Al-H bond.  $\text{LiAlH}_4$  is widely used in synthetic chemistry but it lacks the volatility and thermal stability required of an ALD precursor.  $\text{AlH}_3$ -amine adducts are highly volatile and reactive and have achieved great success as precursors for chemical vapor deposition (CVD) of Al metal. Due to this reactivity, thermal stability and long-term storage is a major problem. There is one report of an  $\text{AlH}_3$ -amine adduct as a vapor phase reducing agent in the low temperature CVD growth of TiAl alloy films using  $\text{TiCl}_4 + \text{AlH}_3(\text{NMe}_3)$ . The Al:Ti ratio could be tuned simply according to the precursor feed ratio with larger  $\text{AlH}_3(\text{NMe}_3)$  exposures producing Al-rich films. The effectiveness of Al hydrides as vapor phase reducing agents was thus demonstrated. In order to achieve self-limiting growth, ALD requires that the precursors do not decompose readily on the growth surface and, accordingly, thermally stable Al hydride reducing agents would be highly valued in ALD of metal and element films.

### **1.7 Thesis Problem**

This dissertation began as an industrial collaboration aimed toward the development of new precursors and processes for thermal ALD of electropositive metal thin films such as titanium, tantalum, molybdenum, tungsten, manganese, and aluminum. Titanium is a very important adhesion layer and contact material due to its strong interaction with silicon. Tantalum is used in a bilayer with tantalum nitride as a copper diffusion barrier. Tungsten is very important as a conductor in interconnects and vias, and molybdenum may have some applications as a tungsten replacement in narrow line width interconnects due to its lower electron mean free path.<sup>145</sup> Manganese may have important uses as a precursor to ultrathin self-forming manganese silicate diffusion barriers. Aluminum was the conductor of choice for integrated circuits for decades before being replaced by copper. Aluminum is currently used as a component of the metal

gate electrode in materials such as TiAl, TiAlN, and TiAlC. Aluminum may find use in future miniaturized integrated circuits due to its much lower electron mean free path than copper and much lower cost compared to alternatives such as cobalt and ruthenium.<sup>145</sup> As shown in Table 1, with the exception of tungsten, these metals have negative electrochemical potentials which makes thermal ALD growth very challenging. Early transition metals such as titanium, tantalum, molybdenum, and tungsten form highly stable carbide and nitride phases which introduces additional challenges when choosing a reducing co-reactant.

Table 1. Selected standard reduction potentials for metal ions and applications of the metals in microelectronics devices.<sup>94</sup>

<u>Element</u>	<u>Reduction</u>	<u>E° (V)</u>	<u>Use</u>
Cu	$\text{Cu}^{2+} + 2\text{e}^- \rightleftharpoons \text{Cu}^0$	0.342	Interconnects
W	$\text{W}^{3+} + 3\text{e}^- \rightleftharpoons \text{W}^0$	0.100	Fill for contacts/vias
Ni	$\text{Ni}^{2+} + 2\text{e}^- \rightleftharpoons \text{Ni}^0$	-0.257	Contacts, electrodes
Co	$\text{Co}^{2+} + 2\text{e}^- \rightleftharpoons \text{Co}^0$	-0.280	Copper seed/capping layer
Fe	$\text{Fe}^{2+} + 2\text{e}^- \rightleftharpoons \text{Fe}^0$	-0.447	Magnetic devices
Ta	$\text{Ta}^{3+} + 3\text{e}^- \rightleftharpoons \text{Ta}^0$	-0.600	Cu barrier, gate electrode
Cr	$\text{Cr}^{2+} + 2\text{e}^- \rightleftharpoons \text{Cr}^0$	-0.913	Copper seed layer
Mn	$\text{Mn}^{2+} + 2\text{e}^- \rightleftharpoons \text{Mn}^0$	-1.185	Self-forming Cu barriers
Ti	$\text{Ti}^{2+} + 2\text{e}^- \rightleftharpoons \text{Ti}^0$	-1.630	W barrier, Cu/Ti, Al/Ti
Al	$\text{Al}^{3+} + 3\text{e}^- \rightleftharpoons \text{Al}^0$	-1.676	Gate electrode, Al/Ti
Dy	$\text{Dy}^{3+} + 3\text{e}^- \rightleftharpoons \text{Dy}^0$	-2.295	Magnetic devices (lanthanides)
Mg	$\text{Mg}^{2+} + 2\text{e}^- \rightleftharpoons \text{Mg}^0$	-2.372	???????

These metals have many important applications in microelectronics devices, but ALD processes for these metals either do not exist or have less optimal aspects such as the use of plasma hydrogen as the reducing agent or production of corrosive byproducts. To solve these problems, new reducing chemistries must be developed. Requirements for new ALD precursors

include high volatility, thermal stability at both the growth temperature and long-term (weeks, months) at the bubbler temperature, and preferably low cost, straightforward syntheses. Liquid precursors are also advantageous for their consistent evaporation rate which results in a consistent precursor delivery rate.

Aluminum hydrides were explored in this project for their high reactivities and potential to produce highly volatile compounds based on their low molecular weights. A major challenge has been preparing aluminum hydride containing molecules with sufficient thermal stability to enable self-limited ALD film growth. Proper ligand design is the main tool in preparing stabilized main group hydride complexes, so inspiration was taken from previously reported aluminum hydride complexes with modifications based on successful ALD precursors.

## CHAPTER 2

### ATOMIC LAYER DEPOSITION OF ALUMINUM METAL FILMS USING A THERMALLY STABLE ALUMINUM HYDRIDE REDUCING AGENT

Reprinted (adapted) with permission from Blakeney, K. J.; Winter, C. H. *Chem. Mater.* **2018**, *30*, 1844–1848. Copyright 2018 American Chemical Society.

#### 2.1 Introduction

Atomic- and nano-scale films of aluminum (Al) metal have current high-interest uses in microelectronics,<sup>60,111,113,146</sup> plasmonics,<sup>95,147–151</sup> energetic materials,<sup>97,98</sup> and hydrogen storage.<sup>152–154</sup> Advanced fabrication techniques for thin films such as chemical vapor deposition (CVD)<sup>5,155</sup> and atomic layer deposition (ALD)<sup>1,6,7,24</sup> provide greater control, conformality, and selectivity over traditional physical vapor deposition techniques such as sputtering and evaporation. Al metal has a more negative electrochemical potential than any element deposited by thermal ALD to date ( $\text{Al}^{3+} \leftrightarrow \text{Al}^0$   $E^\circ = -1.676$  V).<sup>94</sup> As a result, Al metal has not been deposited by a thermal ALD process due to the lack of sufficiently strong and thermally stable reducing precursors. Herein, this chapter reports the thermal ALD of high purity, low resistivity Al films enabled by a thermally stable Al hydride reducing agent. This reducing agent may also permit film growth of other electropositive elements that have not been deposited by thermal ALD to date.

CVD of high purity, low resistivity Al films has been achieved using a variety of Al precursors,<sup>5,101,102,104–107,139,140,155</sup> but the miniaturization demands of Moore's Law<sup>2</sup> are not completely satisfied by CVD in terms of uniformity and conformality. ALD is uniquely suited to deposit uniform films with Angstrom-level thickness control due to its self-limiting growth mechanism.<sup>1,6,7,24</sup> There have been two reports of the plasma-enhanced ALD (PEALD) of Al metal films using  $\text{AlMe}_3$  and  $\text{H}_2$  plasma.<sup>114,115</sup> PEALD has been used to deposit many materials



that remain challenging for thermal ALD, but step coverage may be limited by rapid hydrogen atom recombination in high aspect ratio features and substrate damage may occur from energetic plasma species.<sup>20</sup>

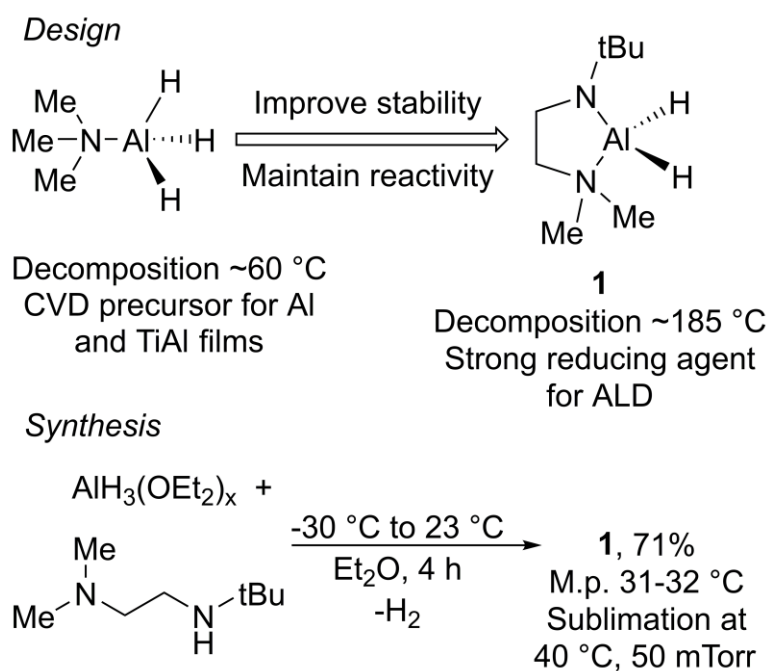
The lack of strong reducing precursors severely limits thermal ALD growth of electropositive metals and elements.<sup>27</sup> Al hydrides are powerful reducing agents and are widely used in synthetic chemistry, but are generally either non-volatile or insufficiently thermally stable for ALD. The most common Al hydride,  $\text{LiAlH}_4$ , is not volatile, but  $\text{AlH}_3(\text{NMe}_3)$  is highly volatile and is a precursor to Al metal films by CVD at temperatures as low as 100 °C.<sup>104</sup> Furthermore,  $\text{AlH}_3(\text{NMe}_3)$  has been used with  $\text{TiCl}_4$  to deposit Ti-Al alloy films by CVD at 60-127 °C.<sup>156</sup> In this process,  $\text{TiCl}_4$  is reduced by  $\text{AlH}_3(\text{NMe}_3)$ , which produces volatile  $\text{AlCl}_3$  as a by-product.  $\text{AlH}_3(\text{NMe}_3)$  has low thermal stability and decomposes at  $\geq 60$  °C to Al metal, so Ti-Al films are produced. The reducing power of Al hydrides for metal film growth was thus demonstrated. The aim of this project was to prepare Al hydride complexes with improved thermal stability that should be powerful reducing agents for ALD film growth.

## 2.2 Results and Discussion

Careful ligand design is the primary tool for preparing stabilized main group hydrides.<sup>136,137,157</sup> Volatile *dimeric* Al dihydride complexes coordinated by simple amido-amine ligands of the formula  $(\text{RN})\text{CH}_2\text{CH}_2(\text{NMe}_2)$  ( $\text{R} = \text{Me}, \text{Et}$ ) have been reported.<sup>142,143</sup> These dimeric Al dihydride complexes serve as CVD precursors to Al metal films at temperatures as low as 70 °C and are thus insufficiently thermally stable for ALD.<sup>144</sup> A *tert*-butyl-substituted amido-amine ligand was envisioned that could produce *monomeric* Al dihydride complexes with high thermal stability based on (1) the chelate effect, (2) a saturated carbon backbone, thereby preventing reduction of the ligand by Al-H, and (3) the steric bulk and strong electron donating

ability of the *tert*-butylamido group (Scheme 1). Complex **1** was synthesized in 71% yield from 1-(*tert*-butylamino)-2-dimethylaminoethane and  $\text{AlH}_3(\text{OEt}_2)_x$  and was found to exhibit high volatility and good thermal stability. Complex **1** is a low melting (Mp 31-32 °C) colorless crystalline solid, and is extremely air and moisture sensitive, but not pyrophoric. Solution molecular weight measurements support a monomeric structure in benzene and thermogravimetric analysis (TGA) revealed that **1** sublimes without decomposition through a quantitative, single-step weight loss event (Figure 9). The vapor pressure of **1** is ~0.75 Torr at 70 °C.

Scheme 1. Design and synthesis of the thermally stable Al hydride complex **1**.



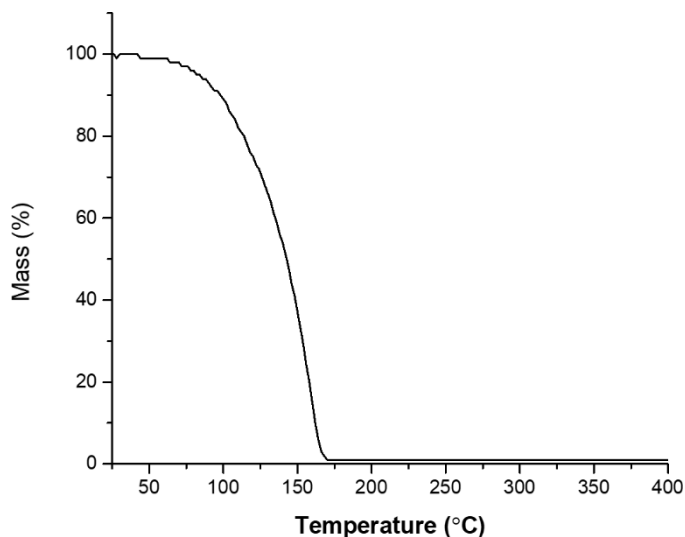
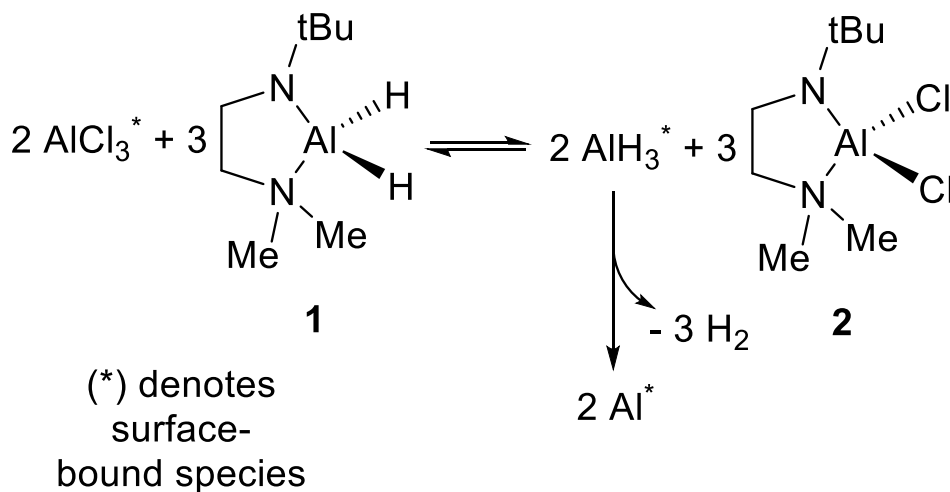


Figure 9. TGA curve of **1**.

Since metal chlorides are widely used ALD precursors, the reaction between **1** and  $\text{AlCl}_3$  was considered as a starting point in initial studies of **1**. The hydride-halide ligand exchange reaction between two Al centers could produce surface-bound Al-H species, which would quickly decompose to Al and  $\text{H}_2$ ,<sup>5</sup> along with the dichloride analogue of **1** as a reaction product (Scheme 2). Dichloride complex **2** was synthesized by treatment of  $\text{AlCl}_3$  with  $\text{Li}[1-(\textit{tert}$ -butylamino)-2-dimethylaminoethane] in toluene and sublimes at 100 °C, 50 mTorr and decomposes above 280 °C. Since the decomposition of surface  $\text{AlH}_3$  to Al metal and  $\text{H}_2$  is irreversible at the growth temperatures, the equilibrium in Scheme 2 should be shifted to the right.

Scheme 2. Proposed reaction between  $\text{AlCl}_3$  and **1** leading to Al metal film growth with formation of  $\text{H}_2$  and **2** as by-products.



Encouraged by the promising physical properties of **1** and **2**, ALD film growth trials were undertaken using  $\text{AlCl}_3$  and **1**. Several different substrates were tested including Si,  $\text{SiO}_2$ , Pt, Cu, and TiN. Although deposition occurred on all substrates, bright silver-colored reflective films grew on Cu and TiN substrates. These films quickly became less reflective upon air exposure (< 2 min), consistent with surface oxidation. Similarly, Al metal CVD displays selectivity for metallic surfaces over dielectrics and good growth of Al films on Cu and TiN is well documented.<sup>11,105,155</sup> TiN was chosen for this ALD study for its larger resistivity difference versus Al. Pretreatment with  $\text{TiCl}_4$  vapor is reported to enhance nucleation of CVD Al on dielectrics.<sup>11</sup> For the ALD Al metal study herein, however,  $\text{TiCl}_4$  pretreatment did not significantly affect growth on Si and  $\text{SiO}_2$  substrates and also retarded growth and increased Al metal film resistivities on Cu and TiN.

In an ALD process, excess precursor should not contribute to the growth rate once sufficient precursor has been dosed to react with all surface sites.<sup>1,6,7,24</sup> At 140 °C, the pulse lengths of both precursors were varied to determine if the observed Al metal film growth

proceeds through a self-limiting ALD mechanism and to rule out CVD-type growth (Figure 10). Purge lengths were 20 s and 10 s following the  $\text{AlCl}_3$  and **1** pulses, respectively. The growth rate of Al saturates at  $3.5 \text{ \AA}/\text{cycle}$  for pulse lengths  $\geq 1.0 \text{ s}$  for both **1** and  $\text{AlCl}_3$  as measured after 200 cycles. No deposition was observed in the absence of  $\text{AlCl}_3$ , even after 250 5 s pulses of **1** at  $400 \text{ }^\circ\text{C}$ . These results provide strong evidence that this process proceeds by a highly controlled, self-limiting ALD growth mechanism. The growth rate for this process of  $3.5 \text{ \AA}/\text{cycle}$  is higher than most other ALD processes but is not without precedent. For instance, ALD of W metal films from  $\text{WF}_6$  achieves growth rates between  $2.5\text{-}6.7 \text{ \AA}/\text{cycle}$ , depending on the reducing agent.<sup>36,40,158</sup> The high growth rates might arise from adsorption of more than one monolayer of  $\text{AlCl}_3$ . As a comparison, the PEALD Al metal process employing  $\text{AlMe}_3$  and  $\text{H}_2$  plasma afforded a growth rate of  $1.5 \text{ \AA}/\text{cycle}$  at a substrate temperature of  $250 \text{ }^\circ\text{C}$ .<sup>114,115</sup> All films were exposed to air prior to analysis, and it is possible that surface oxidation may affect the measured film thicknesses. Quantification of the surface oxide thicknesses after exposure to air and the error this might introduce into thickness measurements was complicated by the high surface roughnesses of the films.

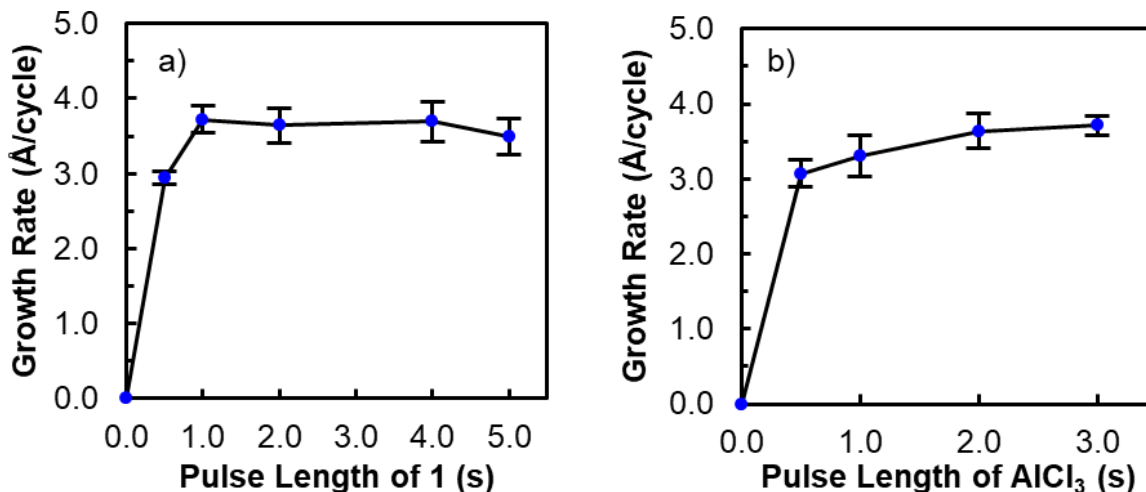


Figure 10. Growth rate versus precursor pulse length after 200 cycles at 140 °C for (a) **1** and (b) AlCl<sub>3</sub>.

The effect of temperature on growth rate and film properties was investigated next (Figure 11a). Mirror-like, low resistivity Al films were deposited at temperatures of  $\leq 140$  °C after 200 cycles. Growth rates increased slightly from 3.5 Å/cycle at 140 °C to 4.1 Å/cycle at 100 °C. Film growth at 160 and 180 °C was characterized by higher surface roughness and resistivity resulting from increased agglomeration of Al particles. Growth rate decreased at 180 °C, which is likely related to the thermal decomposition of **1**. The most conductive films were deposited at 100 °C (83 nm thick) and 120 °C (77 nm thick) after 200 cycles and had calculated bulk resistivities of 3.43 and 3.03  $\mu\Omega\cdot\text{cm}$ , respectively. These resistivity values are only 29 and 14% higher than the resistivity of bulk Al metal (2.65  $\mu\Omega\cdot\text{cm}^{94}$ ), demonstrating that this process can produce high quality Al metal thin films. The resistivities of the previously reported PEALD Al films deposited at 250 °C (100 nm thick) from AlMe<sub>3</sub> and H<sub>2</sub> plasma were  $\sim 10$   $\mu\Omega\cdot\text{cm}^{114,115}$ . Film thickness increased linearly with the number of cycles (Figure 11b). The slope of the trendline (3.47 Å/cycle) matches the saturative growth rate at 140 °C. Films deposited using  $\geq 200$  cycles were electrically continuous with very low sheet resistivity values (0.73-1.02  $\Omega/\text{sq.}$ )

and correspondingly low bulk resistivities ( $5.31\text{-}18.27\ \mu\Omega\cdot\text{cm}$ ). Higher resistivities at higher numbers of cycles may be the result of increased O incorporation due to the longer deposition time or increased surface roughness.

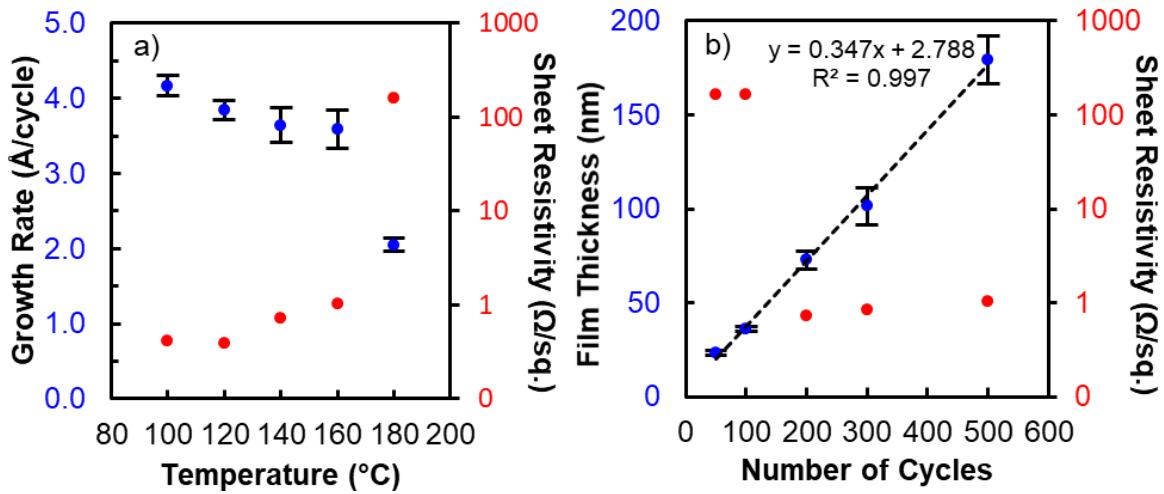


Figure 11. (a) Growth rate and sheet resistivity versus temperature after 200 cycles. (b) Film thickness and sheet resistivity versus number of cycles at  $140\ ^{\circ}\text{C}$ .

Depositions using  $\leq 100$  cycles produced non-conductive discontinuous particles (Figure 12). After 200 cycles, the Al islands coalesced to form a continuous or nearly continuous film (Figure 12).

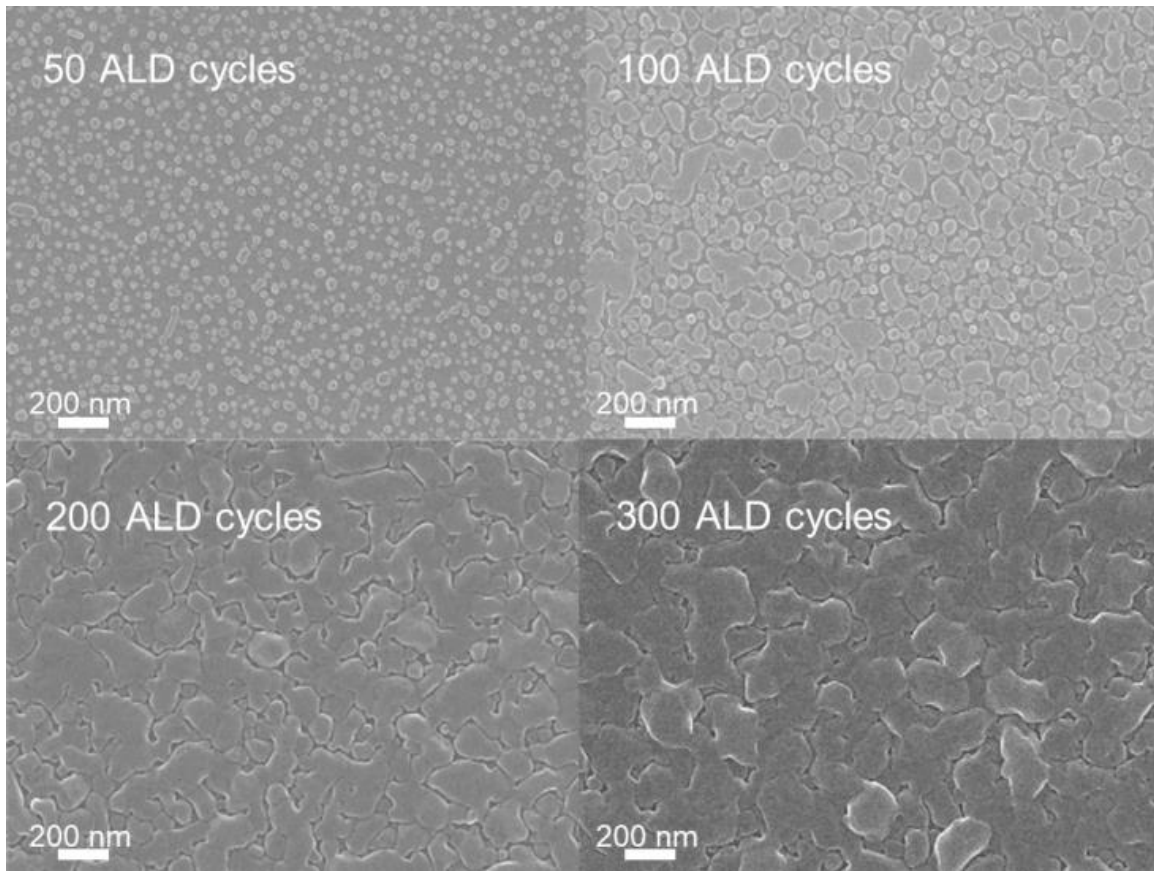


Figure 12. Plane-view scanning electron microscopy images after different numbers of cycles at 140 °C on TiN.

Rms surface roughness was determined by atomic force microscopy to be 17.1 and 19.0 nm for films deposited at 140 °C after 200 (73 nm thick) and 300 (102 nm thick) cycles, respectively (Figure 13). CVD Al metal films often have similar high surface roughnesses.<sup>101,139,159,160</sup> Importantly, the Al films have a smooth, mirror-like appearance immediately upon removal from the reactor, but the films rapidly turn less reflective due to oxidation. Accordingly, some of the surface roughness may arise from surface oxidation.



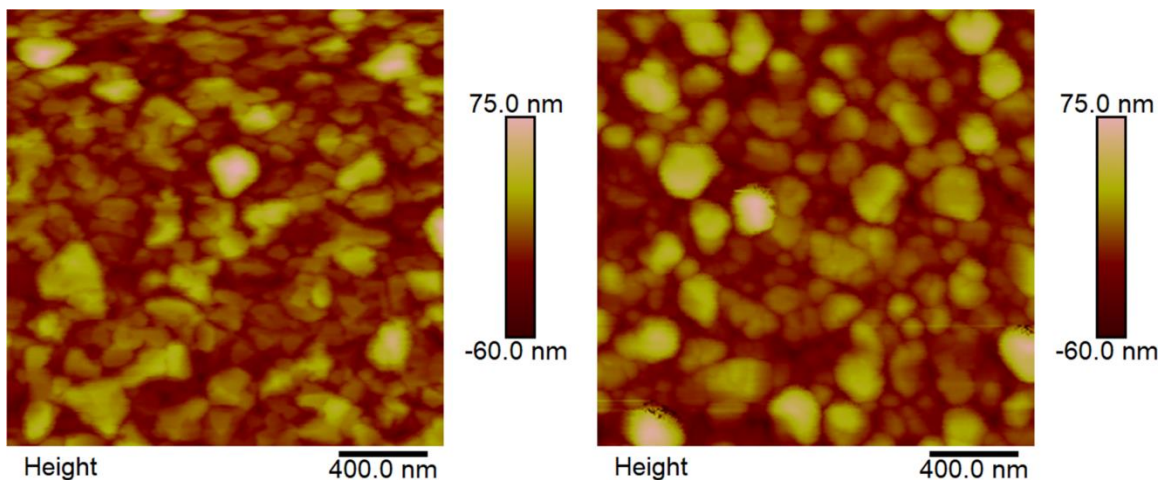


Figure 13. AFM micrographs. (Left) 72.8 nm thick Al film deposited after 200 cycles at 140 °C, Rms roughness = 17.1 nm. (Right) 101.5 nm thick Al film deposited after 300 cycles at 140 °C, Rms roughness = 19.0 nm.

A recent study of initial island growth in low-temperature Cu metal ALD processes examined several contributing factors to the island-type growth mode including temperature, substrate, and number of cycles.<sup>80</sup> The most influential factor in obtaining smooth, continuous metal films at reduced thicknesses is the substrate material. Herein, the substrate was TiN with native oxide. Oxide-free TiN or a different substrate material that forms a strong interface with Al metal might enable smoother films at reduced thicknesses. H<sub>2</sub> plasma-treated TiN has also been shown to improve nucleation of Al CVD.<sup>159</sup>

Figure 14 shows grazing incidence X-ray diffraction (GIXRD) patterns for films deposited after 200 cycles at 100, 120, and 140 °C. The observed reflections exactly match the reference pattern for Al metal. The intensities of the (111) and (200) reflections increase with decreasing growth temperature and the larger crystallite size is likely related to the lower resistivities observed at lower temperatures.

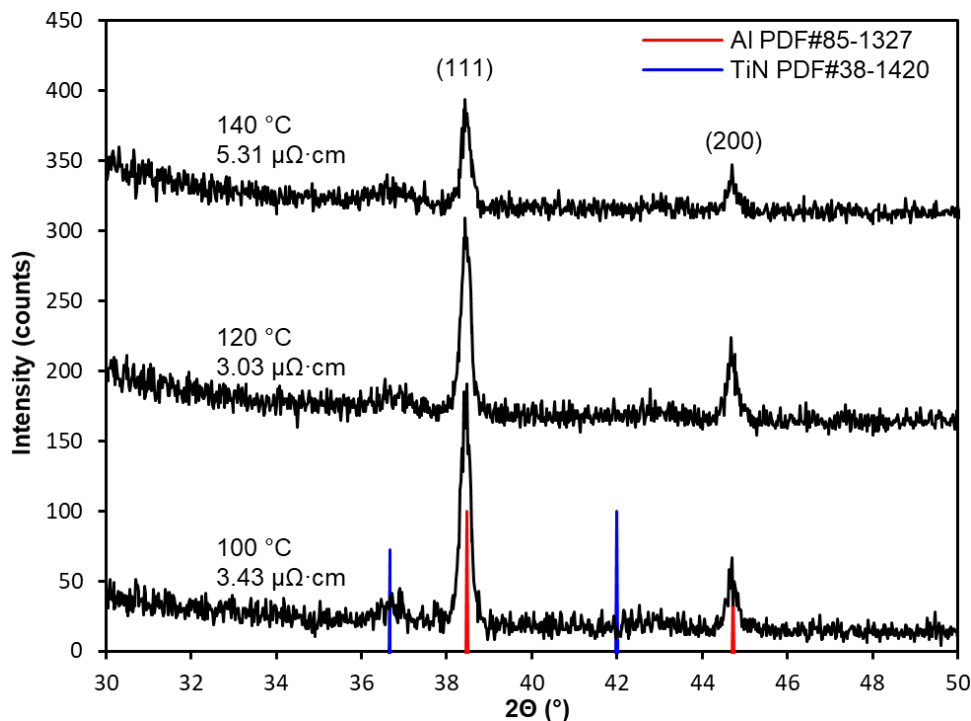


Figure 14. GIXRD patterns after 200 cycles at different temperatures on TiN.

Compositions were measured by X-ray photoelectron spectroscopy (XPS) on films deposited at 100 (120 nm thick) and 140 °C (104 nm thick) after 300 cycles. The films were exposed to air before analysis, so Ar ion sputtering was used to remove the oxidized surface layers. Nevertheless, ionizations corresponding to Al metal were observed prior to any Ar ion sputtering. Figure 15 shows the depth profile, the XPS survey scan, and high-resolution Al 2p region scan for the film deposited at 100 °C after sputtering. The film is high purity Al (> 94 at%) with C and Cl impurities below the detection limit (< 1 and 0.5 at%, respectively). Similar results were observed for the film grown at 140 °C. The major impurity is O due to air exposure, although some O may incorporate during the growth process from the carrier gas or reactor chamber. N is present in 1-2 at% and could be incorporated from the amido-amine ligand in **1**, although C was not detected in the films. The N may also arise from the TiN substrate. In the

reported PEALD process using  $\text{AlMe}_3$  and  $\text{H}_2$  plasma, C impurities were significant at 3 at%.<sup>32,33</sup>

The ionization in the Al 2p region at 72.9 eV exactly matches that of Al metal when calibrated to the surface adventitious C peak of Al native oxide (286.3 eV).<sup>161</sup>

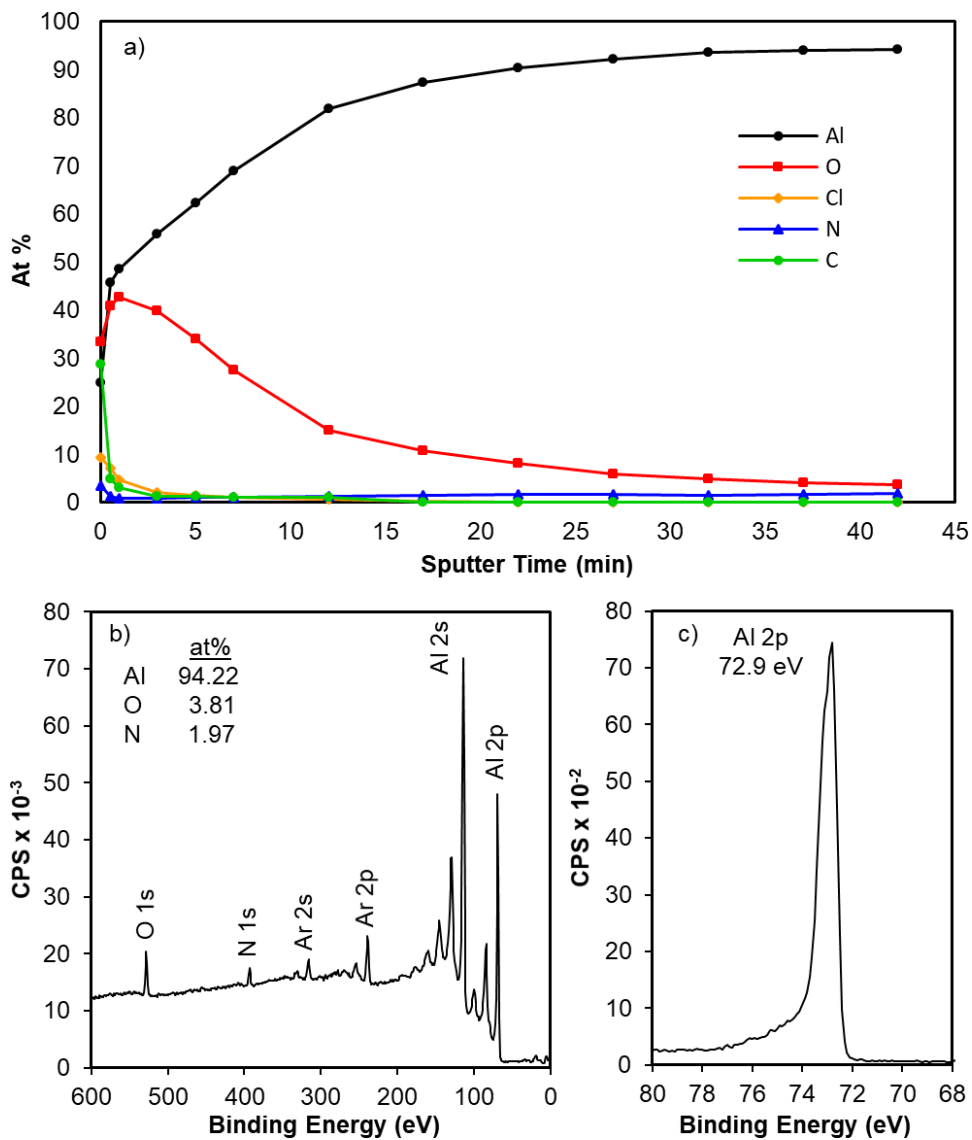


Figure 15. (a) XPS depth profile, (b) survey scan, and (c) high-resolution Al 2p core level scan of a 120 nm thick film (300 cycles) deposited at 100 °C after Ar ion sputtering.

## 2.3 Conclusions

The first growth of metallic Al films by a thermal ALD process was demonstrated. The challenging reduction of  $\text{Al}^{3+}$  to  $\text{Al}^0$  is enabled by the novel and thermally stable Al hydride reducing agent **1**. High purity Al films with C and Cl impurities below 1 and 0.5 at%, respectively, were deposited at very low temperatures with high growth rates between 3.5-4.1 Å/cycle. Film resistivities were as low as  $3.03 \mu\Omega\cdot\text{cm}$ , which is close to the bulk resistivity of Al metal. Similar depositions with **1** and the more common precursor  $\text{AlMe}_3$  did not afford films after 500 cycles at 80 or 150 °C. A possible explanation is that the presumed reaction product, dimethylaluminum hydride ( $\text{Me}_2\text{AlH}$ ), is volatile and stable at these low temperatures.<sup>28</sup> The ability to deposit ALD Al films should enable new applications in many fields such as reflective coatings, plasmonics, microelectronics, hydrogen storage, and energetic materials. The strongly reducing nature of **1** may allow ALD growth of other metal and element films whose ions have electrochemical potentials that are more positive than that of the  $\text{Al}^{3+}$  ion.

## 2.4 Experimental Section

Synthetic manipulations were performed using standard air-free Schlenk line and glovebox techniques. Solvents were dried over purple sodium benzophenone ketyl (diethyl ether) or sodium (toluene) and distilled under Ar atmosphere. Reagents were purchased from Sigma-Aldrich and used as received except  $\text{AlCl}_3$  which was purified by sublimation.  $^1\text{H}$  and  $^{13}\text{C}$  NMR spectra were collected on Agilent MR-400 or DD2-600 MHz spectrometers and referenced to  $\text{C}_6\text{D}_6$  solvent peaks ( $^1\text{H}$ : 7.16 ppm,  $^{13}\text{C}$ : 128.39 ppm). Infrared spectra were measured on a Shimadzu IRTracer-100 spectrometer. Melting points were measured using a Thermo Scientific Mel-temp 3.0 and are uncorrected. Cryoscopic molecular weight measurements were made in benzene using a vacuum-jacketed Schlenk flask that was cooled in liquid nitrogen; temperature

was measured using a Keithley 197A microvoltmeter, an Omega SMCJ-K resistance to voltage converter, and a type K thermocouple. Thermogravimetric analysis (TGA) was performed inside a dry nitrogen-filled glovebox using a Netzsch TG 209F1 Libra thermobalance with a heating rate of 5 °C/min.

Thin film depositions were performed using a Picosun R200 ALD reactor operating at 6-10 torr and equipped with two Picosolid boosters (low vapor pressure precursor delivery systems). Ultrahigh purity N<sub>2</sub> (99.999%, Airgas) which was further purified using an in-line gas purifier (SAES, <100 ppt H<sub>2</sub>O, O<sub>2</sub>) was used as the carrier gas. The reactor used in this study is not equipped with a load-lock, therefore to reduce oxygen and moisture contamination as much as possible, the substrates were loaded and the chamber was then evacuated and heated to the deposition temperature for a minimum of 1-2 h before the deposition was started. Care was also taken to minimize the amount of time the chamber was open to atmosphere. The delivery temperatures of **1** and AlCl<sub>3</sub> were 55 and 95 °C, respectively. Films were deposited on various substrates: Cu (30 nm)/SiO<sub>2</sub> (100 nm)/Si, PVD TiN (10 nm)/SiO<sub>2</sub> (100 nm)/Si, Pt (10 nm)/SiO<sub>2</sub> (100 nm)/Si, Si(100) cleaned by the standard RCA method (Si-OH), and hydrogen-terminated Si(100) (Si-H, 1 % HF solution, 60 s). Substrates were rinsed with isopropanol and dried with a stream of N<sub>2</sub> before loading into the reactor chamber. Film thickness was measured using cross-sectional SEM imaging at a minimum of three points across the substrate using a JEOL-7600-FE SEM. The measured Al film thicknesses on TiN substrates were consistent with the 110 nm thickness of the TiN/SiO<sub>2</sub> stacks. XRD patterns were collected in grazing incidence mode (2°) on a Bruker D8 Advance diffractometer using Cu K $\alpha$  radiation. Sheet resistivity was measured within 1 min of air exposure using a Jandel 4-point probe controlled by a Keithley 2400 Sourcemeter and a Keithley 2182A Nanovoltmeter. AFM analysis was obtained using a Bruker

BioScope Catalyst AFM in contact mode with a 2  $\mu\text{m}$  x 2  $\mu\text{m}$  scan size. XPS characterization was performed on a Kratos Axis Ultra XPS system with a base pressure of  $1 \times 10^{-9}$  torr using a monochromated Al K $\alpha$  X-ray source (1486.6 eV). Ar ion sputtering (3.8 kV) was used to remove surface adventitious C and O and for depth profiling. Binding energies were calibrated to the surface adventitious C peak of Al native oxide (286.3 eV).<sup>161</sup>

*Preparation of 1-(tert-butylamino)-2-dimethylaminoethane.* A 250 mL round-bottomed flask was charged with 2-chloro-N,N-dimethylethylamine hydrochloride (25.0 g, 0.175 mol), *tert*-butylamine (115 mL, 1.1 mol, 6.3 equiv.), water (5 mL), and heated to gentle reflux (70 °C oil bath temperature) for 18 h. After cooling to ambient temperature, hexanes and water (40 mL each) were added and the mixture was transferred to a separatory funnel. The aqueous fraction was washed with hexanes (3 x 20 mL) and the combined hexanes fractions were washed with brine, dried over anhydrous MgSO<sub>4</sub>, and evaporated under reduced pressure to yield a clear, colorless oil (10.898 g, 43 %). The spectroscopically pure product was used routinely without further purification, but it can be purified by vacuum distillation at 65 °C, 18 Torr. <sup>1</sup>H NMR (400 MHz, C<sub>6</sub>D<sub>6</sub>)  $\delta$  = 2.56 (t, 2H), 2.34 (t, 2H), 2.06 (s, 6H), 1.06 (s, 9H) <sup>13</sup>C NMR (100 MHz, C<sub>6</sub>D<sub>6</sub>)  $\delta$  = 60.52, 50.00, 45.74, 40.53, 29.61 HR ESI-MS calcd. for C<sub>8</sub>H<sub>20</sub>N<sub>2</sub> [M+H]<sup>+</sup> 145.1705; found 145.1700.

*Preparation of AlH<sub>2</sub>(*t*BuN)CH<sub>2</sub>CH<sub>2</sub>(NMe<sub>2</sub>) (1).* A solution of AlH<sub>3</sub>(OEt<sub>2</sub>)<sub>x</sub><sup>162</sup> was prepared as follows: a 250 mL Schlenk flask was charged with LiAlH<sub>4</sub> (0.854 g, 22.5 mmol), diethyl ether (70 mL), and cooled to 0 °C on an ice bath. A separate 100 mL Schlenk flask was charged with AlCl<sub>3</sub> (1.000 g, 7.5 mmol) and diethyl ether (50 mL). The AlCl<sub>3</sub> solution was cannulated into the LiAlH<sub>4</sub> solution and the resulting cloudy solution was stirred at ambient temperature for 30 min. The AlH<sub>3</sub>(OEt<sub>2</sub>)<sub>x</sub> solution was cooled to -30 °C and a solution of 1-(*tert*-

butylamino)-2-dimethylaminoethane (3.934 g, 27.3 mmol) in diethyl ether (25 mL) was added. The resulting mixture stirred at ambient temperature over 4 h and was then filtered through Celite and evaporated under reduced pressure. When most of the diethyl ether had been evaporated, the flask was cooled on an ice bath to solidify the low-melting product (3.345 g, 71 %). The spectroscopically pure product was used routinely for ALD without further purification, but it can be purified by vacuum sublimation at 40 °C, 50 mTorr. Mp 31-32 °C Thermal Stability (5 °C/min): In an Ar-filled sealed glass capillary, the compound melted and remained a colorless liquid to 185 °C, at which point it began to darken to a grey solid, likely Al metal, and evolve gas bubbles, likely H<sub>2</sub>. <sup>1</sup>H NMR (600 MHz, C<sub>6</sub>D<sub>6</sub>) δ = 4.52 (bs, 2H), 2.73 (t, 2H), 2.15 (t, 2H), 1.83 (s, 6H), 1.35 (s, 9H) <sup>13</sup>C NMR (150 MHz, C<sub>6</sub>D<sub>6</sub>) δ = 61.62, 51.25, 44.83, 41.73, 30.52 IR (ATR)  $\nu/\text{cm}^{-1}$  = 3001, 2961, 2895, 2853, 2812, 1852, 1782, 1728, 1485, 1462, 1429, 1406, 1383, 1352, 1342, 1290, 1238, 1223, 1205, 1184, 1157, 1118, 1101, 1065, 1057, 1014, 1003, 947, 916, 895, 800, 775, 679, 619, 596, 580, 546, 511, 465 Elemental Analysis calcd. for C<sub>8</sub>H<sub>21</sub>AlN<sub>2</sub> C, 55.78; H, 12.29; N, 16.26 found C, 54.39; H, 11.95; N, 16.05. Cryoscopic Molecular Weight Determination calcd. for C<sub>8</sub>H<sub>21</sub>AlN<sub>2</sub> 172.25 found 179.06, degree of association = 1.04.

*Preparation of AlCl<sub>2</sub>(tBuN)CH<sub>2</sub>CH<sub>2</sub>(NMe<sub>2</sub>) (2).* A 100 mL Schlenk flask was charged with 1-(*tert*-butylamino)-2-dimethylaminoethane (500 mg, 3.47 mmol), toluene (10 mL), and cooled to 0 °C on an ice bath. *n*-Butyllithium solution (1.39 mL, 3.47 mmol) was added dropwise and the mixture was allowed to stir on the ice bath for 30 min then the ice bath was removed and the mixture was warmed to ambient temperature over 2 h. A separate 100 mL Schlenk flask was charged with AlCl<sub>3</sub> (463 mg, 3.47 mmol), toluene (20 mL), and cooled to 0 °C on an ice bath. The ligand solution was then cannulated into the AlCl<sub>3</sub> solution and the resulting mixture was stirred at ambient temperature for 4 h before being filtered through Celite and

evaporated under reduced pressure to yield a slightly orange solid. Sublimation of the crude (100 °C, 50 mTorr) yielded colorless needles (451 mg, 53.9 %). Mp 87-89 °C Thermal Stability (5 °C/min): In an Ar-filled sealed glass capillary, the compound melted and remained a colorless liquid until it began to turn slightly yellow but not obviously decomposed from 250-280 °C. The compound had evaporated out of the heated section of the capillary by 280 °C. <sup>1</sup>H NMR (400 MHz, C<sub>6</sub>D<sub>6</sub>) δ = 2.49 (t, 2H), 1.97 (t, 2H), 1.76 (s, 6 H), 1.27 (s, 9H) <sup>13</sup>C NMR (100 MHz, C<sub>6</sub>D<sub>6</sub>) δ = 60.20, 50.74, 44.92, 39.71, 30.41 IR (ATR) ν/cm<sup>-1</sup> = 3013, 2968, 2957, 2930, 2903, 2886, 2866, 2826, 1489, 1464, 1460, 1447, 1435, 1410, 1385, 1371, 1358, 1344, 1288, 1250, 1236, 1225, 1213, 1188, 1157, 1115, 1065, 1015, 1001, 943, 916, 895, 795, 781, 627, 586, 532, 498, 473 Elemental Analysis calcd. for C<sub>8</sub>H<sub>19</sub>AlCl<sub>2</sub>N<sub>2</sub> C, 39.85; H, 7.94; N, 11.62 found C, 40.22; H, 8.06; N, 11.69.



## CHAPTER 3

### ALUMINUM DIHYDRIDE COMPLEXES AND THEIR UNEXPECTED APPLICATION IN ATOMIC LAYER DEPOSITION OF TITANIUM CARBONITRIDE FILMS

Reprinted (adapted) with permission from Blakeney, K. J.; Martin, P. D.; Winter, C. H. *Dalton Trans.* **2018**, 48, in press, DOI: 10.1039/C8DT02508H. Copyright 2018 The Royal Society of Chemistry.

#### 3.1 Introduction

New chemical approaches are needed to advance the thin film deposition technique known as ALD.<sup>27,28,163–165</sup> ALD is based on surface chemistry and film growth proceeds by sequential, self-limited surface reactions between two or more precursors.<sup>6,7</sup> The self-limited nature of the surface chemistry allows film growth to proceed with a high degree of control over film thickness and composition. Moreover, perfect film conformality in high aspect ratio structures can be achieved. Critical unsolved challenges in ALD include the deposition of many pure elements and industrially important materials. Materials whose thermal ALD growth is currently unknown or limited in scope include electropositive elements such as Ti, Ta, Mn, Zn, Al, Si, Ge, Sn, Mg, and refractory materials such as metal nitrides, carbides, and carbonitrides.<sup>1,24,26</sup>

Early transition metal thin films and their corresponding nitrides, carbides, and carbonitrides have wide-ranging applications in microelectronic devices.<sup>1</sup> As the gate electrode in high-*k*/metal gate (HKMG) transistors, metal nitrides and carbides have advantages over pure metals such as oxidation resistance, chemical inertness, and ease of work function tuning.<sup>69</sup> Carbonitrides have improved physical properties over pure nitride or carbide materials.<sup>67,166</sup> Efforts to deposit these materials by ALD are made especially challenging by a paucity of strong

reducing agents that are sufficiently volatile and thermally stable to be used in ALD. Precursors to incorporate C are also lacking.

Molecular hydrogen is the most commonly investigated reducing agent for thermal ALD, but it exhibits low reactivity toward most electropositive metal precursors at temperatures below 400 °C (Figure 16). Plasma-enhancement (PEALD) can produce atomic hydrogen, which is a very powerful reducing agent and has enabled the ALD of Ti,<sup>21,22</sup> Ta,<sup>23</sup> and many other materials that are difficult to deposit by purely thermal reactions.<sup>20,26</sup> High film conformality is more difficult to achieve with PEALD due to fast recombination of hydrogen atoms on surfaces in high aspect ratio features.<sup>20</sup> Plasma-induced surface damage and particle generation is also problematic. Thus, thermal ALD processes have many advantages if the correct chemistry can be developed.

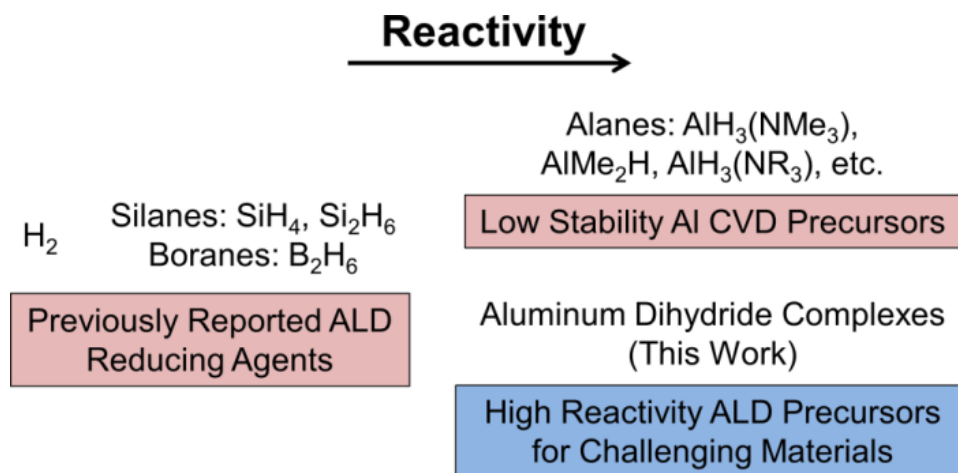


Figure 16. Reducing Agents for ALD.

Silanes and boranes are more reactive hydride donors than molecular hydrogen and have been used in several ALD processes (Figure 16). Mo and W metals can be deposited from the metal hexafluorides and  $Si_2H_6$ ,  $SiH_4$ , or  $B_2H_6$ .<sup>36,41,158</sup> This chemistry does not extend to Ta metal

and TaSi<sub>x</sub> films are produced instead.<sup>42,43</sup> Subsequently, BH<sub>3</sub>(NHMe<sub>2</sub>) has been used to deposit Cu and other first row transition metal films<sup>76,77,167</sup> and has also been evaluated for Ag<sup>168</sup> and Au<sup>169</sup> metal ALD, but film growth in all cases is highly substrate dependent. Thus, there is a great need to develop new volatile reducing agents for ALD of these challenging elements and materials.

Al hydrides are powerful reducing agents due to the highly polarized Al-H bond.<sup>157</sup> LiAlH<sub>4</sub> is widely used in synthetic chemistry but it lacks the volatility and thermal stability required of an ALD precursor. AlH<sub>3</sub>-amine adducts are highly volatile but decompose to Al metal in chemical vapor deposition (CVD) processes at temperatures as low as 60 °C (Figure 16).<sup>104,106,137</sup> There is one report of an AlH<sub>3</sub>-amine adduct as a vapor phase reducing agent in the low temperature CVD growth of TiAl alloy films using TiCl<sub>4</sub> + AlH<sub>3</sub>(NMe<sub>3</sub>).<sup>156</sup> The Ti:Al ratio could be tuned simply according to the precursor feed ratio, with larger AlH<sub>3</sub>(NMe<sub>3</sub>) exposures producing Al-rich films.

A thermally stable Al dihydride complex and its use as a reducing agent in the first thermal ALD growth of Al metal films was presented in Chapter 2.<sup>170</sup> Herein, this chapter reports the synthesis and thermal characterization of several Al dihydride complexes. Their unexpected application in the thermal ALD growth of TiC<sub>x</sub>N<sub>y</sub> films from TiCl<sub>4</sub> is then reported. Ti has a high affinity for C and N which explains the formation of the highly stable carbonitride instead of the pure metal ( $\Delta H(\text{TiN}) = -338 \text{ kJ/mol}$ ,<sup>171</sup>  $\Delta H(\text{TiC}) = -420 \text{ kJ/mol}$ <sup>172</sup>). Although the C and N content originates from the Al dihydride precursor, competitive Al incorporation is not observed even at temperatures as high as 400 °C, producing films with low Al content.

### 3.2 Results and Discussion

*Synthesis and Characterization.* The widely used Al CVD precursor  $\text{AlH}_3(\text{NMe}_3)$  decomposes first by dissociation of  $\text{NMe}_3$ , and then loss of  $\text{H}_2$  to form Al metal.<sup>104</sup> Coordination of an anionic, bidentate ligand to  $\text{AlH}_2^+$  would produce a stabilized Al hydride complex on the basis of ionic versus dative bond strengths as well as the chelate effect. Amido-amine ligands are easily synthesized with a variety of substitution patterns and readily form stable complexes with group 13 metals.<sup>142,143,173</sup> These ligands are non-planar and asymmetric, which is advantageous for producing highly volatile compounds.<sup>174</sup> Although Al dihydride complexes bearing amido-amine ligands have been previously studied, only dimeric complexes have been reported. Beachley first reported complexes of this type with  $\text{R} = \text{Me}$  and  $\text{Et}$  which sublimed at low temperature (50 °C) and discovered their dimeric structures through cryoscopic solution molecular weight measurements (Figure 17).<sup>142</sup> Barron later reported their crystal structures and confirmed their dimeric structures in the solid state.<sup>143</sup> These same complexes were also used as single-source precursors in the CVD growth of Al metal films at temperatures as low as 70 °C.<sup>144</sup> ALD requires high precursor thermal stability and, therefore, these dimeric Al dihydride precursors may not afford self-limited film growth.

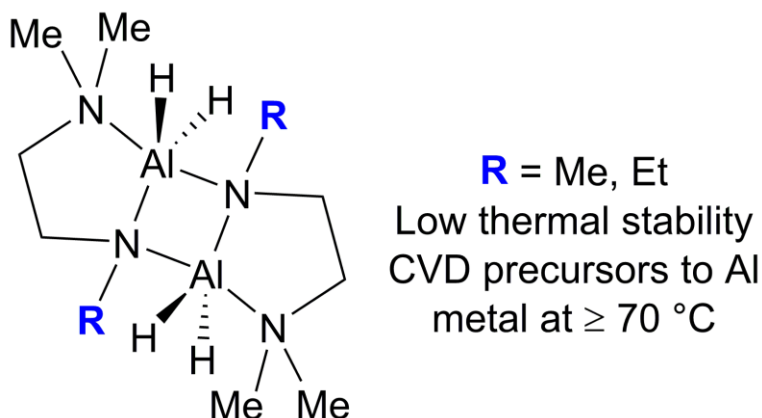
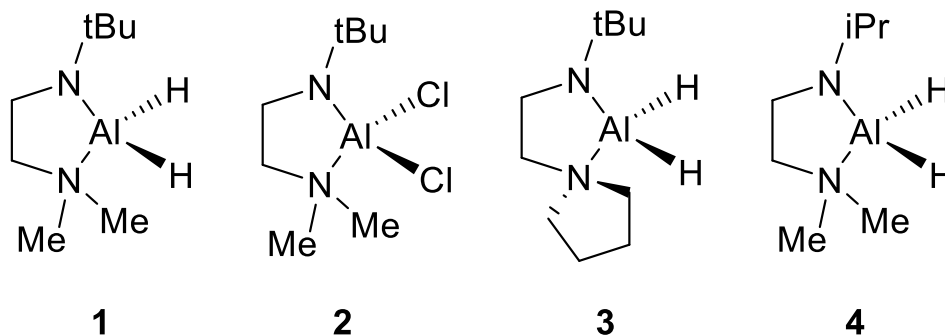


Figure 17. Structure of previously reported dimeric Al dihydride complexes coordinated by a methyl or ethyl-substituted amido-amine ligand.

In Figure 17, the bridging amido R group should largely control the degree of association for these complexes. Therefore, monomeric Al dihydride complexes could be synthesized by employing bulkier *tert*-butyl or isopropyl amido groups. Al dihydride complex **1** and the dichloride complex **2** were synthesized as reported in Chapter 2.<sup>170</sup> Additional Al dihydride complexes  $\text{AlH}_2(\text{tBuNCH}_2\text{CH}_2\text{NC}_4\text{H}_8)$  (**3**),  $\text{AlH}_2(\text{iPrNC}_2\text{H}_4\text{NMe}_2)$  (**4**) were obtained in 56 and 60% yields, respectively, by treatment of a diethyl ether solution of  $\text{AlH}_3$ <sup>162</sup> with the corresponding amido-amine ligand at  $-30$  °C (Table 2). The dihydride complexes **1**, **3**, and **4** were characterized by IR,  $^1\text{H}$ , and  $^{13}\text{C}$  NMR spectroscopy, cryoscopic molecular weight measurements, melting point, and thermogravimetric analysis (TGA) (Table 2). Highly volatile complexes **1** and **3** are noteworthy as they display excellent thermal stability which should, in turn, yield self-limiting ALD film growth.

Table 2. Physical properties of **1-4**.

Complex	Mp (°C)	T <sub>decomposition</sub>	T <sub>sublimation</sub>	Degree of Association
<b>1</b>	31-32	185	40	1.04
<b>2</b>	87-89	> 280	100	*
<b>3</b>	28-29	190	55	1.03
<b>4</b>	70.5-71.4	170	75	1.74

\*Monomeric in solid-state according to X-ray crystal structure

The characteristically broad <sup>1</sup>H NMR Al-H signal was observed near  $\delta$  4.5 for **1**, **3**, and **4**. The remaining <sup>1</sup>H NMR resonances for **1-3** were sharp, but broad signals were observed for **4**, likely from a dynamic process at 23 °C. In the IR spectra, strong Al-H stretches were observed at 1728 (shoulder at 1782) and 1755 (shoulder at 1786) cm<sup>-1</sup> for **1** and **3**, respectively. Complex **4** displayed two equally strong Al-H stretches at 1672 and 1761 cm<sup>-1</sup>. Complexes **1** and **3** are monomeric according to cryoscopic molecular weight measurements in benzene. Complex **4** is mostly dimeric in benzene solution with a degree of association of 1.74. The degree of aggregation and broad NMR peaks of **4** in benzene-*d*<sub>6</sub> suggest a monomer/dimer exchange in solution. A dimeric solid-state structure for **4** would be consistent with the observed higher

melting and sublimation points, relative to **1** and **3**. The isopropyl group in **4** is apparently not sterically bulky enough to produce a monomeric complex.

The X-ray crystal structure of **2** was determined to understand the molecular structure and degree of aggregation (Figure 18). Table 2 gives selected bond lengths and angles for **2**. Complex **2** exists as a monomer with distorted tetrahedral geometry at the Al center. The Al-N distances are 1.792(2) (amido) and 1.966(2) (amine) Å. As expected, the Al-N bond length is much shorter for the amido N atom, compared to the amine N atom. The Cl-Al-Cl angle is 106.26(3)° and the Cl-Al-N angles associated with the dimethylamino N atom are 107.19(5) and 109.98(6)°. These angles are close to those expected for ideal tetrahedral geometry about the Al ion. By contrast, the Cl-Al-N angles associated with the amido N atom are 119.61(7) and 120.40(6)°, which are much larger than the related angles for the dimethylamino N atom. The origin of these larger angles resides with the bulky *tert*-butyl substituent as well as the shorter Al-N<sub>amido</sub> bond length. The large angles clearly delineate the sizeable steric effect of the *tert*-butyl group and provide insight into why **1** and **3** are monomeric.

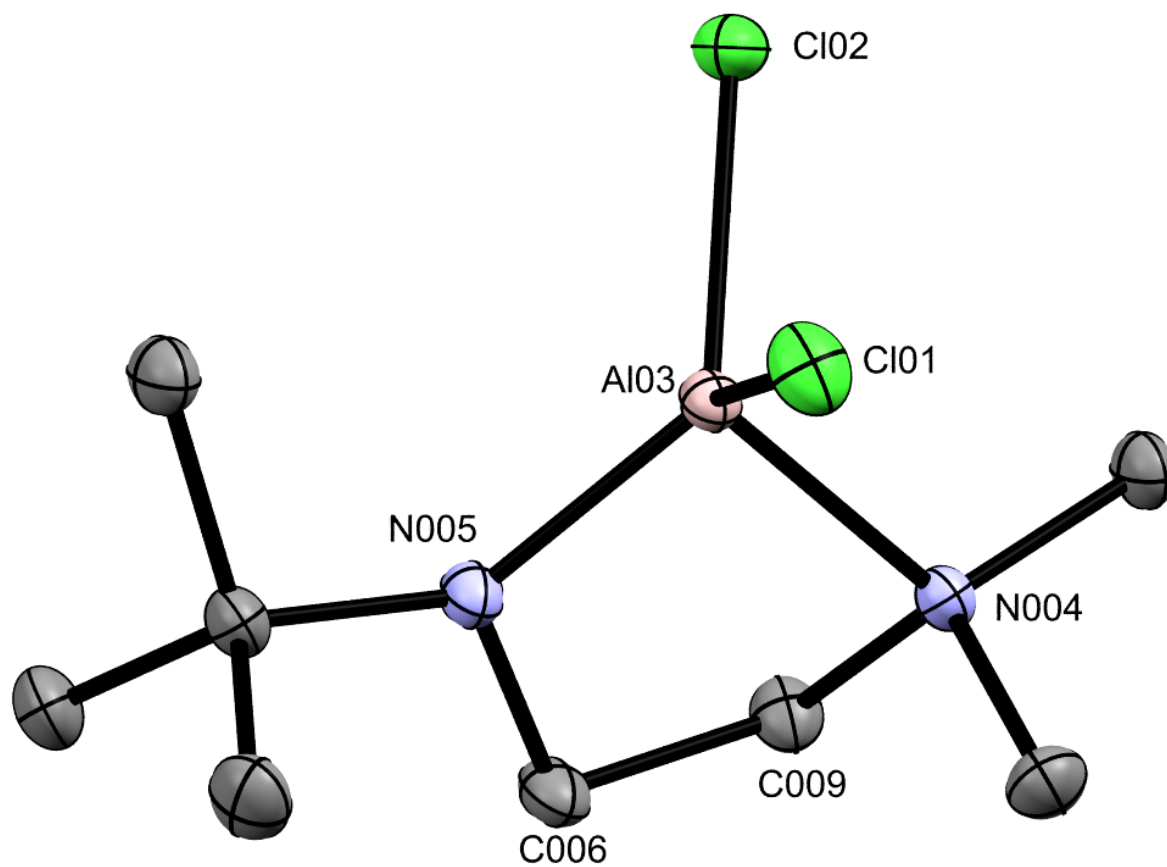


Figure 18. Perspective view of **2** with thermal ellipsoids at the 50% level. Hydrogen atoms are omitted for clarity.

Table 3. Selected bond lengths (Å) and angles (°) for **2**.

Al03-N005	1.792(2)
Al03-N004	1.966(2)
Al03-Cl01	2.1405(7)
Al03-Cl02	2.1430(7)
Cl01-Al03-Cl02	106.26(3)
Cl01-Al03-N004	109.98(6)



Cl01-Al03-N005	120.40(6)
Cl02-Al03-N04	107.19(5)
Cl02-Al03-N005	119.61(7)
N004-Al03-N005	91.43(7)

Complexes **1** and **3** have low melting points and are liquids at their respective ALD process delivery temperatures. Liquid precursors provide a consistent evaporation rate, reduced risk of particle contamination, and are much preferred over solid precursors.<sup>164</sup> Thermal decomposition experiments were conducted where **1-4** melted and remained clear liquids while heated at 5 °C/min in Ar-filled sealed glass capillary tubes until their decomposition points (Table 2). Complexes **1**, **3** and **4** decomposed with gas evolution (likely H<sub>2</sub>) to dark grey solids (likely Al) between 170-190 °C. Dichloride **2** displayed much higher thermal stability and only a slight color change from clear colorless to pale yellow liquid was observed from the melting point (~89 °C) until 280 °C, at which point the liquid had evaporated to the colder end of the capillary. TGA analyses revealed that **1-3** volatilize without decomposition through single-step weight loss events (Figure 19). Complex **4** exhibited very different behaviour and underwent significant decomposition during the TGA experiment. Mass loss began at ~75 °C but only 44 % of the sample mass had evaporated by 400 °C. The poor volatilization of **4** is likely a result of its higher degree of association (1.74) compared to **1** and **3**, as well as the easily eliminated  $\beta$ -hydrogen atom of the isopropyl group. These results likely preclude the use of **4** as an ALD reducing agent, although it may behave similarly to previously reported dimeric amido-amine Al dihydride complexes as CVD precursors to Al metal films.<sup>144</sup>

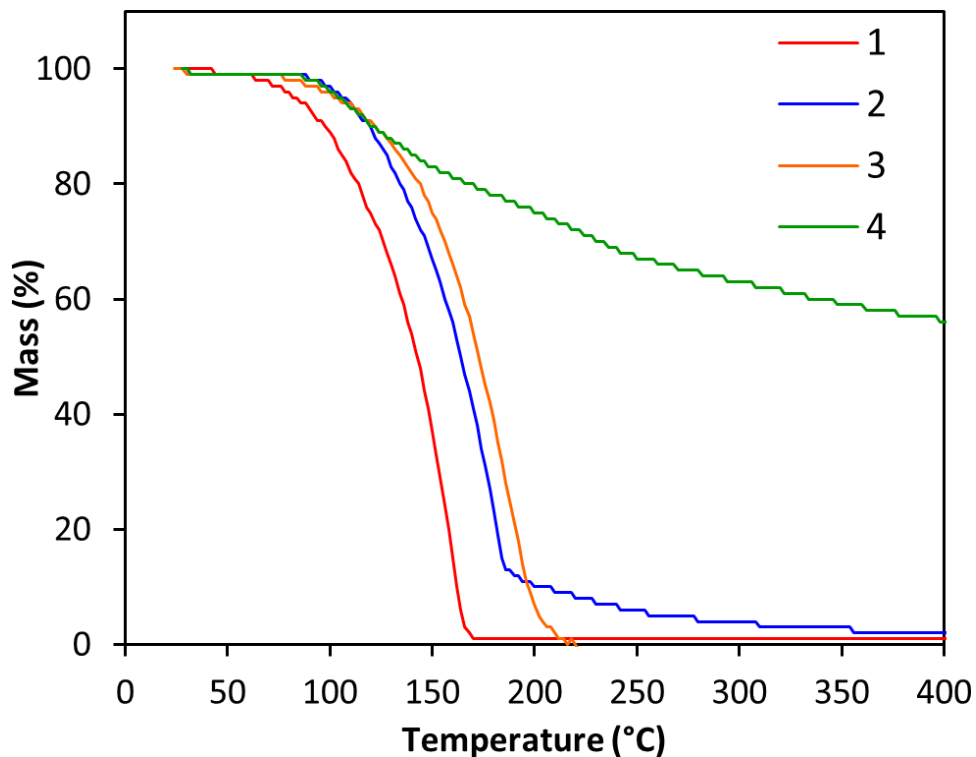


Figure 19. TGA curves for 1-4.

*ALD Film Growth.* ALD growth of thin films was evaluated using **1** and  $\text{TiCl}_4$  on  $\text{SiO}_2$  substrates (100 nm thermal oxide on Si) in a Picosun R-75 ALD reactor equipped with a load-lock and ultra-high purity  $\text{N}_2$  (<100 parts per trillion  $\text{H}_2\text{O}$ ,  $\text{O}_2$ ) as carrier gas. Precursor vapors were pulsed into the deposition chamber sequentially using inert gas valving and separated by 10 s purge periods.  $\text{TiCl}_4$  was chosen as the metal precursor due to its ease of vapor delivery, low cost, high reactivity, and the high interest in Ti-based thin films. Although selective ALD film growth was not investigated in this study,  $\text{TiCl}_4$  is also known to display selective deposition on hydroxyl-terminated versus hydrogen-terminated Si surfaces.<sup>175</sup> This is notable since area-selective ALD has experienced a huge growth in interest recently, largely driven by its ability to reduce device patterning steps.<sup>12</sup>

Depositions at temperatures below 180 °C resulted in very high growth rates (3-6 Å/cycle) and produced poorly conductive films that reacted rapidly with air, becoming moist, changing color, and essentially disintegrating. Significant Cl and Al content was observed by EDS for a film that was exposed to air for ~3 minutes. These observations are consistent with incomplete surface reactions between TiCl<sub>4</sub> and **1**, leading to low density films containing significant Cl, Al, and likely organic impurities. These results contrast with our recent report of ALD Al metal film growth from AlCl<sub>3</sub> and **1** at temperatures below 180 °C.<sup>170</sup> Although the electrochemical potentials of Ti and Al are similar (Ti<sup>2+</sup> ↔ Ti<sup>0</sup>,  $E^\circ = -1.628$  V, Al<sup>3+</sup> ↔ Al<sup>0</sup>,  $E^\circ = -1.676$  V),<sup>94</sup> the film growth results of TiCl<sub>4</sub> and AlCl<sub>3</sub> with **1** are quite different. More details about these differences in surface chemistry would require *in situ* characterization equipment.

Above 180 °C, the growth rates decreased and the films were very conductive and stable in air with little change in sheet resistivity after 24 h. Self-limited growth was demonstrated for TiCl<sub>4</sub> and **1** at 300 °C by investigating growth rate as a function of precursor pulse length. Growth rates were constant at 1.7 Å/cycle after 250 ALD cycles for pulse lengths  $\geq 0.2$  s for TiCl<sub>4</sub> and  $\geq 2.0$  s for **1** (Figure 20). Similar self-limited behavior for TiCl<sub>4</sub> has been observed in this reactor,<sup>87</sup> but the observation of self-limited behavior for **1** came as a surprise since the film growth temperature of 300 °C is well above its solid-state thermal decomposition temperature of 185 °C. Above precursor decomposition temperatures, loss of self-limited growth and increasing growth rate is usually observed. Depositions carried out with TiCl<sub>4</sub> only and no pulse of **1**, and **1** only and no pulse of TiCl<sub>4</sub> gave no film growth at temperatures up to 400 °C.

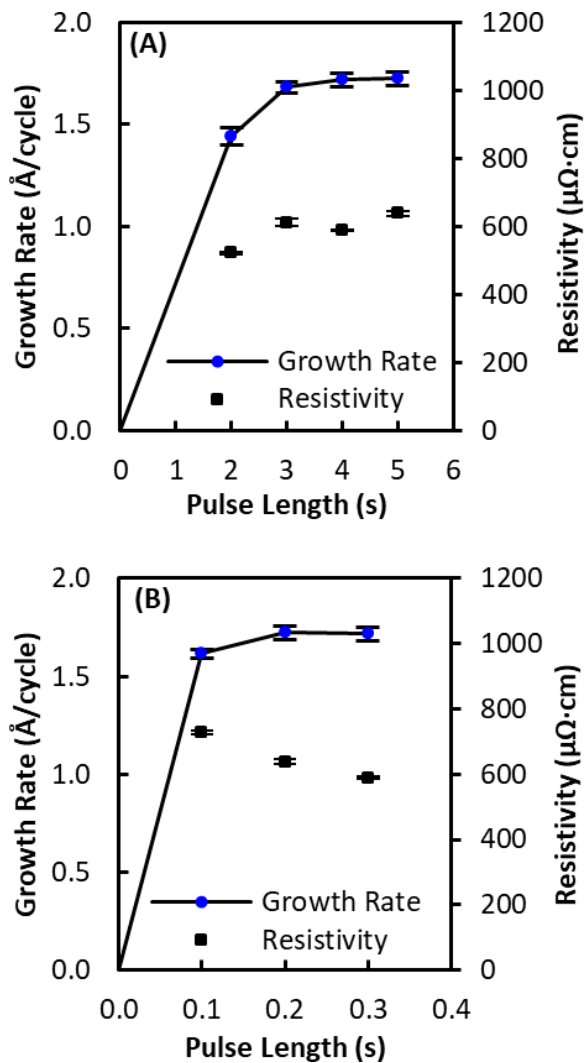


Figure 20. A) Growth rate and bulk resistivity versus pulse length of **1**. B) Growth rate and resistivity versus pulse length of  $\text{TiCl}_4$ .

Using the saturative pulse scheme of 0.2 s  $\text{TiCl}_4$ , 5 s **1**, and 10 s  $\text{N}_2$  purges, growth rate after 250 cycles was evaluated as a function of substrate temperature (Figure 21a). Between 220-400 °C, growth rate was approximately independent of substrate temperature at 1.6-2.0 Å/cycle. Film resistivities were between 600-650  $\mu\Omega\cdot\text{cm}$  across the temperature range 280-400 °C. A plot of film thickness versus number of cycles was linear between 75-375 cycles with a slope of 1.78

Å/cycle (Figure 21b). The y-intercept of -16.577 could indicate a slight nucleation delay before steady-state growth is reached.

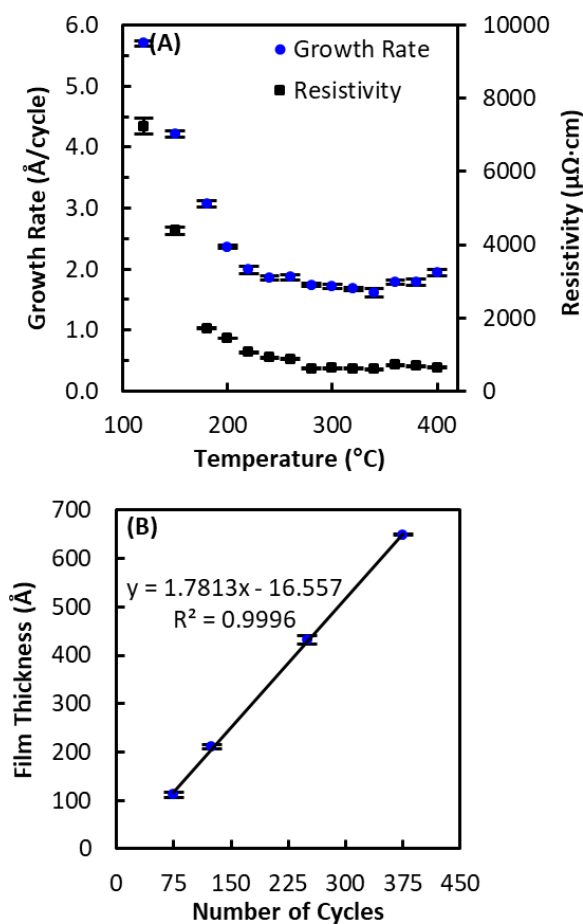


Figure 21. A) Growth rate and resistivity versus temperature. B) Film thickness versus number of cycles.

*Film Characterization.* XPS was used to determine film compositions and Figure 22a shows the survey spectrum of a film deposited at 300 °C after 250 cycles using  $\text{TiCl}_4$  and **1** after Ar ion sputtering to remove adventitious C and O from air exposure. Ti, C, and N are present along with small amounts of O, Cl, and Al. Figure 22b-d show high resolution core level scans of the Ti 2p, N 1s, and C 1s regions with binding energies of 454.9 (Ti), 397.1 (N), and 282.0 eV

(C). An additional C 1s ionization at 284.7 likely corresponds to C-H bonds or amorphous C.<sup>54</sup> TiC<sub>0.5</sub>N<sub>0.5</sub> films deposited by CVD were reported to have Ti, N, and C binding energies of 455.4, 397.2, 282.8 eV, respectively.<sup>68</sup> Binary TiN and TiC films have reported Ti, N, and C binding energies of 455.2, 455.1, 397.4, and 281.6 eV, respectively.<sup>63,176</sup> Accordingly, the ionizations observed for the ALD TiC<sub>x</sub>N<sub>y</sub> films in this study correspond well to previously reported values for the TiN/TiC system.

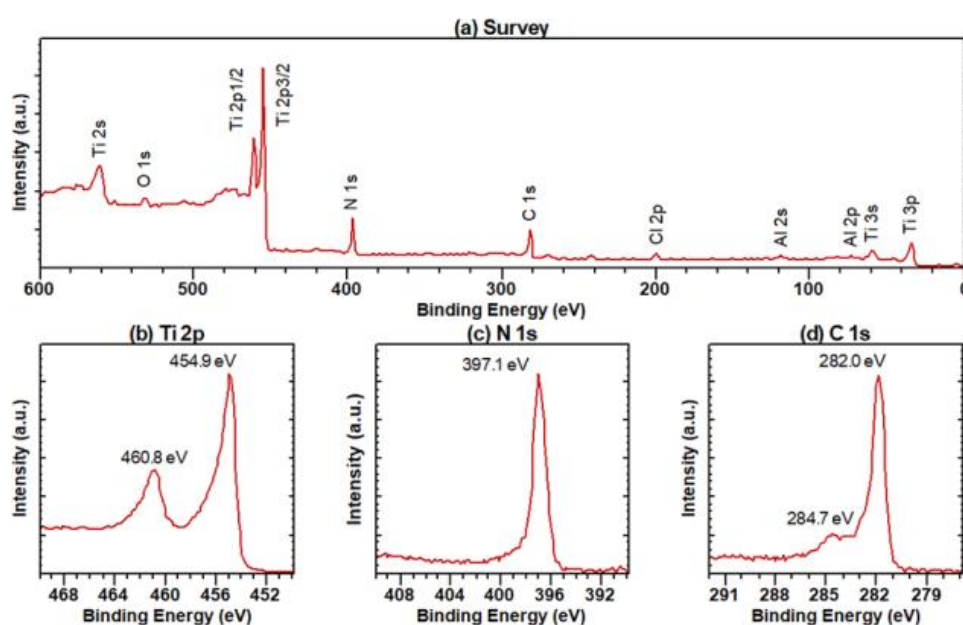


Figure 22. A) XPS survey spectrum after Ar ion sputtering of a film deposited at 300 °C after 250 cycles using TiCl<sub>4</sub> and **1**. High-resolution core level scans of B) Ti 2p, C) N 1s, and D) C 1s regions.

Table 4 summarizes the film compositions obtained using TiCl<sub>4</sub> and **1**. At 300 °C, the film stoichiometry is approximately TiC<sub>0.8</sub>N<sub>0.5</sub>. The observation of C-rich films is either due to preferential sputtering of N, which is documented for TiN,<sup>176</sup> or is a result of the higher C:N ratio of the ligand of **1**. At 400 °C, N content increased slightly and Cl content decreased slightly, but the films deposited at 300 and 400 °C have quite similar compositions. Al content is remarkably

low since this ALD process is operating well above the decomposition point of **1**. Analysis of a film deposited using Ar carrier gas showed a similar composition to the films grown with N<sub>2</sub>, ruling out N incorporation from the carrier gas. The closest related thermal ALD process uses TiCl<sub>4</sub>, AlMe<sub>3</sub>, and NH<sub>3</sub> and produces nitrogen-rich Ti(Al)(C)N films.<sup>61</sup> The C content is lower using this method (6-16 at%) and the use of NH<sub>3</sub> produces corrosive HCl as a by-product and also requires high deposition temperatures (> 350 °C) to minimize NH<sub>4</sub>Cl impurities. Growth rates were also < 0.6 Å/cycle, which are much lower than the present study.

Table 4. Film compositions from XPS using TiCl<sub>4</sub> and **1**.

Temperature	Ti / at%	C / at%	N / at%	Al / at%	Cl / at%	O / at%
<b>300 °C</b>	36.8	30.0	19.9	5.6	4.1	3.7
<b>300 °C (Ar)</b>	34.6	29.4	18.8	7.0	6.0	4.3
<b>400 °C</b>	29.2	31.5	23.4	6.0	2.8	7.1

The structure of the films was found to be polycrystalline TiN/TiC by GIXRD analysis of 40-50 nm films deposited at 280 and 400 °C (Figure 23a). Low intensity, broad reflections were observed corresponding to the 111 and 200 lattice planes of either TiN or TiC. AFM analysis of a 43 nm TiC<sub>x</sub>N<sub>y</sub> film deposited at 300 °C for 250 cycles showed very low roughness (Figure 23b). The Rms surface roughness was 0.558 nm, which corresponds to 1.3 % of the film thickness.

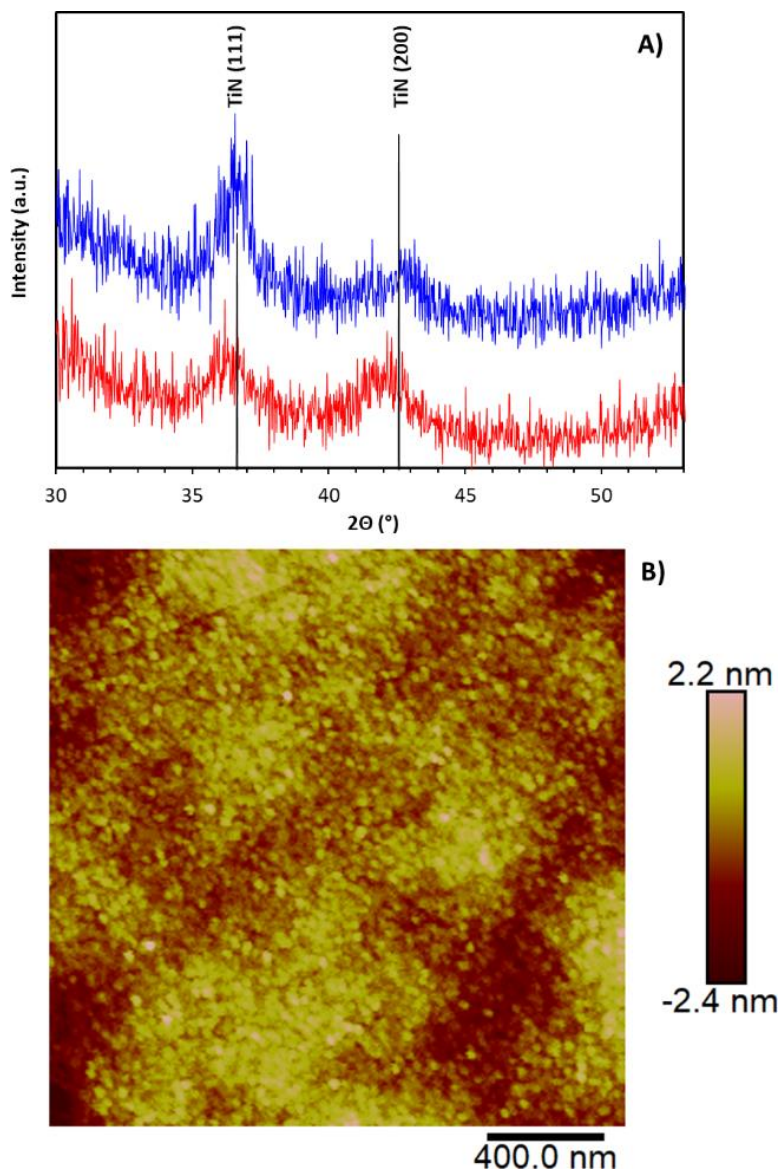


Figure 23. A) GIXRD patterns of TiC<sub>x</sub>N<sub>y</sub> films deposited at 280 °C (red, bottom) and 400 °C (blue, top). B) AFM micrograph of a TiC<sub>x</sub>N<sub>y</sub> film deposited at 300 °C for 250 cycles.

*Film Growth using 3.* Al dihydride complex **3** was also found to deposit films with TiCl<sub>4</sub>. This precursor was designed to have improved resistance toward ligand transfer to TiCl<sub>4</sub>, thereby leading to lower C and N incorporation into the films. The neutral dimethylamino group in **1** forms a weaker bond to Al compared to the ionic *tert*-butylamido bond. Strengthening this dative bond could therefore improve the thermodynamic stability of the complex. Pyrrolidine ( $pK_a =$



11.27) is more basic than dimethylamine ( $pK_a = 10.73$ ), so **2** was synthesized to test the stability prediction. Indeed, **3** was found to be slightly more thermally stable than **1**, as summarized in Table 2. Despite the differences in structure and thermal properties between **1** and **3**, similar film growth results were observed. At 300 °C, **3** produced a growth rate of 1.78 Å/cycle, which is nearly identical to the growth rate obtained using **1** under the same conditions (Figure 24). Film composition according to XPS resulting from **3** at 300 °C was 34.4 at% Ti, 32.8 at% C, 17.0 at% N, 8.3 at% Al, 5.9 at% Cl, 1.6 at% O. The film composition was similar to those obtained with **1**. At 300 °C, films deposited using **1** and **3** had bulk resistivities of 639 and 703  $\mu\Omega\cdot\text{cm}$ , respectively. Accordingly, the film resistivities obtained from **1** and **3** were similar.

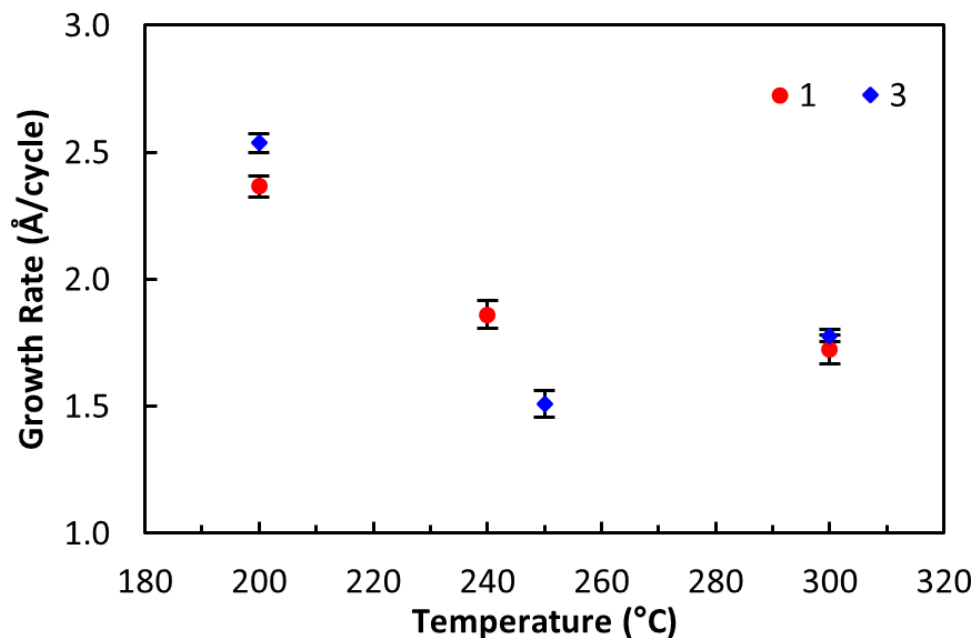


Figure 24. Comparison of growth rates using Al dihydride complexes **1** and **3**.

### 3.3 Conclusions

There are significant chemical challenges in the ALD growth of thin films. Although applications of ALD are increasing in both basic research and industrial products, ALD chemistry for many elements and compounds remains unknown or very limited in scope. Metal hydrides should enable new routes to thin film growth of difficult elements and materials by ALD if these highly reactive compounds can be stabilized and designed to be volatile. Explorations of this new class of ALD precursor have begun by synthesizing volatile and thermally stable Al dihydride complexes coordinated by bulky amido-amine ligands. Monomeric complexes **1** and **3** have excellent ALD precursor properties such as low melting and sublimation points and high thermal decomposition points compared to other common Al hydride thin film precursors such as  $\text{AlH}_3(\text{NMe}_3)$ . In ALD experiments using  $\text{TiCl}_4$ , these two complexes were found to deposit conductive titanium carbonitride films with low Al content and high growth rates (1.5-2.0 Å/cycle). Importantly, self-limited growth was demonstrated using **1** at 300 °C. Titanium has a large negative electrochemical potential and forms highly stable carbide and nitride phases, which renders this metal extremely challenging to deposit as a pure metal film by ALD. Synthetic work toward designing metal hydride complexes with further improved stability may enable atomic-layer growth of important electropositive metals such as Ti, Ta, Mg, Zn, and others.

### 3.4 Experimental Section

*General Information.* All manipulations involving Al hydride compounds were performed using standard Schlenk and glovebox techniques under Ar. Diethyl ether was distilled under Ar from purple sodium benzophenone ketyl. Reagents were purchased from Sigma-Aldrich or Strem Chemical and used as received. Complexes **1** and **2** were synthesized as

reported in Chapter 2.<sup>170</sup> NMR spectra were acquired on Agilent MR-400 or DD2-600 MHz spectrometers and internally referenced to protio impurities ( $C_6D_6$   $\delta = 7.16$  ppm ( $^1H$ )) or solvent carbon atoms ( $C_6D_6$  128.39 ppm ( $^{13}C$ )). Melting point and thermal decomposition experiments were performed in Ar-filled sealed glass capillaries on a Mel-temp 3.0 apparatus. Infrared (IR) spectra were acquired on a Shimadzu IRTracer-100 spectrometer. Solution molecular weight measurements were acquired in benzene using a vacuum-jacketed Schlenk flask cooled with liquid nitrogen. Temperature was measured using a Keithley 197A microvoltmeter, an Omega SMCJ-K resistance to voltage converter, and a type K thermocouple. Thermogravimetric analysis (TGA) was performed with a Netzsch TG 209F1 Libra thermobalance contained in a dry nitrogen-filled glovebox at a 5 °C/min heating rate.

*Synthesis of 1-(tert-butylamino)-2-pyrrolidinoethane.* A 250 mL round-bottomed flask was charged with 1-(2-chloroethyl)pyrrolidine hydrochloride (24.850 g, 0.146 mol), *tert*-butylamine (115 mL, 1.1 mol), and water (5 mL). The resulting mixture was refluxed for 18 h. After cooling to ambient temperature, hexane and water (40 mL each) were added to the flask and the flask contents were transferred to a separatory funnel. The aqueous fraction was washed with hexane (3x20 mL) and the combined hexanes fractions were washed with brine, dried over anhydrous  $MgSO_4$ , and evaporated under reduced pressure to a pale red oil that was purified by vacuum distillation at 100 °C and 18 Torr to yield a colorless oil (14.466 g, 58.1 % yield).  $^1H$  NMR (400 MHz,  $C_6D_6$ )  $\delta = 2.64$ -2.54 (m, 4H), 2.37 (t, 4H), 1.58 (p, 4H), 1.06 (s, 9H).  $^{13}C$  NMR (100 MHz,  $C_6D_6$ )  $\delta = 57.27$ , 54.53, 50.12, 41.77, 29.54, 24.24. HR ESI-MS calcd. for  $C_{10}H_{23}N_2$   $[M+H]^+$  171.1861; found 171.1866.

*Synthesis of 1-(isopropylamino)-2-dimethylaminoethane.* In a similar fashion to 1-(*tert*-butylamino)-2-pyrrolidinoethane, treatment of 2-chloro-*N,N*-dimethylamine hydrochloride

(25.000 g, 0.175 mol) with isopropylamine (94.5 mL, 1.1 mol) afforded a colorless liquid after vacuum distillation at 47 °C, 18 Torr (10.582 g, 46.4 % yield).  $^1\text{H}$  NMR (400 MHz,  $\text{C}_6\text{D}_6$ )  $\delta$  = 2.66 (sept, 1H), 2.56 (t, 2H), 2.29 (t, 2H), 2.04 (s, 6H), 1.00 (d, 6H).  $^{13}\text{C}$  NMR (100 MHz,  $\text{C}_6\text{D}_6$ )  $\delta$  = 60.01, 49.52, 45.79, 45.71, 23.65. HR ESI-MS calcd. for  $\text{C}_7\text{H}_{18}\text{N}_2$   $[\text{M}+\text{H}]^+$  131.1548; found 131.1542.

*Synthesis of  $\text{AlH}_2(\text{tBuNCH}_2\text{CH}_2\text{NC}_4\text{H}_8)$  (3).* A 250 mL Schlenk flask was charged with  $\text{LiAlH}_4$  (0.925 g, 24.37 mmol), diethyl ether (70 mL), and was cooled to 0 °C in an ice bath. A separate 100 mL Schlenk flask was charged with  $\text{AlCl}_3$  (1.083 g, 8.12 mmol) and diethyl ether (50 mL). The  $\text{AlCl}_3$  solution was cannulated into the  $\text{LiAlH}_4$  solution and the resulting cloudy solution was stirred at ambient temperature for 30 min. This solution was then cooled to -30 °C and a solution of 1-(*tert*-butylamino)-2-pyrrolidinoethane (5.531 g, 32.48 mmol) in diethyl ether (25 mL) was added. The resulting mixture stirred at ambient temperature for 4 h and was then filtered through Celite and evaporated under reduced pressure. When most of the diethyl ether had been evaporated, the flask was cooled in an ice water bath to solidify the colorless, low-melting product (3.600 g, 56%). Mp 28-29 °C. Thermal Stability (5 °C/min): In an Ar-filled sealed glass capillary, the compound melted and remained a colorless liquid to 190 °C, at which point it began to darken to a grey solid, likely Al metal, and evolve gas bubbles, likely  $\text{H}_2$ .  $^1\text{H}$  NMR (400 MHz,  $\text{C}_6\text{D}_6$ )  $\delta$  = 4.47 (bs, 2H), 3.08 (m, 2H), 2.82 (t, 2H), 2.43 (t, 2H), 1.66 (m, 4H), 1.37 (s, 9H), 1.22 (m, 2H).  $^{13}\text{C}$  NMR (100 MHz,  $\text{C}_6\text{D}_6$ )  $\delta$  = 59.45, 54.84, 51.52, 42.99, 30.48, 23.23. IR (ATR)  $\nu/\text{cm}^{-1}$  = 2959, 2920, 2876, 2857, 2847, 2795, 2669, 1786, 1755, 1460, 1447, 1382, 1362, 1352, 1340, 1310, 1273, 1248, 1221, 1202, 1121, 1097, 1053, 1036, 1009, 968, 895, 789, 677, 619, 586, 552, 521, 496. Elemental Analysis calcd. for  $\text{C}_{10}\text{H}_{23}\text{AlN}_2$  C, 60.57; H, 11.69;

N, 14.13 found C, 59.12; H, 11.36; N, 13.71. Solution molecular weight calcd. for  $C_{10}H_{23}AlN_2$  198.29 found 205.17, degree of association = 1.03.

*Synthesis of  $AlH_2(iPrN)CH_2CH_2(NMe_2)$  (4).* A 250 mL Schlenk flask was charged with  $LiAlH_4$  (1.200 g, 31.62 mmol), diethyl ether (100 mL), and was cooled to 0 °C in an ice water bath. A separate 100 mL Schlenk flask was charged with  $AlCl_3$  (1.405 g, 10.54 mmol) and diethyl ether (30 mL). The  $AlCl_3$  solution was cannulated into the  $LiAlH_4$  solution and the resulting cloudy solution was stirred at ambient temperature for 30 min. The mixture was cooled to -30 °C and a solution of 1-(isopropylamino)-2-dimethylaminoethane (4.992 g, 38.33 mmol) in diethyl ether (30 mL) was added. The resulting mixture stirred at ambient temperature over 4 h and was then filtered through Celite and evaporated under reduced pressure to afford a white paste. The crude product was recrystallized from diethyl ether at -25 °C overnight, which yielded colorless cubic crystals (3.638 g, 60%). Mp 70.5-71.4 °C. Thermal Stability (5 °C/min): In an Ar-filled sealed glass capillary, the compound melted and remained a colorless liquid to 170 °C, at which point it began to darken to a grey solid, likely Al metal, and evolve gas bubbles, likely  $H_2$ .  $^1H$  NMR (600 MHz,  $C_6D_6$ )  $\delta$  = 4.32 (bs, 2H), 3.43 (bs, 1H), 2.76 (bs, 2H), 2.20 (bs, 2H), 1.92 (bs, 6H), 1.36 (d, 6H).  $^{13}C$  NMR (150 MHz,  $C_6D_6$ )  $\delta$  = 60.02, 50.36, 44.61, 43.55, 24.22. IR (ATR)  $\nu/cm^{-1}$  = 3038, 2988, 2967, 2932, 2889, 2862, 2853, 2833, 2795, 1761, 1672, 1456, 1402, 1393, 1373, 1362, 1354, 1304, 1279, 1248, 1182, 1142, 1113, 1099, 1078, 1057, 1034, 1018, 964, 947, 926, 880, 806, 787, 735, 698, 608, 544, 461, 434, 413. Elemental Analysis calcd. for  $C_7H_{19}AlN_2$  C, 53.14; H, 12.10; N, 17.71 found C, 51.86; H, 11.60; N, 17.07. Solution molecular weight calcd. For  $C_7H_{19}AlN_2$  158.22 found 275.66, degree of association = 1.74.

*ALD Experiments.* Thin films were deposited in a Picosun R75-BE ALD reactor equipped with a load-lock at 6-8 hPa working pressure.  $TiCl_4$  (99.9 %) was delivered from a

vapor-draw ampoule held at ambient temperature. Al dihydride complexes **1** and **3** were delivered using a low vapor pressure precursor delivery system (Picosolid booster) at 60 and 85 °C, respectively. Nitrogen (> 99.999%, Airgas) was used as the carrier gas, and was further purified with an SAES in-line gas purifier. Some experiments used argon as the carrier gas (> 99.9997%, Airgas). Substrates were 1-2 cm<sup>2</sup> coupons of Si with 100 nm of thermally grown SiO<sub>2</sub> that were rinsed with deionized water and isopropanol and blown dry with nitrogen. A JEOL-7600 field emission scanning electron microscope was used to measure film thicknesses. Energy-dispersive X-ray spectra (EDS) was carried out on the scanning electron microscope with an Ametek EDAX system with Genesis Spectrum software. Growth rates were measured by dividing the average film thickness measured at a minimum of three points by the number of cycles. Atomic force microscopy (AFM) was used to measure surface roughness using a Bruker BioScope Catalyst in contact mode with a 2 μm x 2 μm scan size. Grazing incidence X-ray diffraction (GIXRD) patterns were acquired on a Bruker D8 Advance diffractometer using Cu Kα radiation and a 2° incidence angle. Sheet resistivity was measured using a Keithley 2400 sourcemeter, a Keithley 2182A nanovoltmeter, and a Jandel 4-point probe. Film composition was measured by X-ray photoelectron spectroscopy (XPS) with a Kratos Axis Ultra XPS system using a monochromated Al Kα X-ray source (1486.6 eV) at a chamber pressure of ~1x10<sup>-9</sup> Torr. Binding energies were calibrated to the surface C 1s ionization at 284.8 eV. Adventitious C and O was removed by Ar ion sputtering (3.8 kV). CasaXPS software was used for XPS analysis.

## CHAPTER 4

### THERMAL ATOMIC LAYER DEPOSITION OF TUNGSTEN CARBIDE FILMS FROM $WCl_6$ AND $AlMe_3$

Reprinted (adapted) from Blakeney, K. J.; Winter, C. H. *J. Vac. Sci. Technol. A* **2018**, *36*,

01A104, with the permission of the American Vacuum Society

#### 4.1 Introduction

Tungsten carbides ( $W_2C$ , WC; hereafter  $WC_x$ ) are refractory materials with very high hardnesses, melting points, and chemical resistance.<sup>45,94</sup> Thin films of  $WC_x$  have been investigated as diffusion barriers and adhesion layers for Cu interconnects in integrated circuits.<sup>51,177,178</sup>  $WC_x$  thin films are typically grown by physical vapor deposition (PVD) using W metal and methane<sup>177,178</sup> or a WC target,<sup>179–181</sup> or by chemical vapor deposition (CVD) using a variety of molecular tungsten precursors.<sup>49–53</sup> Future applications in microelectronics devices will require precise film thickness control and perfect conformality in high aspect ratio features, in order to meet increasingly strict demands associated with smaller device dimensions.<sup>6,7</sup> Atomic layer deposition (ALD) is a thin film deposition process that enables sub-nanometer control of film thickness and inherently gives perfect conformal coverage of shaped features because of the self-limited growth mechanism.<sup>6,7</sup> There have been limited reports of  $WC_x$  film growth by ALD methods. ALD growth of  $WC_x$  films was achieved at 250 °C using  $W(NtBu)_2(NMe_2)_2$  with a hydrogen plasma,<sup>182</sup> and use of  $W(CO)(EtC\equiv CEt)_3$  with a 10:1  $H_2:N_2$  plasma at 250 °C afforded  $WC_x$  films.<sup>183</sup> However, plasma-based ALD processes can lead to substrate damage from the reactive plasma species and may afford poor conformal coverage in high aspect ratio features because the plasma constituents react with the feature walls before they reach the bottom of the feature.<sup>20</sup> Brief mentions of the thermal ALD of  $WC_x$  films appeared in two recent review articles.<sup>17,24</sup> This approach used  $WF_6$  and  $SiEt_2H_2$  at 150–300 °C.<sup>17,24</sup> There

have been several reports in the patent literature about the ALD growth of early transition metal carbide films using  $\text{AlMe}_3$  as the carbon source.<sup>184</sup> Only recently has this method been studied and disclosed in the scientific literature. An ALD process for tantalum carbide ( $\text{TaC}_x$ ) films was briefly described in a 2007 review article.<sup>17</sup> The  $\text{TaC}_x$  films were produced from  $\text{TaCl}_5$  and  $\text{AlMe}_3$  or  $\text{AlEt}_3$  at 325 °C and afforded resistivities of 1400 and 700  $\mu\Omega\cdot\text{cm}$ , respectively.<sup>17</sup> These low resistivity processes for ALD  $\text{TaC}_x$  are in stark contrast to TaN ALD, which generally produces high resistivity  $\text{Ta}_3\text{N}_5$  films because the reduction of precursors in the Ta(V) oxidation state to the Ta(III) oxidation state in TaN is very difficult.<sup>1</sup> Other reports of metal carbide ALD using  $\text{AlMe}_3$  have included Nb, Hf, and Ti carbides, but significant incorporation of Al in the films was also observed.<sup>65,185,186</sup>

The most commonly used tungsten vapor deposition precursor is  $\text{WF}_6$ , which is a highly reactive gas that hydrolyzes to form toxic HF.<sup>38,40,187-190</sup>  $\text{WF}_6$  is also reactive toward other common semiconductor device materials such as Si, Al, or Ti and can lead to spontaneous etching.<sup>1,188</sup> Tungsten metal films can be deposited by ALD using  $\text{WF}_6$  and  $\text{Si}_2\text{H}_6$ .<sup>7,36,38,40,187</sup> The only reported thermal ALD process for  $\text{WC}_x$  films used  $\text{WF}_6$  and  $\text{H}_2\text{SiEt}_2$ .<sup>17,24</sup> Although saturation behavior was not reported,  $\text{WC}_x$  films were deposited with a growth rate of 0.8-0.9 Å/cycle within an ALD window of 150-300 °C and had resistivities between 400-500  $\mu\Omega\cdot\text{cm}$ .<sup>17,24</sup>  $\text{WN}_x\text{C}_y$  films were deposited by thermal ALD from  $\text{WF}_6$ ,  $\text{NH}_3$ , and  $\text{BEt}_3$  and were found to be excellent barriers to Cu diffusion.<sup>191</sup>

Since  $\text{WF}_6$  is toxic, HF is corrosive, and fluorine impurities may be harmful to device performance, fluorine-free tungsten precursors have recently received attention.<sup>183,192</sup> Tungsten hexachloride ( $\text{WCl}_6$ ) is an obviously fluorine-free, comparatively easy to handle volatile solid.  $\text{WCl}_6$  has not been reported in an ALD process to date, but it has been used in CVD growth of

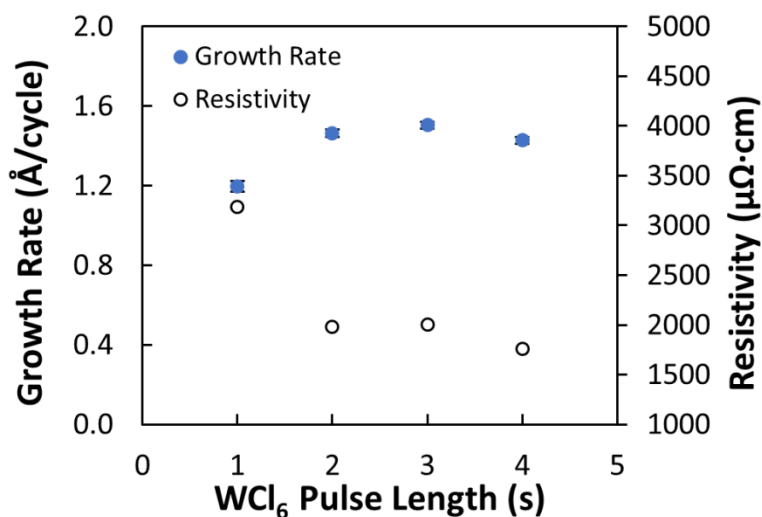


WC<sub>x</sub> films.<sup>50</sup> Herein, this chapter reports the thermal ALD of WC<sub>x</sub> films with low Al and Cl impurities using WCl<sub>6</sub> and AlMe<sub>3</sub>.

## 4.2 Results and Discussion

The ALD process characteristics for WCl<sub>6</sub> and AlMe<sub>3</sub> were evaluated on a variety of substrates including Pt, TiN, TaN, Si(100) with native oxide, and 100 nm thermal SiO<sub>2</sub> substrates. Similar growth rates were observed on all substrates according to cross-sectional SEM images. All film growth results reported herein were conducted on the 100 nm thermal SiO<sub>2</sub> substrates. As shown in Figure 25, self-limited growth was demonstrated for both precursors at 325 °C, where the growth rate was constant at ~1.5 Å/cycle with pulse lengths of ≥ 0.1 s for AlMe<sub>3</sub> and ≥ 2.0 s for WCl<sub>6</sub>, as measured after 500 cycles. The purge length following each precursor pulse was kept at 10 s. Due to the high vapor pressure of AlMe<sub>3</sub>, pulse lengths of ≥ 0.1 s supplied sufficient precursor to afford self-limiting growth. WCl<sub>6</sub> was delivered by solid-state booster at 125 °C, and films deposited using WCl<sub>6</sub> pulses of ≥ 2.0 s were in the self-limited growth regime, as evidenced by their equivalent growth rates and resistivities.

(a)



(b)

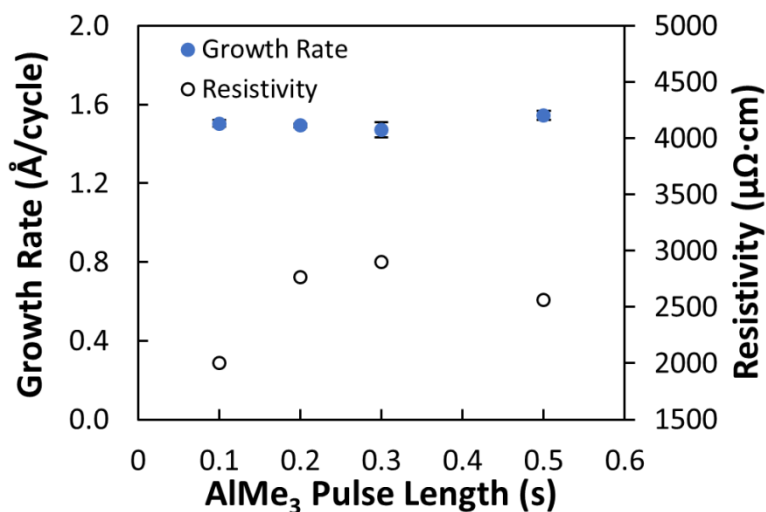


Figure 25. Plots of growth rate versus precursor pulse length of (a)  $\text{WCl}_6$  and (b)  $\text{AlMe}_3$  after 500 cycles at  $325\text{ }^\circ\text{C}$ .

Using these saturative precursor exposures, the growth rate after 500 cycles was approximately independent of substrate temperature between  $275\text{-}350\text{ }^\circ\text{C}$ , as determined by a plot of growth rate versus substrate temperature (Figure 26).  $\text{AlMe}_3$  is reported to decompose thermally at temperatures above  $300\text{ }^\circ\text{C}$ ,<sup>193,194</sup> but this decomposition does not appear to affect the growth rate for this process below  $350\text{ }^\circ\text{C}$ . The growth rate increases outside of the ALD window, which is likely due to increased rate of  $\text{AlMe}_3$  decomposition at higher temperatures and incomplete surface reactions at lower temperatures.

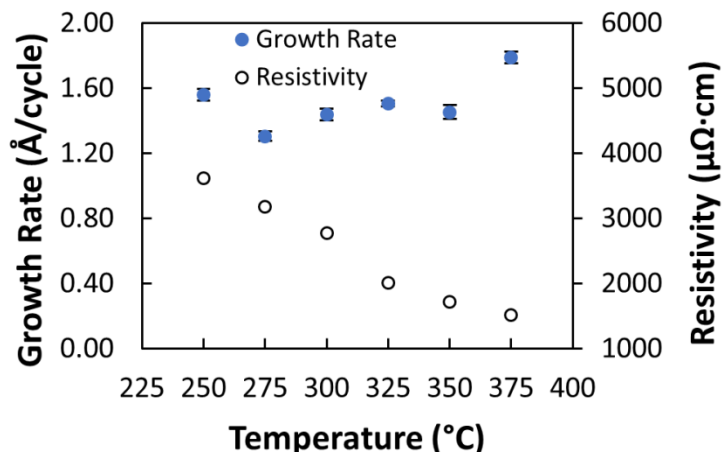
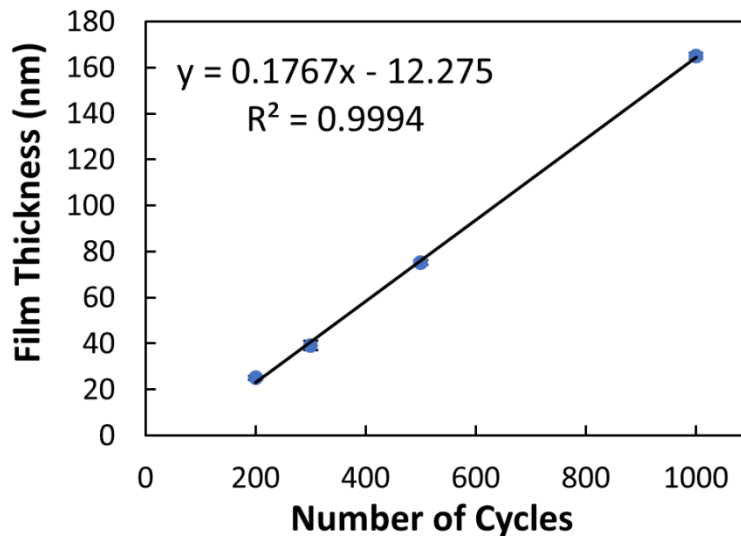


Figure 26. Plot of growth rate versus substrate temperature after 500 cycles using  $WCl_6$  and  $AlMe_3$ .

To investigate the growth behavior after differing numbers of ALD cycles, a plot of film thickness versus number of cycles was generated with a substrate temperature of 325 °C using the previously established pulse sequence (Figure 27a). This plot was linear between 200-1000 cycles with a slope corresponding to a growth rate of 1.77 Å/cycle, which is higher than the measured growth rate after 500 cycles of ~1.5 Å/cycle. An “ideal” ALD process would have x- and y-intercepts at the origin, but in this case they are 69 and -12.275, respectively. These values indicate an apparent nucleation delay at 325 °C on  $SiO_2$  of about 69 cycles. When growth rate is plotted versus number of cycles, it is clear that the growth rate increases with increasing number of cycles and likely plateaus at > 1000 cycles (Figure 27b). Nucleation delays are common features in film growth of metals on dielectric substrates.<sup>18</sup> In a review of ALD process characteristics, Puurunen discussed the variation of growth rate versus number of cycles.<sup>18</sup> For the process herein, this observation is consistent with substrate-inhibited growth, which indicates that the number of surface reactive sites is lower on the substrate than on the growing  $WC_x$  film.

(a)



(b)

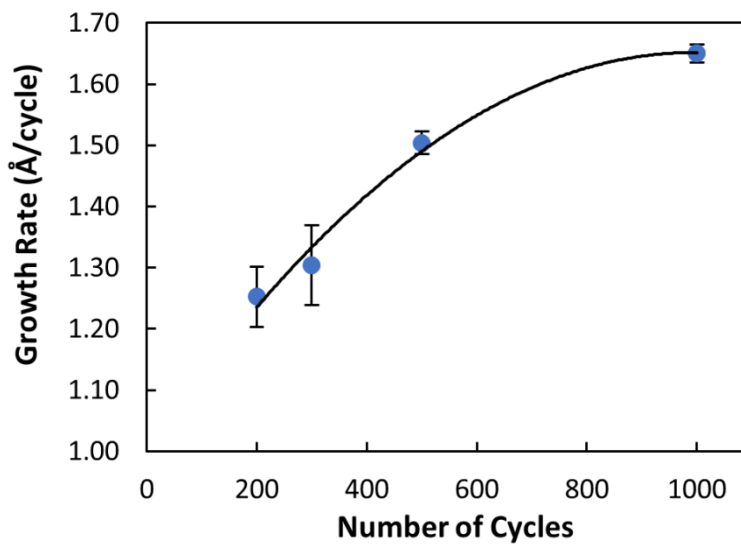


Figure 27. (a) Plot of film thickness versus number of cycles at 325 °C. (b) Plot of growth rate versus number of cycles at 325 °C.

X-ray photoelectron spectroscopy (XPS) was used to determine film composition. Analysis of a film deposited at 300 °C showed approximately 1:1 WC stoichiometry with low levels of O, Al, and Cl impurities after argon ion sputtering to remove adventitious carbon and oxygen (Figure 28a). The XPS data are consistent with a WC stoichiometry, and not  $W_2C$ . The

concentration of Al was below the detection limit, Cl was 1.3 at%, and O was 2.4 at%. The Al concentration increased at 325 and 375 °C to 20.2 and 28.5 at%, respectively. Since  $\text{AlMe}_3$  is reported to decompose thermally above 300 °C,<sup>193,194</sup> the Al incorporation is likely due to  $\text{AlMe}_3$  decomposition and is higher with increasing temperature.  $\text{AlMe}_3$  decomposition is also likely the cause of the higher growth rate at 375 °C. The high-resolution W 4f and Al 2p XP spectra are shown in Figure 28b and c, respectively. The observed W 4f<sub>7/2</sub> binding energy of 31.6 eV and the C 1s binding energy of 283.2 eV agree well with previously reported values for WC<sub>3,12</sub>. Another ionization in the C 1s spectrum at a higher binding energy of 284.2 eV may correspond to C-H species or to amorphous C.<sup>52,63,185</sup> A possible ionization in the Al 2p region is difficult to discern from the noise, but the Al content is certainly less than 1 at. % at 300 °C.

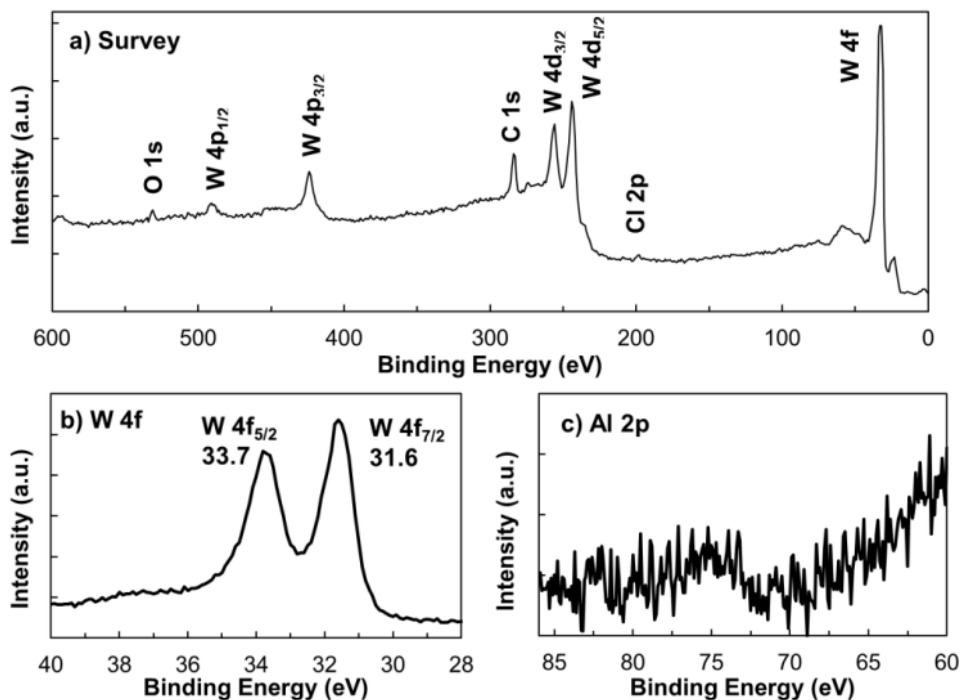


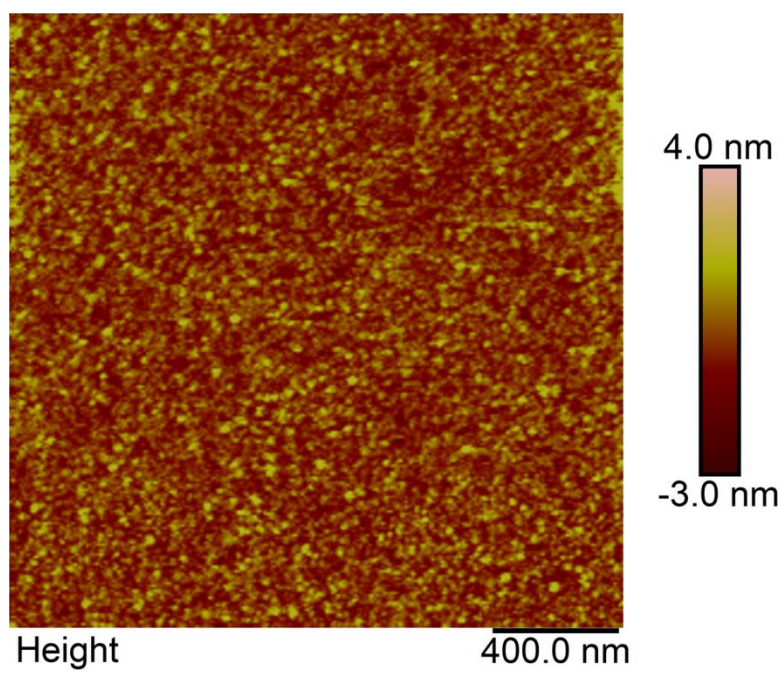
Figure 28. (a) XPS survey scan of a  $\text{WC}_x$  film deposited at 300 °C after Ar ion sputtering to remove adventitious carbon and oxygen. High resolution XPS (b) W 4f and (c) Al 2p core level scans of a  $\text{WC}_x$  film deposited at 300 °C after Ar ion sputtering to remove adventitious carbon and oxygen.

Reports of Hf and Ti carbides deposited using  $\text{AlMe}_3$  had significant Al and Cl incorporation. At 270 °C, films deposited from  $\text{HfCl}_4$  and  $\text{AlMe}_3$  had Al contents between 7.7-12.5% and Cl contents between 10.1-20%.<sup>186</sup> Films deposited between 300-400 °C from  $\text{TiCl}_4$  and  $\text{AlMe}_3$  had Al contents between 5-8% and Cl contents between 3-10%.<sup>65</sup> Al content was not reported for  $\text{NbC}_x$  films deposited from  $\text{NbCl}_5$  and  $\text{AlMe}_3$ , but for films deposited using  $\text{NbF}_5$  and  $\text{AlMe}_3$ , the Al content was between 2-6%.<sup>185</sup> At 300 °C, the F content was ~12% (from  $\text{NbF}_5$ ) and Cl content was ~9% (from  $\text{NbCl}_5$ ).<sup>185</sup> Regardless of the Nb precursor, the films were carbon-rich. At 350 °C, the Nb content was 26-28% and the C content was 61-63% as measured by both XPS and Rutherford backscattering spectrometry.<sup>185</sup>

The structure of the as-deposited  $\text{WC}_x$  films was investigated with grazing incidence X-ray diffraction. No distinct reflections were observed, indicating amorphous material.  $\text{WC}_x$  films deposited from  $\text{WF}_6$  and  $\text{H}_2\text{SiEt}_2$ , the only other reported thermal tungsten carbide ALD process, were reported to be polycrystalline.<sup>17,24</sup> Since diffusion is enhanced along grain boundaries, the amorphous films prepared herein could be superior barrier layers to Cu diffusion.

Film roughness was assessed by atomic force microscopy (AFM). Films with thicknesses of 39 and 51 nm were deposited at 325 and 375 °C, respectively, were very smooth and found to have rms roughness values of 0.651 and 0.851 nm, respectively, which corresponds to 1.7% of the film thickness in both cases (Figure 29). Crystalline films tend to be rougher, so these low roughness values correspond well with the observed amorphous structure of the films.

(a)



(b)

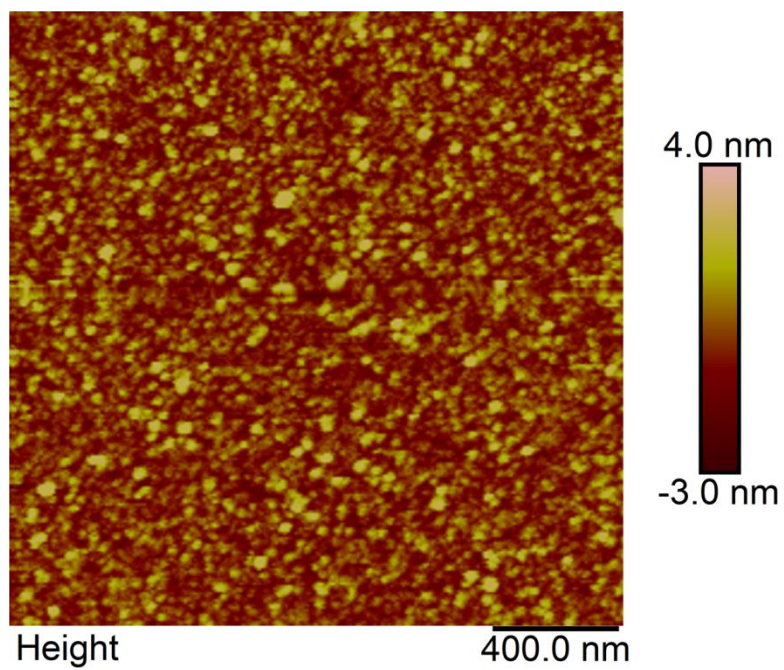


Figure 29. AFM micrographs of films deposited from  $WCl_6$  and  $AlMe_3$  at (a) 300 °C and (b) 375 °C after 500 cycles on  $SiO_2$  substrates.

The resistivity of a 72 nm thick film deposited after 500 cycles at 300 °C on SiO<sub>2</sub> was 2770 μΩ·cm. Film resistivity decreased with increasing deposition temperature, reaching a minimum value of 1500 μΩ·cm for an 89 nm thick film at 375 °C (Figure 26). Lower film resistivity is likely a result of more efficient removal of hydrogen and denser films at higher temperatures. Infrared spectroscopy was used to investigate the possible presence of C-H bonds in a film deposited at 325 °C. No absorbance was observed in the typical C-H stretching region of 2800-3100 cm<sup>-1</sup>. The lack of a C-H absorption in the infrared spectrum suggests that C-H defects are either not present or at low concentrations. Accordingly, the XPS C 1s ionization at 284.2 eV likely corresponds to amorphous carbon.<sup>52,185</sup> For comparison, WC<sub>x</sub> films deposited by thermal ALD from WF<sub>6</sub> and SiEt<sub>2</sub>H<sub>2</sub> had resistivities between 400-500 μΩ·cm.<sup>17,24</sup> The effectiveness of the ethyl group in producing low resistivity carbide films could be due to efficient β-hydride elimination, which removes ethylene and may produce the metal-rich phase W<sub>2</sub>C or metallic W. The Si-H bonds in SiEt<sub>2</sub>H<sub>2</sub> may also serve as a reducing agent for WF<sub>6</sub>, which may lead to lower resistivity films.

In this ALD process, AlMe<sub>3</sub> behaves as both a carbon source and a reducing agent. Film growth likely begins with ligand exchange between AlMe<sub>3</sub> and surface-bound WCl<sub>x</sub> to afford a tungsten-methyl surface and volatile byproduct AlMe<sub>2</sub>Cl (Figure 30). The mechanism of carbide formation likely involves α-hydride elimination. Similar mechanisms have been proposed in CVD TiC<sub>x</sub> and WC<sub>x</sub> processes using tetrakis(neopentyl)titanium and tris(neopentyl)(neopentylidyne)tungsten, respectively.<sup>52,63,64</sup> By extension of Girolami's proposed mechanism,<sup>63,64</sup> α-hydride elimination from tungsten-methyl bonds would produce tungsten-methylidene and tungsten hydride bonds. Reductive elimination of H<sub>2</sub>, or possibly CH<sub>4</sub>, reduces tungsten from the 6+ oxidation state in the starting WCl<sub>6</sub> to the required 4+ oxidation



state in WC. The tungsten-methylidenes can then undergo intramolecular hydrogen transfer to produce methane and WC. Methane production via intramolecular hydrogen transfer was also observed in a surface chemistry study of Ta(NMe)<sub>5</sub>.<sup>195</sup>

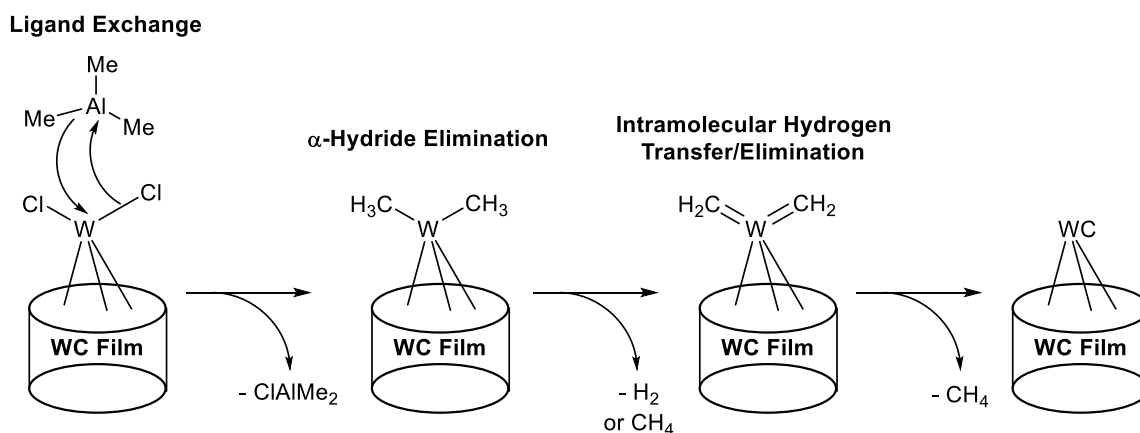


Figure 30. Possible mechanism of WC<sub>x</sub> formation.

### 4.3 Conclusions

Tungsten carbide films were deposited by thermal ALD using WCl<sub>6</sub> as the metal precursor and AlMe<sub>3</sub> as both the carbon source and the reducing agent. WCl<sub>6</sub> is successfully used as an ALD precursor for the first time, resulting in a high growth rate of 1.5-1.8 Å/cycle within an ALD window from 275-350 °C. Self-limited growth was confirmed at 325 °C. The as-deposited films were amorphous, which could be advantageous if this material were used as a Cu diffusion barrier. The films were conductive and had a minimum resistivity value of 1500 μΩ·cm at 375 °C. The film composition was found to have a nearly 1:1 W to C ratio with very low levels of Al, Cl, and O impurities when deposited at 300 °C. At temperatures greater than 300 °C, AlMe<sub>3</sub> thermal decomposition leads to increased Al content but does not affect the growth rate below 350 °C.

#### 4.4 Experimental Section

Films for this study were deposited in a Picosun R75-BE ALD reactor operating at 6-8 hPa.  $\text{WCl}_6$  (99.9%, Strem) was heated to 125 °C in a Picosolid booster to produce adequate vapor pressure.  $\text{AlMe}_3$  (97%, Sigma-Aldrich) was delivered at ambient temperature by vapor-draw ampoule. Nitrogen was used as carrier gas (> 99.999%, Airgas). Films were deposited on 1-2  $\text{cm}^2$  coupons of  $\text{SiO}_2$  (100 nm)/Si that were rinsed with deionized water and isopropanol and dried under a stream of nitrogen. Film thickness was measured at a minimum of three points on the films by cross-sectional SEM imaging using a JEOL-7600 field emission scanning electron microscope. Surface roughness was measured on a Bruker BioScope Catalyst atomic force microscope in contact mode with a 2  $\mu\text{m}$  x 2  $\mu\text{m}$  scan size. Grazing incidence X-ray diffraction patterns were collected on a Bruker D8 Advance diffractometer using a 2° incidence angle. Sheet resistivity measurements were made using a Jandel 4-point probe controlled by a Keithley 2400 Sourcemeter and a Keithley 2182A Nanovoltmeter. X-ray photoelectron spectra were collected using a Kratos Axis Ultra XPS system employing a monochromated Al  $\text{K}\alpha$  (1486.6eV) X-ray source at a chamber pressure of  $10^{-9}$  torr. Argon ion sputtering (4 keV) was used to remove surface adventitious carbon and oxygen. XPS data were analyzed using CasaXPS software. Infrared spectroscopy measurements were taken in transmission mode using a Shimadzu IRTracer-100 spectrometer.

## CHAPTER 5

### ATOMIC LAYER DEPOSITION OF TUNGSTEN-RICH TUNGSTEN CARBIDE FILM USING $WCl_6$ AND $AlH_2(tBuNCH_2CH_2NMe_2)$ AS PRECURSORS

Reprinted (adapted) with permission from Blakeney, K. J.; Ward, C. L.; Winter, C. H. *ECS*

*Trans.* **2018**, 86, in press. Copyright 2018 The Electrochemical Society.

#### 5.1 Introduction

Tungsten-based thin films are essential components of microelectronic devices due to their high melting points, high densities, and low resistivities. Tungsten carbides have been heavily investigated as diffusion barriers,<sup>51,179,191,196–198</sup> and also as work function metals and adhesion layers.<sup>177,199</sup> Tungsten carbides are also important catalytic materials.<sup>46–48</sup> These reports most often use physical or chemical vapor deposition (PVD or CVD) to deposit the thin films. Atomic Layer Deposition (ALD) is an alternative technique for depositing highly conformal and uniform thin films.<sup>6,7,16,165</sup> ALD is a variation of CVD where the growth surface is exposed sequentially to two or more precursors which are separated in time by inert gas purge periods. Film growth is based on self-limiting surface chemical reactions which deposit approximately one monolayer of material with each cycle. ALD is used in the microelectronics industry to fabricate transistors with atomic level precision.<sup>200</sup> Other fields such as catalysis have recently began to employ ALD to fabricate precise structures.<sup>4,201</sup>

Industrial tungsten-based film growth is dominated by  $WF_6$  as the tungsten precursor. Tungsten metal deposited by ALD from  $WF_6$  is increasingly used in high aspect ratio contact holes and gate trenches.<sup>39,158</sup> Unfortunately,  $WF_6$  readily etches Si surfaces through formation of strong Si-F bonds and conversion to volatile fluorosilanes. To combat this facile reaction, an etch stop layer, such as TiN, must be used to prevent undesirable pitting of the Si substrate. It is desirable to eliminate extra processing steps and unnecessary materials from integrated circuits

due to the miniaturization demands of Moore's Law.<sup>2</sup> Additionally,  $\text{WF}_6$  hydrolyzes to form toxic and corrosive HF, which presents serious safety concerns for the handling of this precursor.<sup>36,187-190</sup> Fluorine-free tungsten processes would therefore have immediate applications in semiconductor manufacturing.<sup>183,192,199</sup>

As part of a project to develop new reducing precursors and ALD processes for electropositive metal and metal-containing films, Chapter 2 reports the aluminum dihydride complex **1** and its use in ALD of aluminum metal films.<sup>170</sup> The structure of **1** is shown in Figure 31. In Chapter 3, where **1** was tested with  $\text{TiCl}_4$  as the metal precursor, titanium metal films were not deposited. Instead, titanium carbonitride films were deposited, which were highly air stable and conductive when grown above 180 °C.<sup>70</sup> Thermal ALD of pure metallic films of early transition metals is extremely challenging. Tungsten has a much more positive electrochemical potential than titanium ( $\text{W}^{3+} \leftrightarrow \text{W}^0 E^\circ = 0.100 \text{ V}$ ,  $\text{Ti}^{2+} \leftrightarrow \text{Ti}^0 E^\circ = -1.628 \text{ V}$ ), which prompted an exploration of tungsten ALD film growth using **1**.

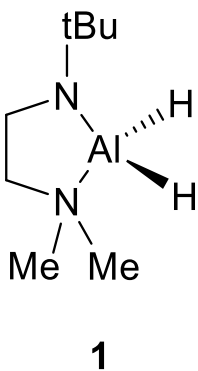


Figure 31. Structure of the co-reactant **1**.

Herein, this chapter reports the thermal ALD growth of tungsten-rich tungsten carbide films using  $\text{WCl}_6$  and **1**. The films are deposited with a growth rate of 1.6 Å/cycle within an

ALD window of 275-350 °C. High purity tungsten carbide films are deposited with a tungsten:carbon ratio between 2.8-3.7, which is greater than the tungsten-rich  $W_2C$  phase. The observed self-limited growth and low aluminum content (<1 at. %) show that aluminum hydride complexes such as **1** are promising co-reactants for thermal ALD growth of transition metal and metal-containing films. Rational design of improved derivatives of **1** could reduce carbon incorporation and yield high purity metallic films.

## 5.2 Experimental Section

ALD experiments were conducted on a Picosun R-200 system using nitrogen carrier gas (5N, Airgas) that was passed through an in-line gas purifier (SAES, <100 ppt  $H_2O$ ,  $O_2$ ). The operating pressure was 5-8 Torr.  $WCl_6$  was purchased from Strem Chemicals and was purified by sublimation. Thermogravimetric analysis (TGA) was performed on a TA Instruments SDT-2960 TGA with a heating rate of 10 °C/min. Complex **1** was synthesized as described previously.<sup>170</sup>  $WCl_6$  and **1** were heated to 125 and 55 °C, respectively, using Picosolid boosters (bubbler-style precursor source) and pulsed into the deposition chamber with inert gas valving. Films were deposited on Si(100) substrates which were cleaned by the standard RCA method.<sup>202</sup> Some films were deposited on uncleaned Si(100) with native oxide and  $SiO_2$  (100 nm thermal oxide on Si) substrates. Film thickness was measured primarily by cross-sectional scanning electron microscopy (SEM) using a JEOL 7600 FE-SEM. X-ray reflectivity (XRR) and grazing-incidence X-ray diffraction (GIXRD) measurements were performed with a Bruker D8 Advance diffractometer using  $Cu K\alpha$  (1.5418 Å) radiation at 40 kV/40mA tube power. Thin film samples were rigorously aligned using Z-height beam splitting and rocking curve scans (2-3 iterations). Annealing studies were carried out in an Anton-Paar XRK-900 XRD chamber at  $5 \times 10^{-2}$  Torr. XRR patterns were modeled using open-source GenX (v2.4.10) software. Resistivity was

measured using a four-point probe (Keithley 2400 sourcemeter, Keithley 2182A nanovoltmeter, Jandel four-point probe). Film elemental composition was investigated by X-ray photoelectron spectroscopy (XPS) using a Kratos Axis Ultra XPS system with a monochromatic Al K $\alpha$  (1486.6 eV) source. Argon ion sputtering (3.8 kV) was used for depth profiling and to remove surface adventitious carbon and oxygen. XPS spectra were analyzed with CasaXPS software.

### 5.3 Results and Discussion

*Precursor Properties.* WCl<sub>6</sub> is a solid with a vapor pressure of 9.75 Torr at 190 °C.<sup>203</sup> For comparison, HfCl<sub>4</sub>, which has achieved widespread adoption as an industrial ALD precursor, is a solid with a vapor pressure of 1 Torr at 190 °C.<sup>204</sup> The TGA plot of WCl<sub>6</sub> shows a mass loss event between 150-230 °C which is visible in both the TGA and differential thermogravimetric (DTG, first derivative) curves (Figure 32). There is only 0.78% residual mass, which indicates clean volatilization of WCl<sub>6</sub> without decomposition. There is a small amount of mass loss at ~120 °C, which is likely volatile tungsten oxychloride impurity caused by brief air exposure during sample loading.

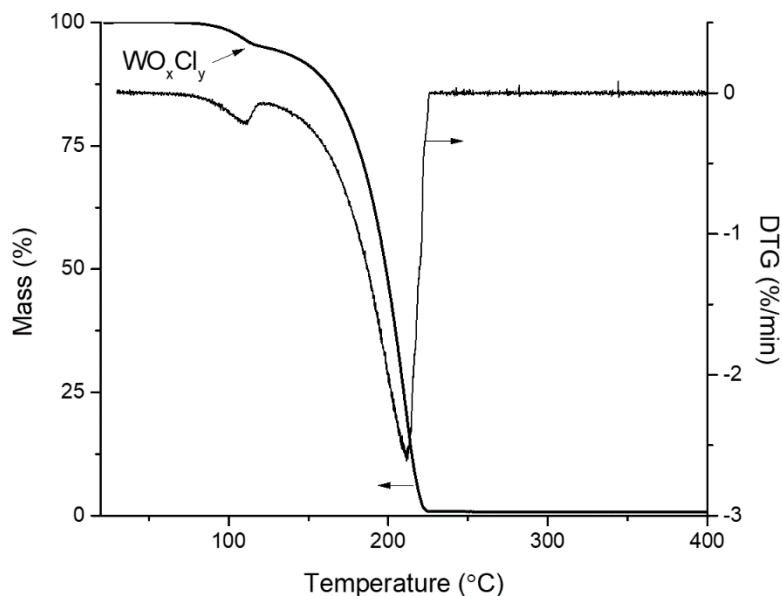


Figure 32. TGA and DTG (first derivative) curves for  $\text{WCl}_6$ . A small amount of tungsten oxychloride is present due to brief air exposure during sample loading.

Chapter 2 reports a volatile aluminum dihydride complex coordinated by a bulky *tert*-butylamido-amine ligand ( $\text{AlH}_2(\text{tBuNCH}_2\text{CH}_2\text{NMe}_2)$ , **1**).<sup>170</sup> Complex **1** has improved thermal stability compared to other volatile aluminum hydride complexes, which enabled a self-limiting thermal ALD process for aluminum metal films.<sup>170</sup> The vapor pressure of **1** is 0.75 Torr at 70 °C, its solid state thermal decomposition temperature is ca. 185 °C, and it has low melting point of 31-32 °C.<sup>170</sup> Complex **1** also displays a quantitative, single-step weight loss in its TGA curve.<sup>170</sup> Thus,  $\text{WCl}_6$  and **1** exhibit good ALD precursor characteristics.

*ALD Film Growth.* Thin film deposition experiments using  $\text{WCl}_6$  and **1** were carried out between 150-400 °C.  $\text{WCl}_6$  and **1** were evaporated at 125 °C and 55 °C, respectively, and were sequentially pulsed into the deposition chamber separated by 10 s nitrogen purge periods. Films were deposited on 1-2  $\text{cm}^2$  coupons of Si(100) cleaned by the standard RCA method. Films deposited at 150 and 200 °C for 250 cycles had sheet resistivities  $> 10^6 \Omega/\text{square}$  and were highly unstable in air, becoming powdery after several minutes. Poor film growth below 200 °C

was also observed when using  $\text{TiCl}_4$  as the metal precursor (Chapter 3).<sup>70</sup> Higher deposition temperatures afforded stable, reflective, silvery-grey films which allowed for a study of ALD process characteristics.

Pulse lengths of both precursors were varied at a deposition temperature of 300 °C to determine if the film growth proceeds via self-limited steps. First, the pulse length of **1** was varied while the pulse length of the  $\text{WCl}_6$  was constant (3 s) (Figure 33a). A 1 s pulse length yielded a lower growth rate of 1.1 Å/cycle while the growth rate saturated for pulse lengths  $\geq 2$  s at 1.5 Å/cycle. The pulse length of  $\text{WCl}_6$  was then varied while keeping the **1** pulse length constant at 3 s (Fig. 3b). A 1 s pulse produced a much lower growth rate of 0.6 Å/cycle, while pulse lengths  $\geq 2$  s yielded identical growth rates of 1.5 Å/cycle. Chapter 4 reports similar saturation characteristics for  $\text{WCl}_6$ .<sup>54</sup> A control experiment was conducted at 300 °C with 300 cycles in which **1** (3 s) was pulsed into the chamber, but no  $\text{WCl}_6$  pulses were used. No film growth was detected by SEM. A similar experiment was carried out at 300 °C with 300 cycles of  $\text{WCl}_6$  (3 s) pulses. Again, no film growth was observed by SEM. The observed saturative behavior of **1** at 300 °C is remarkable, since the solid state thermal decomposition point of **1** is 185 °C.<sup>170</sup> Accordingly, **1** must undergo thermal decomposition during the film growth, but the reaction products must be able to transfer the ligand from **1** to a surface-bound tungsten species to afford carbon in the films. Detailed insights into the mechanism of carbon incorporation will require additional experimentation.



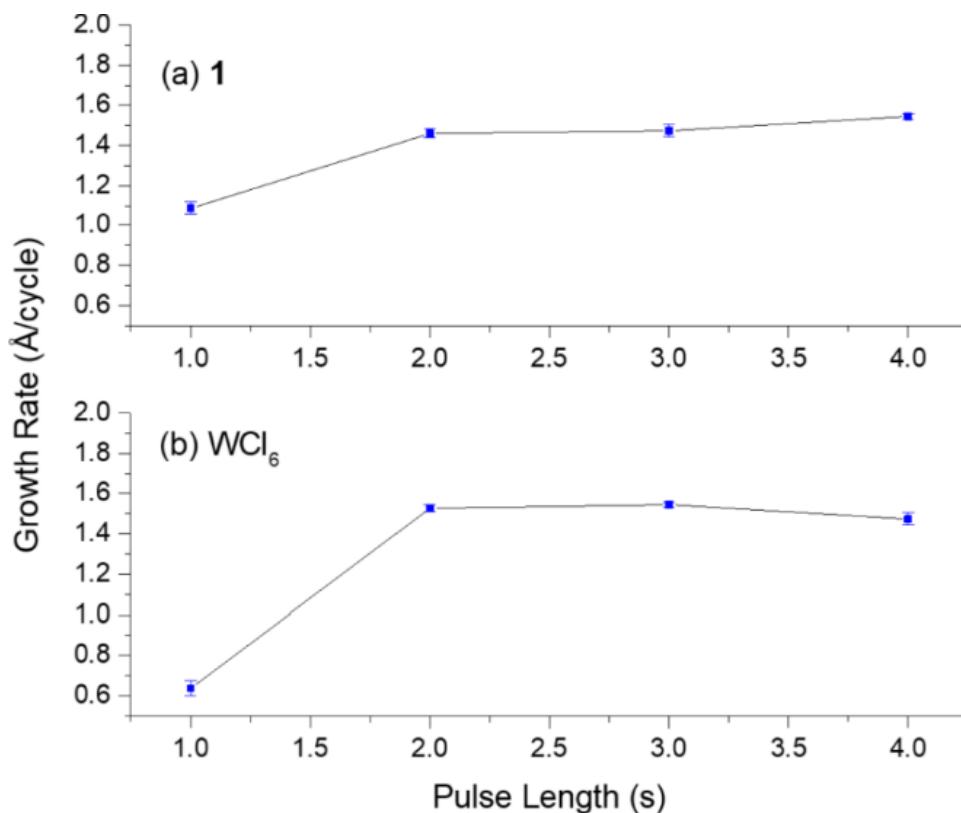


Figure 33. Growth rate versus precursor pulse length for (a) **1** and (b)  $\text{WCl}_6$  at 300 °C.

Using a saturative pulse sequence of  $\text{WCl}_6$  (3 s),  $\text{N}_2$  purge (10 s), **1** (3 s),  $\text{N}_2$  purge (10 s), growth rate was measured as a function of temperature between 250-400 °C after 300 cycles (Figure 34). An ALD window, where growth rate was approximately independent of temperature, was observed between 275-350 °C with a growth rate of 1.6 Å/cycle. Growth rate increased at temperatures > 350 °C which could be related to increased thermal decomposition of **1**.

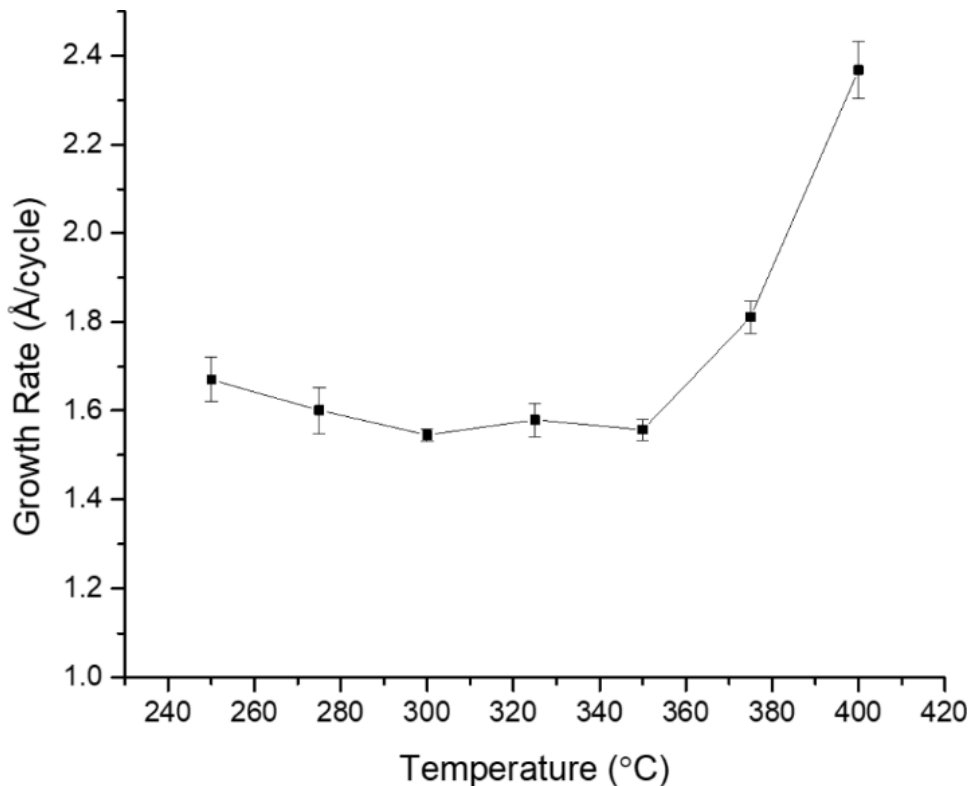


Figure 34. Growth rate versus temperature after 300 ALD cycles.

A plot of film thickness versus number of cycles at 300 °C was linear between 35-400 cycles (Figure 35). Film thicknesses measured by both cross-sectional SEM and XRR were in agreement. The slope of the trendline fitted to XRR thickness measurements was 1.607 Å/cycle which is consistent with the growth rates measured after 300 cycles for the saturation and ALD window plots. The y-intercept of the trendline was close to zero, indicating negligible nucleation delay on RCA-cleaned Si substrates.

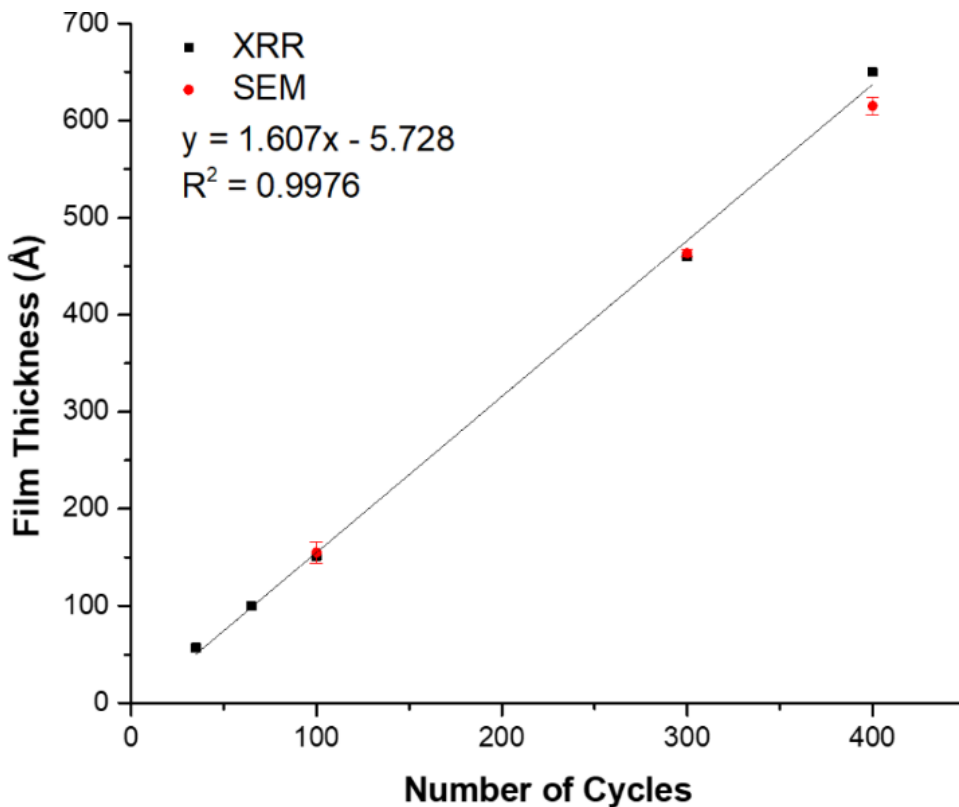


Figure 35. Film thickness versus number of ALD cycles at 300 °C.

*Film Structure and Composition.* XRR was used as a secondary thickness measurement and also to determine film density and surface roughness (Figure 36). The XRR model is described pictorially in Figure 6 which included a thin interfacial SiO<sub>2</sub> layer, but the fit was not improved by adding an oxidized tungsten surface layer, so this was not included. The model and calculated film densities were based on a film composition of W<sub>3</sub>C. Root mean square surface roughness values ( $\sigma$ ) decreased with increasing film thickness from 9.0 Å (93 Å thick film) to 1.8 Å (647 Å thick film). Film densities ( $\rho$ ) ranged from 9.1-7.5 g/cm<sup>3</sup> for films deposited at 300 °C between 93 and 648 Å thick. These densities are 50-60 % of the ideal bulk densities of WC (15.7 g/cm<sup>3</sup>) and W<sub>2</sub>C (17.3 g/cm<sup>3</sup>).<sup>36,199</sup> In general, densities of films grown by thermal ALD can vary significantly depending on the precursors. For example, high density tungsten nitride or

tungsten carbonitride films can be deposited using  $\text{WF}_6$ ,  $\text{B}_2\text{H}_6$  or  $\text{BEt}_3$ , and  $\text{NH}_3$  with densities of 15 and  $15.4 \text{ g/cm}^3$ , respectively.<sup>189,191</sup> By contrast, a report of thermal ALD of  $\text{NbC}_x$  films from  $\text{NbF}_5$  and  $\text{AlMe}_3$  reported densities roughly 50 % of bulk  $\text{NbC}$ .<sup>185</sup>

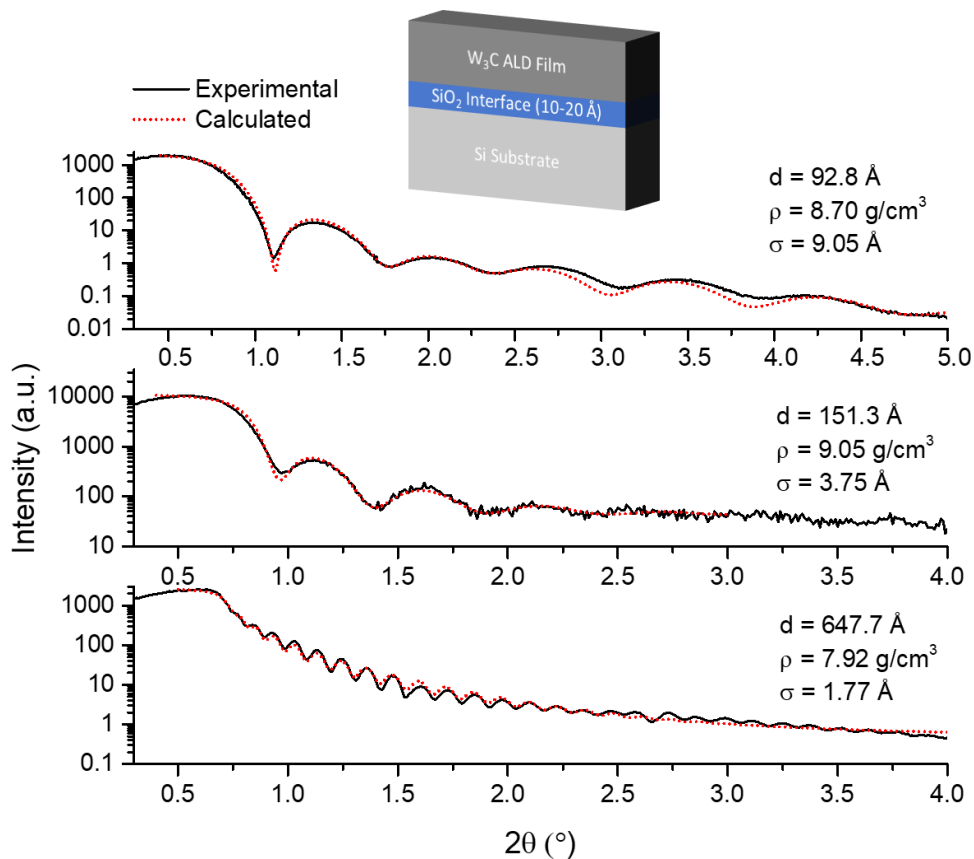


Figure 36. XRR analysis for films deposited on Si using  $\text{WCl}_6$  and **1** at  $300 \text{ }^\circ\text{C}$  after 65 (top), 100 (middle), and 400 (bottom) cycles.

Film crystallinity was evaluated using GIXRD. The as-deposited films displayed a broad reflection centered at  $2\theta = 37.5^\circ$ , which is a common feature of vapor deposited tungsten carbide films (Figure 37).<sup>51,179,183,191,199,205</sup> A film deposited at  $300 \text{ }^\circ\text{C}$  for 300 cycles was annealed under vacuum and its structure was evaluated between  $600\text{-}900 \text{ }^\circ\text{C}$ . The film structure converts to the non-stoichiometric  $\beta\text{-WC}_{1-x}$  phase above  $600 \text{ }^\circ\text{C}$ .<sup>183,199,205,206</sup> At  $900 \text{ }^\circ\text{C}$ , the structure changes

significantly and strong reflections are observed at  $2\theta = 40$  and  $58^\circ$ , which match cubic tungsten metal. The major reflection at  $2\theta = 40^\circ$  also matches the (111) reflection of  $W_2C$ . A similar annealing experiment of a tungsten carbide film deposited at  $300^\circ\text{C}$  using  $WCl_6$  and  $AlMe_3$  also produced reflections corresponding to tungsten metal (Data not shown). Trace amounts of oxygen present in the films or in the low vacuum of the annealing chamber ( $5 \times 10^{-2}$  Torr) could allow removal of carbon from the films, forming  $CO_2$  and tungsten metal. No evidence for tungsten silicide formation was observed, which is similar to previous annealing experiments of ALD WCN films.<sup>191</sup>

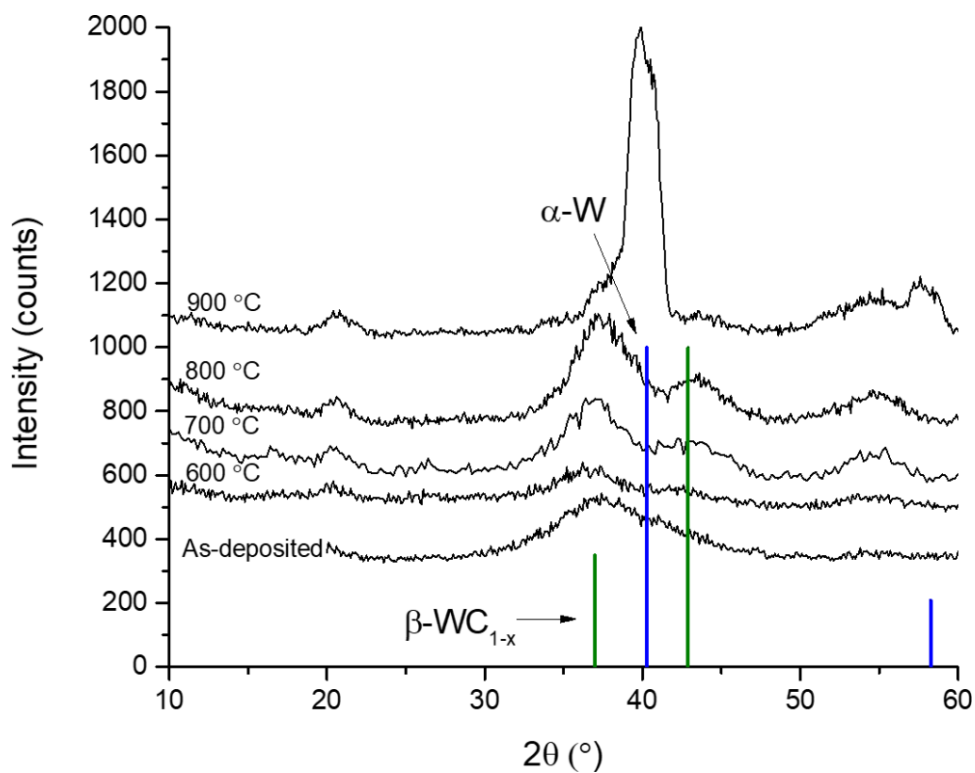


Figure 37. GIXRD patterns of a film deposited from  $WCl_6$  and **1** at  $300^\circ\text{C}$  after 300 cycles. Reference patterns are included for  $\alpha$ -W metal (blue lines, PDF#04-0806) and  $\beta$ - $WC_{1-x}$  (green lines, PDF#20-1316). Weak reflections at  $2\theta = 21^\circ$  and  $54^\circ$  were indexed to  $WO_3$  (reference not included for clarity).

Film composition according to XPS after Ar ion sputtering to remove surface contamination showed tungsten and carbon as the major components with low levels of nitrogen (< 4 at.%), oxygen (< 4 at.%), chlorine (< 3 at.%), and aluminum (< 1 at.%) (Figure 38). The tungsten:carbon ratio  $x$  for  $W_xC$  after sputtering was 2.8-3.7, which is higher than the more common  $W_2C$  phase, and indicates that this ALD process produces tungsten-rich films. The high resolution core level scans are shown in Figure 8. The W  $4f_{7/2}$  ionization was between 31.5-31.4 eV when the C 1s ionization was calibrated to 283.2 eV. For comparison, the previous report of WC ALD in Chapter 4 using  $WCl_6$  and  $AlMe_3$  had W  $4f_{7/2}$  and C 1s binding energies of 31.6 and 283.2 eV, respectively.<sup>54</sup> W metal has a  $4f_{7/2}$  binding energy of 31.4 eV and, therefore, the tungsten-rich films deposited herein display a W  $4f_{7/2}$  binding energy which is intermediate between tungsten metal and WC films. Additionally, previous reports of transition metal carbide ALD processes have observed two ionizations in the C 1s region at ~283.2 and 284.2 eV that have been attributed to metal carbide and amorphous carbon species, respectively.<sup>54,185</sup> For this tungsten carbide ALD process the C 1s region showed a single ionization (283.2 eV) corresponding to W-C and no evidence for amorphous carbon within the films.

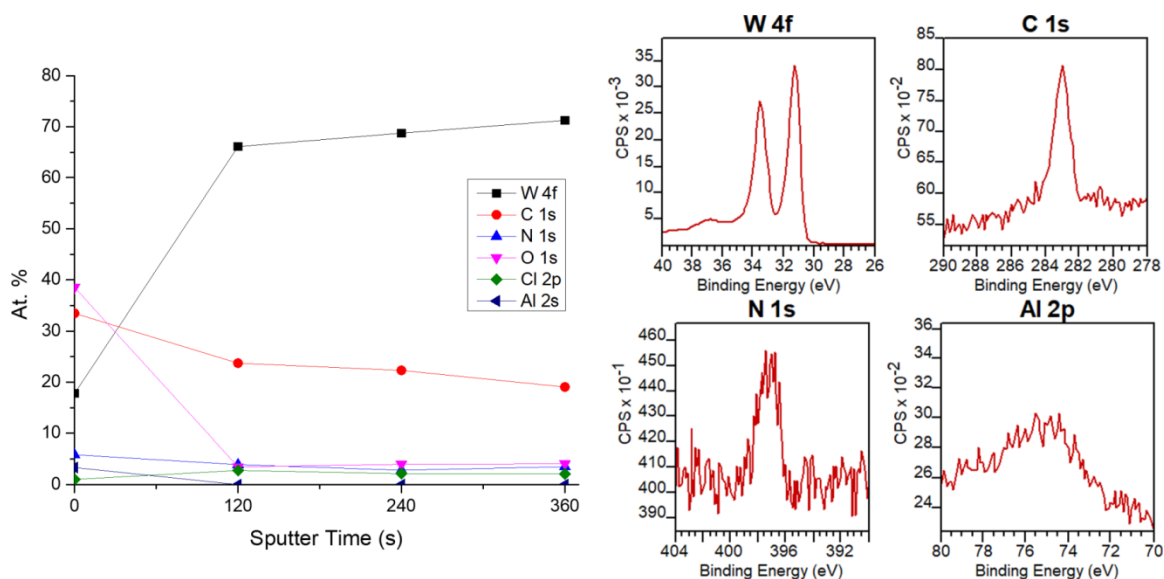


Figure 38. (Left) XPS depth profile of a film deposited from  $WCl_6$  and **1** after 250 cycles at 300 °C. (Right) High resolution XPS scans of W 4f, C 1s, N 1s, and Al 2p regions after sputtering.

Although the film composition is tungsten-rich and high purity tungsten carbide, film resistivities were much higher than bulk values. The low film densities as measured by XRR likely explain these higher than expected resistivities. No clear trend with temperature was observed. Resistivities were  $1140 \mu\Omega\cdot\text{cm}$  at 300 °C,  $840 \mu\Omega\cdot\text{cm}$  at 325 °C, and  $900 \mu\Omega\cdot\text{cm}$  at 400 °C for films deposited after 300 cycles on Si. Resistivities were slightly higher on  $SiO_2$ :  $1800 \mu\Omega\cdot\text{cm}$  at 300 °C and  $1600 \mu\Omega\cdot\text{cm}$  at 350 °C. For comparison, tungsten carbide ALD films grown on  $SiO_2$  from  $WCl_6$  and  $AlMe_3$  had resistivities of  $2770 \mu\Omega\cdot\text{cm}$  at 300 °C and  $1500 \mu\Omega\cdot\text{cm}$  at 375 °C.<sup>54</sup> The tungsten carbide films reported herein have lower resistivities than the previously reported tungsten carbide films deposited from  $WCl_6$  and  $AlMe_3$ , which is consistent with the higher tungsten content, but not as conductive as the tungsten carbide films deposited from  $WF_6$  and  $H_2SiEt_2$ , which measured  $400\text{--}500 \mu\Omega\cdot\text{cm}$ .<sup>17,24</sup>

*Mechanistic Speculation.* The only source of carbon in this ALD process is the amidoamine ligand in **1**, which implies that the carbon in the film must arise from ligand transfer from

**1** to the  $WCl_x$  growth surface. It is also possible that a decomposition product of **1** transfers the ligand to the  $WCl_x$  growth surface. Figure 9 shows a possible mechanism for carbon incorporation into the growing tungsten film. After ligand transfer to the growth surface,  $\beta$ -methyl elimination from the *tert*-butyl group may be a facile decomposition pathway for the putative tungsten amido-amine surface species. This would form a methyl-terminated tungsten surface and eliminate a neutral amino-imine as a by-product. Chapter 4 on tungsten carbide ALD from  $WCl_6$  and  $AlMe_3$  described a possible mechanism for carbide formation from a tungsten-methyl surface based on  $\alpha$ -hydride elimination.<sup>54</sup>

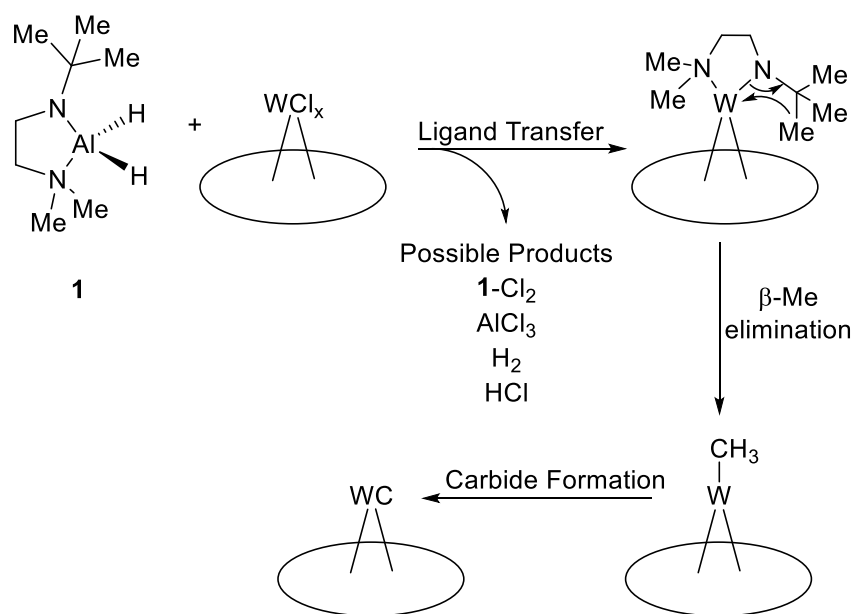


Figure 39. Possible mechanism for carbon incorporation by ligand transfer from **1** to the growth surface and subsequent decomposition and carbide formation.

It is unclear why the ALD process described herein from  $WCl_6$  and **1** produces films with low nitrogen content ( $< 4$  at.%), but the report in Chapter 3 using  $TiCl_4$  and **1** produced titanium carbonitride films ( $\sim 20$  at.% N).<sup>70</sup> Although both processes likely proceed through similar



surface intermediates, differences in ligand decomposition pathways must exist to account for the clearly different film compositions. The much lower degree of carbon and nitrogen incorporation observed herein (~25 at.% versus ~50 at.% for TiCN) implies that there is less ligand transfer from **1** to the growth surface when using  $\text{WCl}_6$  as the metal precursor instead of  $\text{TiCl}_4$ . Future synthetic work will be directed towards designing ligands which can produce volatile and thermally stable aluminum hydride complexes, but which will not readily transfer to the growth surface and incorporate into the film under ALD conditions, and could therefore produce a pure metal film.

### 5.3 Conclusions

A thermal ALD process is described using  $\text{WCl}_6$  and the aluminum dihydride complex  $\text{AlH}_2(\text{tBuNCH}_2\text{CH}_2\text{NMe}_2)$  (**1**) as precursors. The process displays an ALD window between 275-350 °C with a growth rate of 1.6 Å/cycle. Film composition according to XPS is high purity tungsten carbide ( $\text{W}_x\text{C}$ ,  $x = 2.8\text{-}3.7$ ) with low levels of nitrogen, oxygen, chlorine, and aluminum impurities (< 4, 4, 3, 1 at.%, respectively). The as-deposited films are nanocrystalline and are converted to the non-stoichiometric  $\beta\text{-WC}_{1-x}$  phase above 600 °C. Film densities were 50-60% of bulk tungsten carbide values, which may explain the unexpectedly high resistivities (1140  $\mu\Omega\cdot\text{cm}$  at 300 °C) for the tungsten-rich films.

## CHAPTER 6

### A VOLATILE DIALANE COMPLEX FROM RING-EXPANSION OF A SATURATED N-HETEROCYCLIC CARBENE AND ITS USE IN ATOMIC LAYER DEPOSITION OF ALUMINUM METAL FILMS

#### 6.1 Introduction

N-heterocyclic carbene (NHC) complexes of main group element hydrides display rich chemistry and physical properties due to the unique electronic features present in NHCs and the reactivity of the hydride ligands.<sup>132,133,207–209</sup> The high nucleophilicity of the carbene can stabilize molecular main group hydrides, which are generally of low thermal stability. Arduengo reported the first NHC- $\text{AlH}_3$  complex (1,3-bis(2,4,6-trimethylphenyl)-imidazol-2-ylidene- $\text{AlH}_3$ ), which showed very high thermal stability (mp 246 °C).<sup>210</sup> Jones later exploited the stabilizing effect of NHCs in the synthesis of NHC complexes of Al, Ga, and In trihydrides.<sup>211</sup>

Another interesting electronic feature of NHCs is the vacant and electrophilic p orbital of the carbene carbon atom.<sup>208,210</sup> Arduengo immediately reasoned that this interesting feature should in theory preclude stable NHC main group hydride complexes when he remarked, “The stability of (1,3-bis(2,4,6-trimethylphenyl)-imidazol-2-ylidene- $\text{AlH}_3$ ) is remarkable, considering the fact that it contains a potential hydride donor adjacent to an electrophilic carbon center.”<sup>210</sup> However, it was 20 years before hydride attack and resulting ring expansion of an NHC was reported. Following the seminal report from Radius on NHC ring expansion using hydrosilanes,<sup>212</sup> numerous subsequent reports have demonstrated the generality and susceptibility of NHCs to ring expansion by hydride-containing reagents.<sup>213–218</sup> Only two examples of aluminum hydride promoted NHC ring expansion have been reported, both of which involved unsaturated NHCs (Figure 40). Hill reported that treatment of a  $\beta$ -diketiminato aluminum dihydride complex with an NHC led to the corresponding ring expansion product as long as the aryl substituents on both the  $\beta$ -diketiminato ligand and the NHC were not too bulky (Figure

40).<sup>217</sup> Radius then reported ring expansion of stable NHC- $\text{AlH}_3$  complexes bearing small alkyl substituents when heated with a second equivalent of NHC (Figure 40).<sup>218</sup>

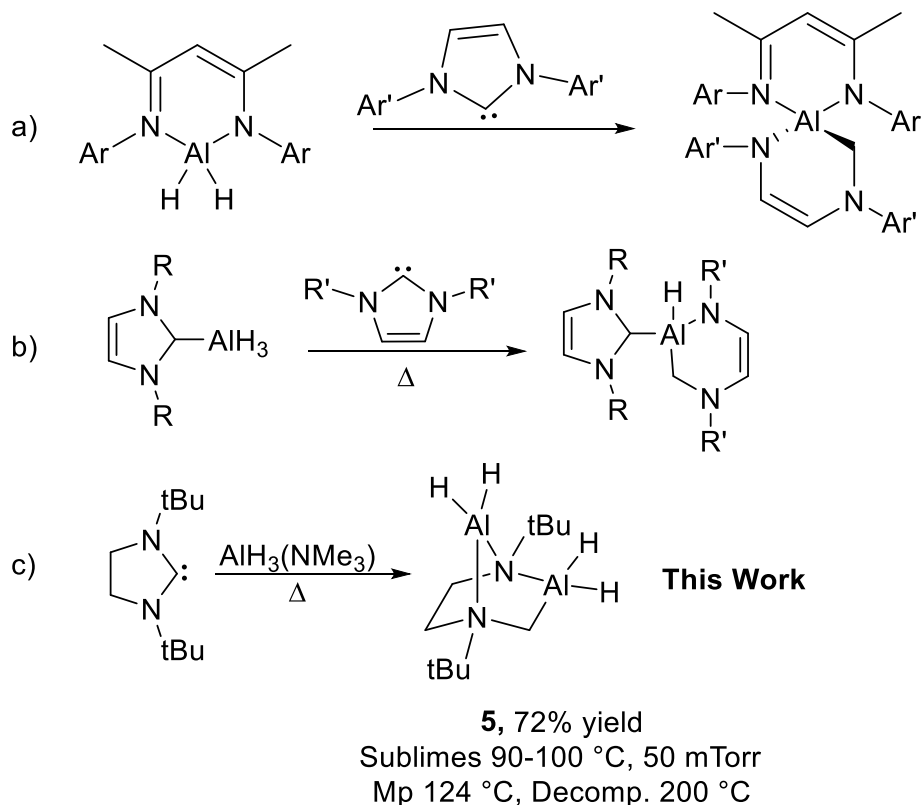


Figure 40. Aluminum hydride promoted NHC ring expansion reactions. A) using  $\beta$ -diketiminato aluminum dihydride complexes,<sup>217</sup> B) using NHC- $\text{AlH}_3$  complexes,<sup>218</sup> and C) this work.

Aluminum metal is important in microelectronics devices as a component of the metal gate electrode and possibly in narrow line width interconnects due to its much lower electron mean free path compared to copper (18.9 versus 39.9 nm, respectively).<sup>60,110–113,145,146</sup> Additionally, aluminum is a very promising plasmonic material which holds several advantages, such as cost and the ability to be used in the ultraviolet region, over noble metals like silver or gold.<sup>95,147,150</sup> Aluminum metal films have been deposited by techniques such as evaporation, sputtering, or chemical vapor deposition (CVD).<sup>155</sup> Ongoing miniaturization of microelectronics

components requires depositing metal films with higher thickness and conformality control than these techniques can achieve.<sup>2</sup>

Atomic layer deposition (ALD), a time-resolved variant of CVD,<sup>10</sup> is now a major technique for depositing thin films in microelectronics devices, but ALD processes for many metals and elements are poorly developed.<sup>1,6,7,24,26,165</sup> ALD enables superior conformality and thickness control over other thin film deposition techniques, but extremely electropositive metals like aluminum require sufficiently strong reducing co-reactants. Plasma-enhanced ALD of aluminum metal has been reported using trimethylaluminum and hydrogen plasma, although some carbon (~3 at.%) was present.<sup>114,115</sup> Thermal ALD is desirable over plasma-based processes due to improved conformality but current thermal chemistries are unable to produce films of many metals and elements.<sup>1,24</sup> Suitable ALD precursors exist for most elements, but strongly reducing precursors must be developed in order to deposit metallic films by thermal ALD.<sup>27</sup> The ALD reducing co-reactant must not readily decompose at the deposition temperature and its by-products must also not contaminate the film. Volatile and thermally stable aluminum hydride complexes would be highly valuable reducing precursors for metal ALD due to their highly polarized Al-H bond.  $\text{AlH}_3(\text{NMe}_3)$  was demonstrated as a reducing co-reagent in low temperature thermal chemical vapor deposition (CVD) of Ti-Al alloy films with  $\text{TiCl}_4$  between 60-127 °C.<sup>156</sup> Chapter 2 reports the highly volatile and thermally stable aluminum dihydride complex  $\text{AlH}_2(\text{tBuNCH}_2\text{CH}_2\text{NMe}_2)$  and its use in the thermal ALD of aluminum metal films.<sup>170</sup> Initial attempts to deposit metallic titanium or tungsten films by ALD using this precursor in Chapters 3 and 5 were unsuccessful, instead producing titanium carbonitride and tungsten carbide films, respectively.<sup>70,219</sup>

In view of the highly stabilizing effect of NHC ligands, NHC-AlH<sub>3</sub> adducts were explored as reducing co-reagents for thermal atomic layer deposition of metal films. No volatility data for these complexes has been reported. As reported by Arduengo, Jones, and Radius, stable AlH<sub>3</sub> complexes of unsaturated NHCs can be readily synthesized by treatment of the free NHC with LiAlH<sub>4</sub> or AlH<sub>3</sub>(NMe<sub>3</sub>).<sup>210,211,220</sup> Efforts to synthesize a volatile and thermally stable N-heterocyclic carbene (NHC) complex of AlH<sub>3</sub> have produced an unusual dialane complex (**5**) from ring expansion of the NHC. Aluminum metal films were deposited by low temperature thermal ALD using AlCl<sub>3</sub> and **5** as precursors. Complex **5** displays promising ALD precursor characteristics and may lead to new valuable ALD processes for metal and element thin films.

## 6.2 Experimental Section

Syntheses and handling of compounds were performed using air-free Schlenk line and glovebox techniques. Solvents were distilled from appropriate drying agents under Ar atmosphere. Reagents were purchased from commercial sources. Unsaturated NHC-alanes (**7-9**) were synthesized according to previous literature reports.<sup>211,220</sup> The saturated NHC 1,3-di-*tert*-butylimidazolin-2-ylidene was synthesized according to a literature procedure.<sup>221</sup> NMR spectra were collected on Agilent MR-400 or DD2-600 spectrometers. A Mel-Temp capillary melting point apparatus was used for melting point and thermal decomposition experiments. Infrared spectra were collected on a Shimadzu IR-Tracer100 spectrometer. Thermogravimetric analysis (TGA) data was obtained in a glovebox using a Netzsch TG 209F1 Libra thermobalance under nitrogen flow at 5 °C/min.

Film deposition experiments were carried out in a Picosun R200 commercial ALD system. The working pressure was 6-8 Torr using ultra high purity nitrogen (Airgas, 5N) which was passed through an inline gas purifier (SAES, < 100 ppt H<sub>2</sub>O, O<sub>2</sub>) as carrier gas. Precursors

were heated using Picosolid boosters (bubbler-style low vapor pressure precursor sources) at 90 and 110 °C for AlCl<sub>3</sub> and **5**, respectively. Aluminum metal films were deposited on 2 cm<sup>2</sup> TiN substrates (10 nm TiN/100 nm SiO<sub>2</sub>/Si) which were loaded into the ALD chamber and heated to the deposition temperature under vacuum for at least 1-2 h prior to the deposition. Film thickness was measured by cross-sectional scanning electron microscopy using a JEOL-7600 FE-SEM. Grazing incidence X-ray diffraction (GIXRD) and X-ray reflectivity (XRR) measurements were made using a Bruker D8 Advance instrument (Cu K $\alpha$ , 1.54056 Å, 1° incidence angle for GIXRD). Sheet resistivity was measured within 60 s of air exposure using a Jandel four-point probe coupled with a Keithley 2400 sourcemeter and 2182A nanovoltmeter. Film composition was measured by X-ray photoelectron spectroscopy (XPS, Kratos Axis Ultra) with a monochromatic Al K $\alpha$  source and using 3.8 kV Ar ion sputtering for depth profiling. The XPS results were analyzed using CASAXPS software. Surface roughness was measured by atomic force microscopy (AFM) over a 2  $\mu$ m<sup>2</sup> area with a Bruker BioScope Catalyst AFM in contact mode.

*Synthesis of 5.* A 100 mL Schlenk flask was charged with AlH<sub>3</sub>(NMe<sub>3</sub>) (196 mg, 2.194 mmol) and toluene (5 mL) and cooled with an ice bath. A separate 100 mL Schlenk flask was charged with 1,3-di-*tert*-butylimidazolin-2-ylidene (200 mg, 1.097 mmol) and toluene (5 mL). The NHC solution was then added *via* cannula to the AlH<sub>3</sub>(NMe<sub>3</sub>) suspension. The ice bath was removed and the mixture was heated to reflux. Evolution of NMe<sub>3</sub> vapor was monitored using an oil bubbler and the mixture was refluxed until the gas evolution ceased after 30 min. The mixture was filtered and evaporated leaving a colorless solid. The product was purified by sublimation at 100 °C and 50 mTorr (192 mg, 72% yield). X-ray quality crystals were grown from a saturated pentane/toluene solution (3:1) at -20 °C over 2 days. The synthesis of **5** was increased to 1-5 g

scales with similar yields, but the reaction mixture should be heated slowly to reflux over the course of 1 h to minimize decomposition of  $\text{AlH}_3(\text{NMe}_3)$ . Mp 122-124 °C. Thermal stability (5 °C/min): In an Ar-filled sealed glass capillary, the compound melted and remained a colorless liquid to 200 °C, at which point it began to darken to a grey solid, likely Al metal, and evolve gas bubbles, likely  $\text{H}_2$ .  $^1\text{H}$  NMR (400 MHz,  $\text{C}_6\text{D}_6$ )  $\delta$  = 5.5-4.5 (bs, 4H), 2.83-2.79 (m, 2H), 2.66-2.59 (m, 1H), 2.14-2.05 (m, 2H), 1.33 (s, 9H), 0.83 (s, 9H).  $^{13}\text{C}$  NMR (100 MHz,  $\text{C}_6\text{D}_6$ )  $\delta$  = 60.27, 54.63, 48.86, 41.75, 29.28, 25.98. IR (ATR)  $\nu/\text{cm}^{-1}$  = 2972, 2962, 2955, 2926, 2886, 1827, 1792, 1771, 1477, 1468, 1400, 1373, 1283, 1231, 1188, 1047, 1030, 959, 939, 922, 791, 760, 696, 615, 592, 559, 548, 521, 500, 447, 417. Elemental Analysis calcd. for  $\text{C}_{11}\text{H}_{28}\text{Al}_2\text{N}_2$  C, 54.52; H, 11.65; N, 11.56. found C, 54.53; H, 11.52; N, 11.14.

*Synthesis of 6.*  $\text{Cp}_2\text{TiCl}_2$  (21 mg, 0.0825 mmol) was suspended in diethyl ether (2 mL). Complex **5** (20 mg, 0.0825 mmol) was dissolved in diethyl ether (2 mL) and added dropwise to the  $\text{Cp}_2\text{TiCl}_2$  mixture. Immediate gas evolution was observed with a rapid color change to purple. Dark purple X-ray quality crystals formed from the resulting clear purple solution after 48 h at -20 °C (18 mg, 45%). Mp 140 °C (dec.). Thermal stability (5 °C/min): In an Ar-filled sealed glass capillary, the dark purple crystals began to simultaneously melt and decompose with gas evolution between 140-160 °C. IR (ATR)  $\nu/\text{cm}^{-1}$  = 2978, 2963, 2928, 2911, 2891, 2866, 2853, 1911, 1908, 1815, 1807, 1468, 1402, 1379, 1356, 1227, 1184, 1123, 1043, 1013, 943, 914, 831, 806, 797, 785, 716, 702, 671, 665, 644, 621, 606, 567, 546, 523, 474, 419, 405. Elemental Analysis calcd. for  $\text{C}_{21}\text{H}_{37}\text{Al}_2\text{Cl}_2\text{N}_2\text{Ti}$  C, 51.45; H, 7.61; N, 5.71. found C, 51.23; H, 7.48; N, 5.58.

### 6.3 Results and Discussion

*Precursor Synthesis and Characterization.* Unsaturated NHC-AlH<sub>3</sub> complexes were previously reported to have outstanding thermal stabilities, with solid state decomposition points above 240 °C.<sup>210,211</sup> First, the volatilities of unsaturated NHC-AlH<sub>3</sub> complexes bearing small alkyl substituents were evaluated. Complexes **7-9** were synthesized from the stable NHC and LiAlH<sub>4</sub> following the reported procedures (Figure 41).<sup>211,218</sup> Sublimation experiments were performed to evaluate **7-9** as ALD precursors. The methyl-substituted complex **7** did not sublime at 50 mTorr and decomposed above 200 °C to a dark grey solid. Complexes **8** and **9** underwent sublimation at 120 °C and 50 mTorr with concurrent decomposition and were recovered in 40 and 58% yields, respectively. TGA analysis of **8** and **9** showed significant thermal decomposition and high residual masses (Figure 43). The percent loss during the first mass loss step was only 34% for **8** and 57% for **9** at 230 °C. Although **8** and **9** display excellent thermal stability with decomposition points above 240 °C, the volatilities of these complexes are disappointingly low and likely insufficient for use in ALD.

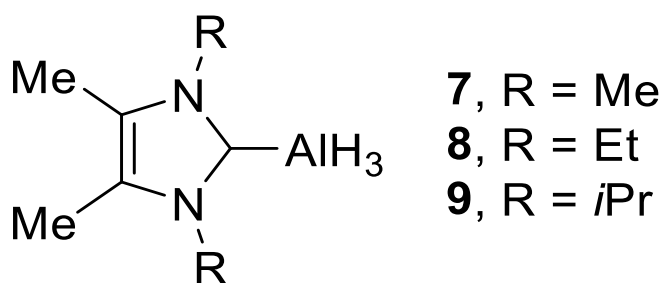


Figure 41. Structures of NHC-AlH<sub>3</sub> complexes **7-9**.

Saturated NHCs show improved volatility over unsaturated NHCs for NHC-Cu complexes, likely due to their lack of a  $\pi$ -electron system and non-planarity.<sup>222</sup> Thus, we began



exploring saturated NHC-AlH<sub>3</sub> complexes as potential ALD precursors. Treatment of the stable NHC 1,3-di-*tert*-butylimidazolin-2-ylidene with LiAlH<sub>4</sub> produced after workup a crude mixture containing the NHC-AlH<sub>3</sub> complex according to NMR analysis. The crude mixture was subjected to sublimation conditions at 100 °C and 50 mTorr which allowed for the separation of a colorless crystalline solid. The <sup>1</sup>H NMR spectrum clearly showed two separate *t*Bu singlets (1.33 and 0.83 ppm) which revealed that the symmetry of the NHC ligand had been broken. The structure of **5** was unambiguously determined by X-ray crystallography from single crystals grown from a saturated pentane/toluene (3:1) solution at -20 °C over two days (Figure 42). The synthesis of **5** was optimized by treating the free NHC with 2 equivalents of AlH<sub>3</sub>(NMe<sub>3</sub>) in refluxing toluene until evolution of NMe<sub>3</sub> ceased. Evaporation of the solvent and sublimation allowed isolation of **5** in 72% yield. Whereas some unsaturated NHC-AlH<sub>3</sub> complexes can be sublimed unchanged, the saturated NHCs are more susceptible to ring expansion due to the lack of aromatic stabilization of the electrophilic carbene p-orbital.<sup>215</sup>

The molecular structure of dialane **5** is shown in Figure 42. The heterocyclic complex has a distorted norbornane-like structure with a C<sub>3</sub>N<sub>2</sub>Al<sub>2</sub> core containing two pseudo-tetrahedral aluminum centers. The two Al-N bond distances for Al2 are 1.971(2) and 1.932(2) Å, and the Al-N and Al-C bond distances for Al1 are 1.971(2) and 2.012(3) Å, respectively. The N1-Al2-N2 and N1-Al1-C7 bond angles are much less than the ideal tetrahedral bond angles at 85.55(9)° and 90.49(10)°, respectively.

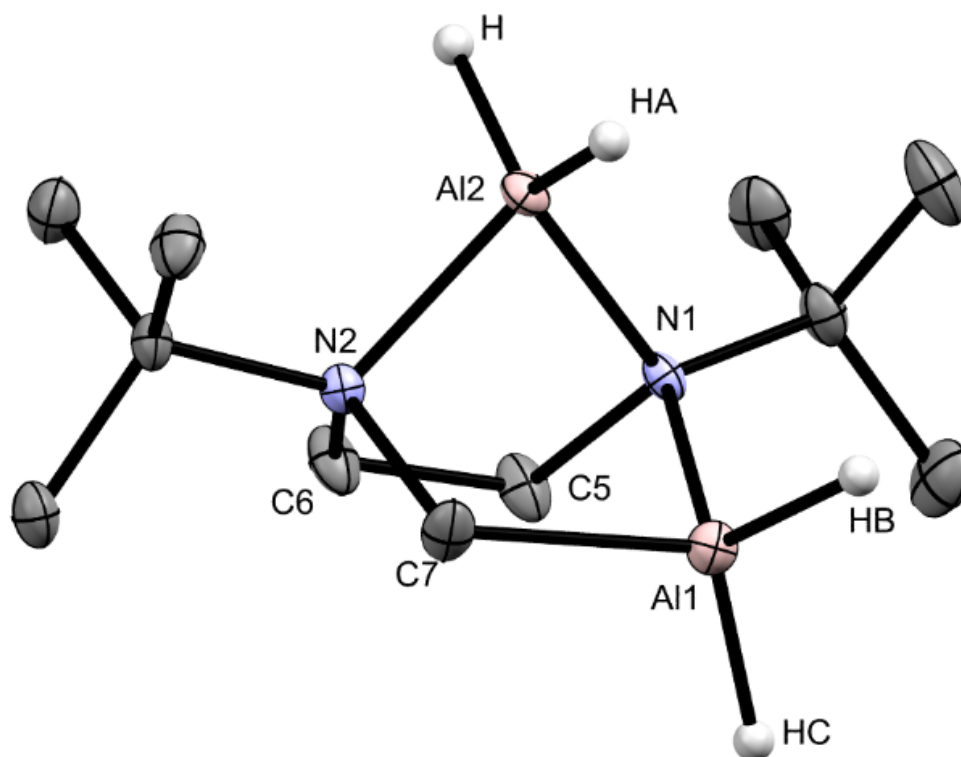


Figure 42. POV-Ray rendered ORTEP plot of the structure of **5**. Hydrogen atoms not bonded to Al are omitted for clarity. Selected bond distances (Å) and angles (°): Al(1)-N(1) 1.971(2), Al(1)-C(7) 2.012(3), Al(2)-N(1) 1.932(2), Al(2)-N(2) 1.971(2), Al(1)-H(B) 1.53(4), Al(1)-H(C) 1.53(3), Al(2)-H 1.50(3), Al(2)-H(A) 1.49(3), N(1)-Al(1)-C(7) 90.49(10), N(1)-Al(2)-N(2) 85.55(9).

Complex **5** sublimes at 90-100 °C and 50 mTorr, melts at 124 °C, and undergoes thermal decomposition at 200 °C, which is higher than most known Al hydride complexes except the unsaturated NHC-AlH<sub>3</sub> complexes previously mentioned. TGA of **5** revealed smooth mass loss and a nearly quantitative single step weight loss from approximately 120-240 °C (Figure 43). The vapor pressure of **1** was determined to be 0.75 Torr at 120 °C. Thus, **5** has promising ALD precursor characteristics.

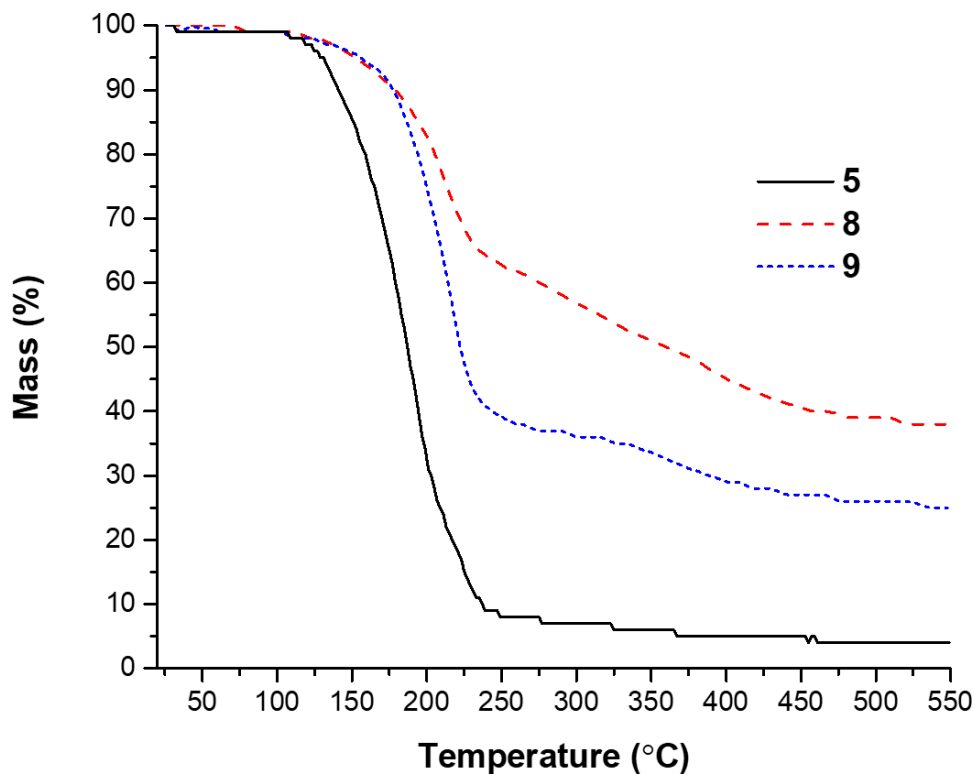


Figure 43. TGA curves of **5**, **8**, and **9**.

Solution chemistry can be helpful in exploring reactivity of vapor-phase thin film precursors.<sup>27,164</sup>  $\text{Cp}_2\text{TiCl}_2$  was chosen as a model metal ALD precursor over, for example,  $\text{TiCl}_4$ , for its greater potential to generate a crystalline product due to the Cp ligands. Treatment of **5** with one equivalent of  $\text{Cp}_2\text{TiCl}_2$  in diethyl ether produced an immediate color change from red to deep purple with gas evolution. Storing the clear purple solution at  $-20\text{ }^\circ\text{C}$  for 48 h produced paramagnetic purple crystals of **6** in 45% yield. The molecular structure of **6** is a hydride-bridged heterobimetallic Ti-Al complex (Figure 44). The Ti(IV) center was reduced to Ti(III) ( $\text{H}_2$  gas evolution) and the two Cl atoms were transferred to Al. Several similar hydride-bridged Ti-Al complexes have been reported and the purple color appears to be characteristic.<sup>125,223,224</sup> The N-Al1-C bond angle increased from  $90.49(10)^\circ$  in **5** to  $100.34(9)$  in **6**.

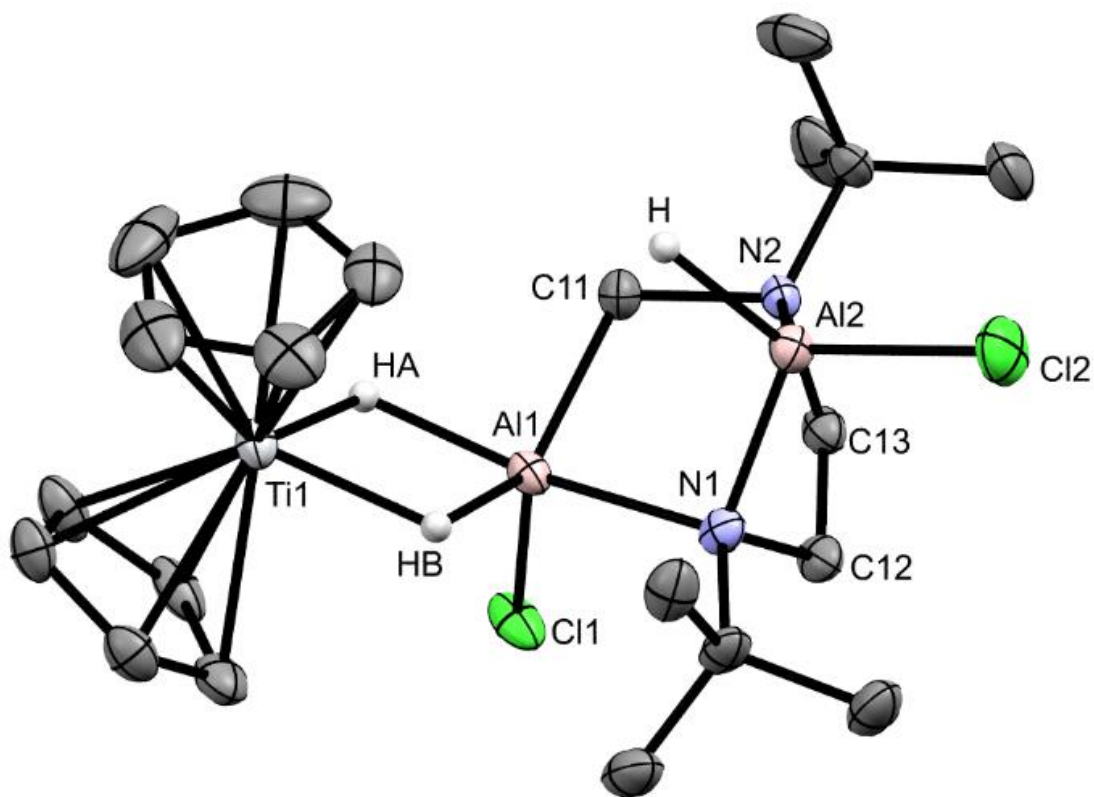


Figure 44. POV-Ray rendered ORTEP structure of **6**. Hydrogen atoms not bonded to Al are omitted for clarity. Selected bond distances (Å) and angles (°): Al(1)-N(1) 2.081(3), Al(1)-C(11) 2.006(40), Al(1)-Cl(1) 2.1823(12), Al(1)-H(A) 1.75(5), Al(1)-H(B) 1.63(4), Ti(1)-H(A) 1.79(4), Ti(1)-H(B) 1.88(6), Al(2)-N(1) 1.917(3), Al(2)-N(2) 1.965(3), Al(2)-Cl(2) 2.1379(13), Al(2)-H 1.78(2), N(1)-Al(1)-C(11) 100.34(9), N(1)-Al(1)-Cl(1) 88.50(12), C(11)-Al(1)-Cl(1) 108.80(10), N(1)-Al(2)-N(2) 87.08(12), N(1)-Al(2)-Cl(2) 113.82(10), N(2)-Al(2)-Cl(2) 113.06(9).

*Aluminum Metal ALD Results.* Complex **5** was evaluated as a reducing agent for the thermal ALD growth of aluminum metal films in deposition experiments with AlCl<sub>3</sub> as the metal precursor. Precursors AlCl<sub>3</sub> and **5** were pulsed sequentially into the reactor chamber which resulted in the deposition of metallic aluminum films. The growth temperature was investigated between 120-150 °C after 100 cycles. Lower temperatures could not be investigated due to the delivery temperature of **5**. An ALD window was observed between 120-140 °C with a constant growth rate of 3.1 Å/cycle (Figure 45). At 150 °C, the growth rate decreased to 2.3 Å/cycle. A

temperature of 140 °C was chosen to investigate the self-limiting growth characteristics of this process.

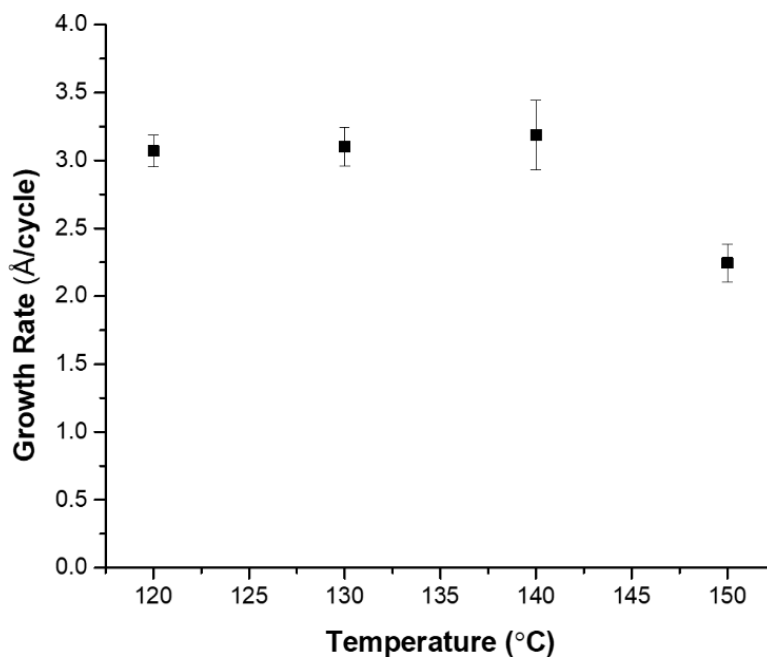


Figure 45. Growth rate versus temperature after 100 cycles of  $\text{AlCl}_3$  and **5** on TiN.

Pulse lengths of  $\text{AlCl}_3$  and **5** were varied independently while depositions were carried out at 140 °C. Film thickness was measured after 100 cycles on TiN substrates and saturative growth rates were observed for pulse lengths  $\geq 1$  s for  $\text{AlCl}_3$  and  $\geq 3$  s for **5**. The saturative growth rates were  $\sim 3.2$ - $3.6$  Å/cycle. Similar saturation characteristics were previously observed for  $\text{AlCl}_3$ .<sup>170</sup>

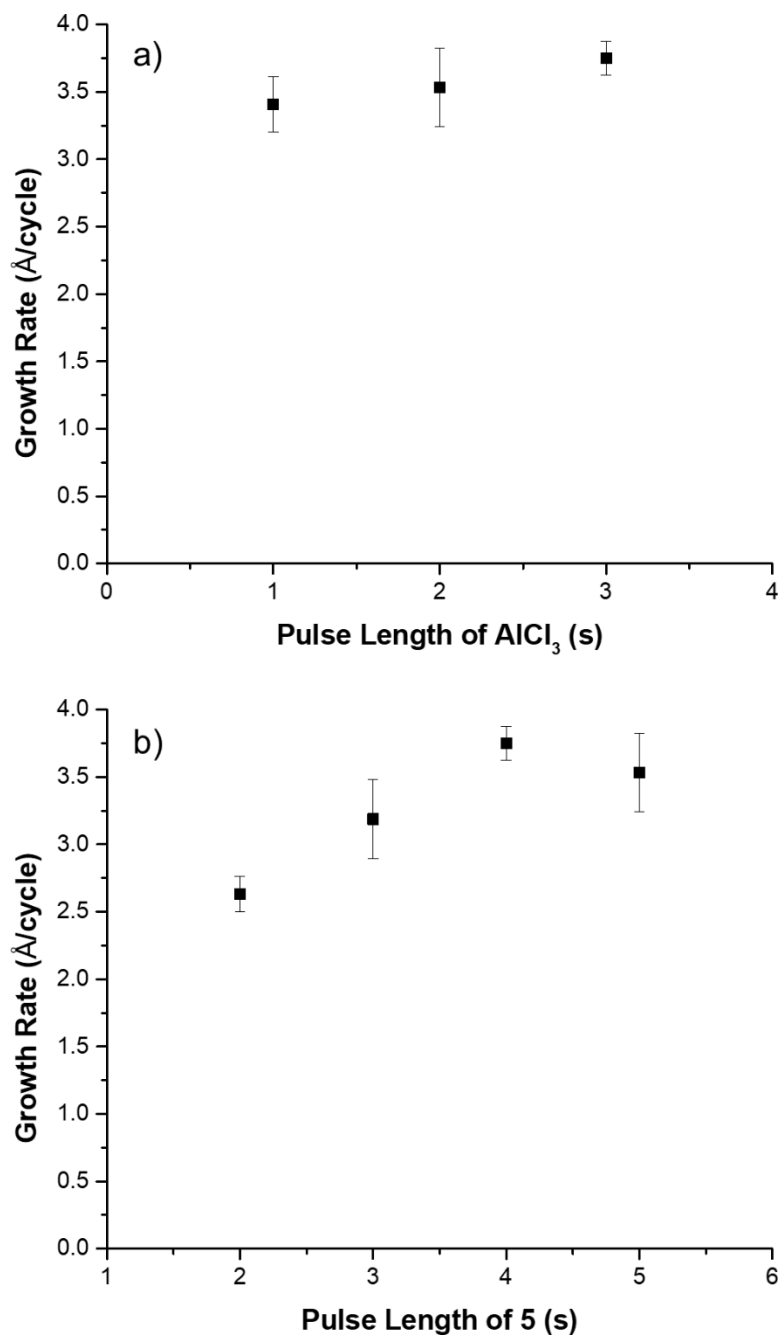


Figure 46. Growth rate versus precursor pulse length for (a) AlCl<sub>3</sub> and (b) 5 after 100 cycles at 140 °C.

Film thickness as a function of the number of ALD cycles was evaluated at 140 °C (Figure 47). Ideal layer-by-layer ALD growth should result in a constant film thickness increase with every ALD cycle and yield a trendline with a y-intercept at the origin and a slope equal to

the measured growth rate value. The y-intercept for the trendline shown in Figure 47 is positive and can be explained by top-view SEM images (Figure 48) where it is clear that the deposited Al metal forms island structures rather than forming a smooth continuous film at low thicknesses. This results in a larger apparent film thickness when measured by cross-sectional SEM due to the island formation. The slope of the trendline is smaller than the measured growth rate after 100 cycles for the same reason, film growth initially proceeds through island formation with many reactive sites but once the film is nearly continuous there are fewer active sites and so the growth rate reaches a steady-state value,  $\sim 1.7 \text{ \AA}/\text{cycle}$  in this case. Similar film thickness versus cycles characteristics have been previously observed in metal ALD processes.<sup>79</sup>

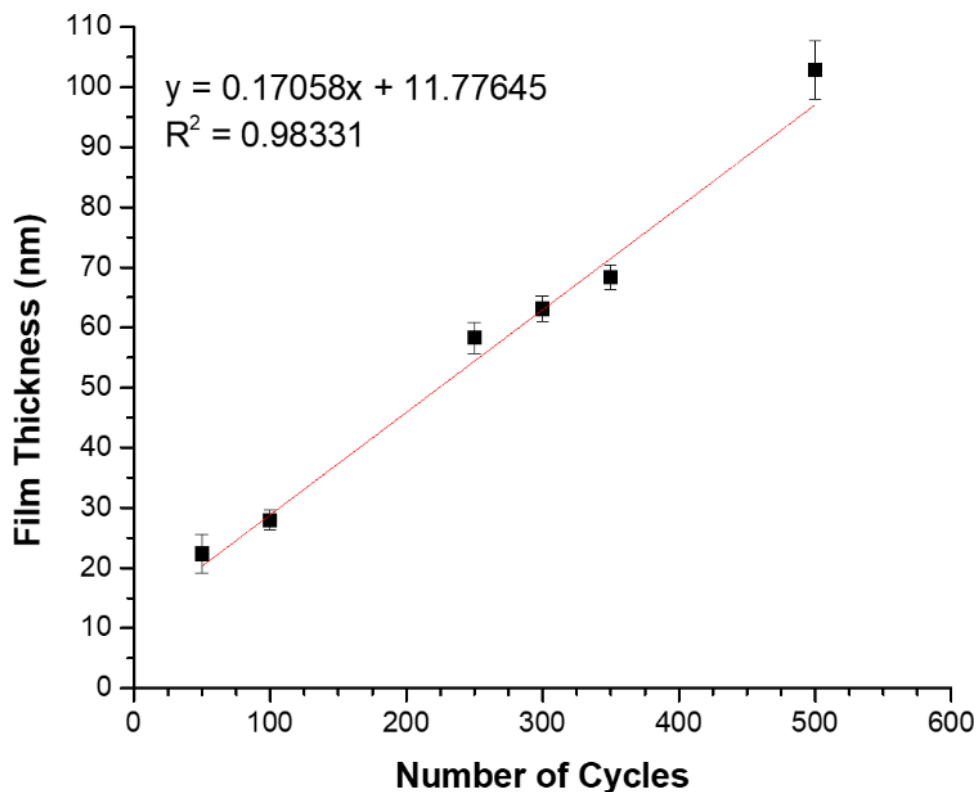


Figure 47. Film thickness versus number of cycles at 140 °C on TiN.

Aluminum metal films deposited using **5** were electrically discontinuous at all thicknesses. Film resistivities were measured immediately upon air exposure by four-point probe and the sheet resistivities were unchanged from the bare TiN substrate values. Figure 48 shows top-view SEM images of film growth at 140 °C after 100 and 300 cycles using AlCl<sub>3</sub> and **5** on TiN. The deposited film consists of discrete, discontinuous metal nanoparticles. No change in resistivity from the bare TiN substrate values was observed. This morphology is significantly different than the previous aluminum metal ALD report, in which the films were continuous and highly conductive at similar film thicknesses.<sup>170</sup> Nevertheless, the films were crystalline aluminum metal according to GIXRD analysis.



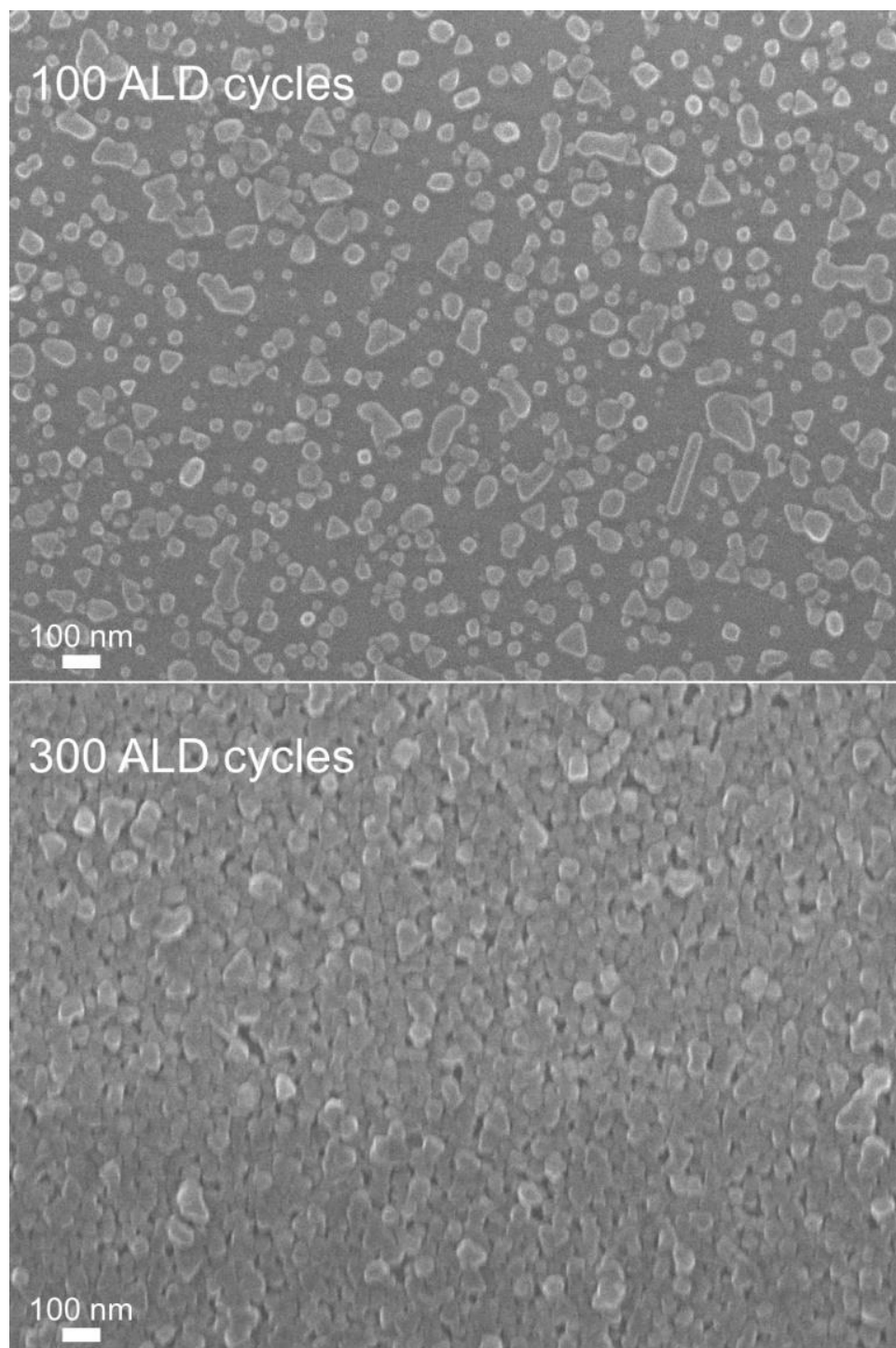


Figure 48. Top-view SEM images of Al metal films grown on TiN substrates at 140 °C after 100 cycles (top) or 300 cycles (bottom) using  $\text{AlCl}_3$  and **5**.

Film composition was measured by XPS on a representative film deposited at 140 °C after 300 cycles. The film was exposed to air prior to XPS analysis. Before Ar ion sputtering, the film surface composition was primarily oxidized aluminum with some adventitious carbon contamination. Ionizations corresponding to the binding energies for both aluminum oxide ( $\text{Al}_2\text{O}_3$ ) and aluminum metal ( $\text{Al}^0$ ) were observed before any sputtering in the Al 2p core level scan and the intensity of the  $\text{Al}^0$  ionization increased after sputtering to remove the oxidized surface layers. After 10 min of Ar ion sputtering, the film composition was 50.23 at.% Al, 38.25 at.% O, 7.01 at.% C, 3.62 at.% N, and 0.88 at.% Cl. In the Al 2p core level scan shown in Figure 49, the ionizations corresponding to  $\text{Al}_2\text{O}_3$  and  $\text{Al}^0$  have approximately equal peak areas. In the previously reported aluminum metal ALD process using  $\text{AlH}_2(\text{tBuNCH}_2\text{CH}_2\text{NMe}_2)$ , the film contained a large amount of oxygen on the surface, but after sputtering the oxygen content was reduced to < 4 at.%.<sup>170</sup> The much higher oxygen content for the air-exposed aluminum metal film reported herein is explained by the discontinuous film morphology, which allows for rapid oxygen diffusion throughout most of the film.

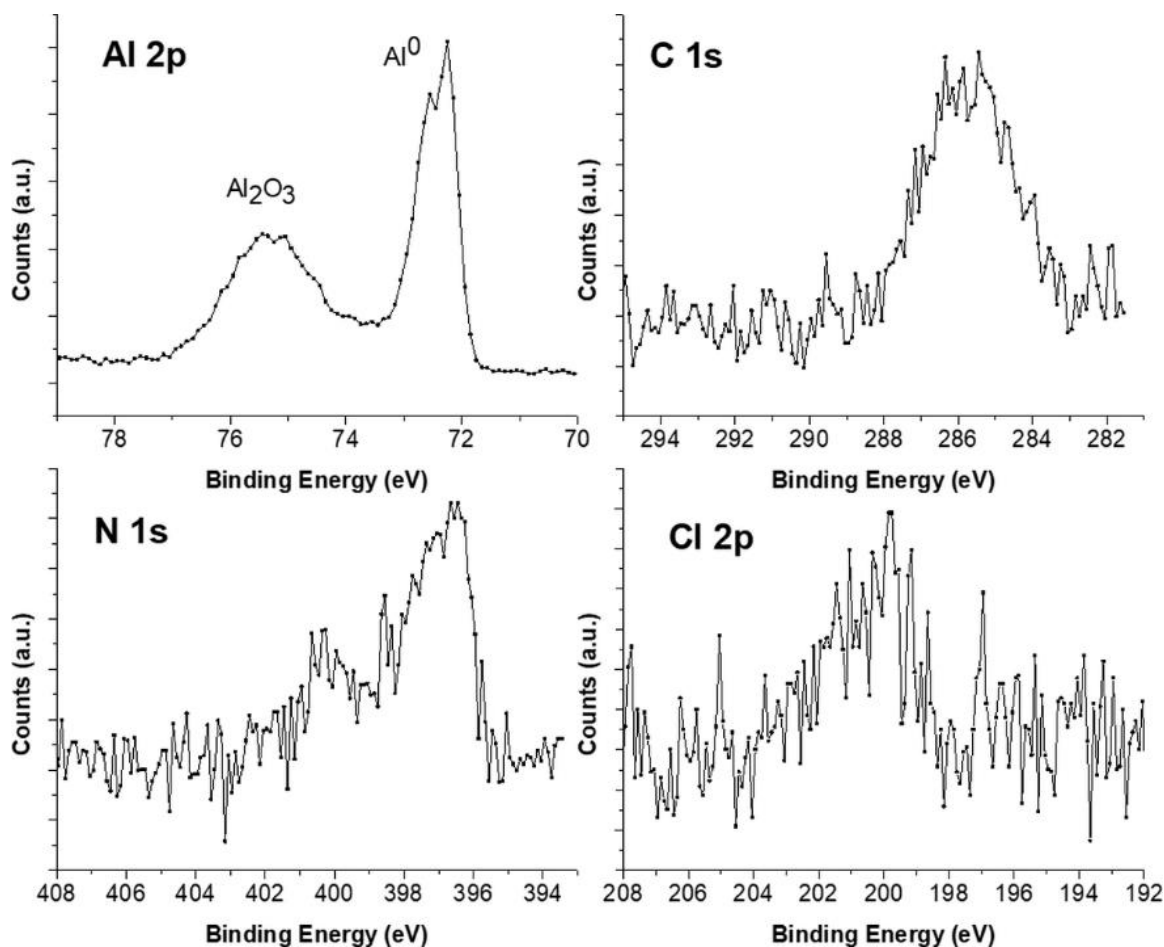


Figure 49. XPS core level scans after Ar ion sputtering of the Al 2p, C 1s, N 1s, and Cl 2p regions of an Al film deposited at 140 °C after 300 cycles.

Separate experiments performed during this study using  $\text{AlH}_2(\text{tBuNCH}_2\text{CH}_2\text{NMe}_2)$  instead of **5** produced highly conductive aluminum metal films. This confirmed that the source of the non-conductive aluminum films was the precursor (**5**) and not a different factor such as a leak in the ALD reactor. At this point it is unclear how **5** is modulating the film morphology in this way, but it may be related to the higher carbon content present in the aluminum metal film deposited using **5** compared to the previously reported process using  $\text{AlH}_2(\text{tBuNCH}_2\text{CH}_2\text{NMe}_2)$ .<sup>170</sup>

## 6.4 Conclusions

This chapter describes the synthesis, molecular structure, and thermal properties of the unexpected dialane complex **5** resulting from ring expansion of the saturated NHC 1,3-di-*tert*-butylimidazolin-2-ylidene. Complex **5** has promising ALD precursor characteristics in terms of volatility, thermal stability, and reactivity. Treatment of **5** with  $\text{Cp}_2\text{TiCl}_2$  as a model for metal-containing ALD precursor produced the structurally characterized hydride-bridged Ti(III)-Al heterobimetallic complex **6**. An aluminum metal ALD film growth study was carried out using  $\text{AlCl}_3$  and **5** as precursors on TiN substrates. Self-limiting film growth was demonstrated for both precursors and an ALD window was observed between 120-140 °C. The films consisted of electrically discontinuous crystalline aluminum metal particles, which is a significantly different film morphology compared to previous aluminum metal ALD processes.<sup>114,115,170</sup> Small differences in ALD precursors, even between aluminum hydride co-reactants, can clearly have a strong influence on film characteristics.

## CHAPTER 7

### CONCLUSIONS

This dissertation reports the synthesis, characterization, and evaluation as ALD precursors of several new aluminum hydride complexes. The complexes were synthesized by protonolysis of the ligand precursor by aluminum trihydride diethyl etherate to generate the corresponding aluminum dihydride complexes **1**, **3**, and **4**, by treatment of a stable NHC with  $\text{LiAlH}_4$  to produce a neutral NHC- $\text{AlH}_3$  complex (**7-9**), or unexpectedly by ring-expansion of a saturated N-heterocyclic carbene by two equivalents of  $\text{AlH}_3(\text{NMe}_3)$  to produce the unusual dialane complex **5**. These complexes were characterized by  $^1\text{H}$  and  $^{13}\text{C}$  NMR spectroscopy, IR spectroscopy, CHN elemental analysis, melting point and solid-state thermal decomposition experiments, thermogravimetric analysis (TGA), and single crystal X-ray diffraction analysis in some cases.

Complex **1** was first evaluated as an ALD reducing co-reactant with  $\text{AlCl}_3$  as the metal precursor, which resulted in the first thermal ALD process for aluminum metal films (Chapter 2). High purity aluminum metal films were grown at low temperatures with an ALD window between 120-160 °C at a growth rate of 3.5 Å/cycle. Importantly, self-limited growth was demonstrated for both precursors and the resulting thin films had resistivities as low as 3.03  $\mu\Omega\cdot\text{cm}$ , which is close to the bulk resistivity of aluminum metal. The development of a low temperature thermal ALD process for aluminum metal films represents a major advance for the field of non-noble metal ALD.

Complex **1** was then tested with  $\text{TiCl}_4$  as the metal precursor in the hopes of developing a titanium metal ALD process. Instead of titanium metal, conductive titanium carbonitride films were deposited with an ALD window between 220-400 °C (Chapter 3). Remarkably, self-limited

growth was establishing at 300 °C, which is well above the solid-state thermal decomposition temperature of **1**, which is ca. 185 °C, leading to films with low aluminum content. A similar aluminum dihydride complex, **3**, also deposited titanium carbonitride films despite its slightly higher solid-state thermal decomposition point and modified structure compared to **1**.

Chapter 4 explored the use of trimethylaluminum, a ubiquitous ALD precursor, and  $\text{WCl}_6$  as the metal precursor in thermal ALD of tungsten carbide films. An ALD window between 275-350 °C was observed with a growth rate of 1.5-1.8 Å/cycle. XPS analysis of a film deposited at 300 °C showed roughly 1:1 tungsten:carbon stoichiometry with aluminum impurities below the detection limit. When **1** was tested with  $\text{WCl}_6$ , tungsten carbide films were also deposited and with a growth rate of 1.6 Å/cycle within an ALD window between 275-350 °C (Chapter 5). Using **1** instead of trimethylaluminum resulted in a tungsten:carbon ratio between 2.8-3.7, which is greater than the tungsten-rich  $\text{W}_2\text{C}$  phase. The resistivities of the tungsten carbide films deposited using **1** were lower than the films deposited using trimethylaluminum, which is consistent with the tungsten-rich composition, but were still quite high compared to bulk tungsten carbide resistivity values. XRR analysis revealed film densities were 50-60% of bulk tungsten carbide values, which likely explain the high resistivities. Once again, aluminum content was low by XPS in a film deposited at 300 °C, but the nitrogen content was also low (< 4 at.%) compared to the titanium carbonitride films also deposited using **1**.

Other aluminum hydride complexes were explored to potentially reduce carbon and nitrogen incorporation in thermal ALD processes for electropositive metal films. The unusual dialane complex **5** was tested in aluminum metal ALD growth (Chapter 6). Aluminum metal films were deposited within an ALD window between 120-140 °C. These films were electrically discontinuous, which highlights the difference small changes in precursors can have on film

properties. The films deposited using **5** had slightly higher carbon content compared to films deposited using **1**, but the source of the dramatically different film morphologies will require further experimentation. Nevertheless, the films were crystalline aluminum metal by GIXRD analysis.

Aluminum hydride-based ALD precursors have not been reported prior to the work presented in this dissertation. The high reactivity of Al-H bonds present great advantages over other reducing co-reactants and useful ALD precursors can be obtained with proper chemical design of the supporting ligand. The reports of ALD processes using aluminum hydride co-reactants presented in this dissertation are barely scratching the surface of potential precursor combinations and many useful ALD processes will be discovered using aluminum hydride-based ALD chemistry in the coming years.

## APPENDIX PERMISSION/LICENSE AGREEMENTS FOR COPYRIGHTED MATERIAL

Permission for Blakeney, K. J.; Winter, C. H. *Chem. Mater.* **2018**, *30*, 1844–1848. Copyright 2018 American Chemical Society.

7/2/2018

Rightslink® by Copyright Clearance Center



# RightsLink®

Home

Create Account

Help



**ACS Publications**  
Most Trusted. Most Cited. Most Read.

**Title:** Atomic Layer Deposition of Aluminum Metal Films Using a Thermally Stable Aluminum Hydride Reducing Agent

**Author:** Kyle J. Blakeney, Charles H. Winter

**Publication:** Chemistry of Materials

**Publisher:** American Chemical Society

**Date:** Mar 1, 2018

Copyright © 2018, American Chemical Society

### LOGIN

If you're a [copyright.com](#) user, you can login to RightsLink using your [copyright.com](#) credentials. Already a [RightsLink](#) user or want to [learn more?](#)

### PERMISSION/LICENSE IS GRANTED FOR YOUR ORDER AT NO CHARGE

This type of permission/license, instead of the standard Terms & Conditions, is sent to you because no fee is being charged for your order. Please note the following:

- Permission is granted for your request in both print and electronic formats, and translations.
- If figures and/or tables were requested, they may be adapted or used in part.
- Please print this page for your records and send a copy of it to your publisher/graduate school.
- Appropriate credit for the requested material should be given as follows: "Reprinted (adapted) with permission from (COMPLETE REFERENCE CITATION). Copyright (YEAR) American Chemical Society." Insert appropriate information in place of the capitalized words.
- One-time permission is granted only for the use specified in your request. No additional uses are granted (such as derivative works or other editions). For any other uses, please submit a new request.

[BACK](#)
[CLOSE WINDOW](#)

Copyright © 2018 [Copyright Clearance Center, Inc.](#) All Rights Reserved. [Privacy statement.](#) [Terms and Conditions.](#) Comments? We would like to hear from you. E-mail us at [customercare@copyright.com](mailto:customercare@copyright.com)



Permission for Blakeney K. J.; Martin, P. D.; Winter, C. H. *Dalton Trans.* **2018**, 48, in press,  
DOI: 10.1039/C8DT02508H. Copyright 2018, The Royal Society of Chemistry.

The Royal Society of Chemistry does not require authors to obtain official permission to reproduce published papers in their own dissertation as long as proper acknowledgment is given.

Permission for Blakeney, K. J.; Winter, C. H. *J. Vac. Sci. Technol. A* **2018**, *36*, 01A104.

Copyright 2018 AIP Publishing

“AIP Publishing permits authors to include their published articles in a thesis or dissertation. It is understood that the thesis or dissertation may be published in print and/or electronic form and offered for sale on demand, as well as included in a university’s repository. Formal permission from AIP Publishing is not needed.”

<https://publishing.aip.org/authors/copyright-reuse>, accessed July 2, 2018.

Permission for Blakeney, K. J.; Ward, C. L.; Winter, C. H. *ECS Trans.* **2018**, 86, in press.

Copyright 2018 The Electrochemical Society.

The Electrochemical Society does not require authors to obtain official permission to reproduce their own published papers as long as proper acknowledgment is given and the ECS-formatted version is not used for this purpose.

<http://ecsdl.org/site/ecs/copyright.xhtml>, accessed July 23, 2018.

## REFERENCES

- (1) Kim, H. *J. Vac. Sci. Technol. B* **2003**, *21*, 2231–2261.
- (2) Moore, G. E. *Electronics* **1965**, *38*, 114–117.
- (3) *International Technology Roadmap for Semiconductors*; 2015. <http://www.itrs2.net>.
- (4) Kim, H.; Lee, H. B. R.; Maeng, W. J. *Thin Solid Films* **2009**, *517*, 2563–2580.
- (5) Creighton, J. R.; Parmeter, J. *Crit. Rev. Solid State Mater. Sci.* **1993**, *18*, 175–237.
- (6) Leskelä, M.; Ritala, M. *Angew. Chem. Int. Ed.* **2003**, *42*, 5548–5554.
- (7) George, S. M. *Chem. Rev.* **2010**, *110*, 111–131.
- (8) Levy, R. A.; Green, M. L. *J. Electrochem. Soc.* **1987**, *134*, 37C–49C.
- (9) Zhang, Z.; Lagally, M. G. *Science* **1997**, *276*, 377–383.
- (10) Pedersen, H. *Chem. Mater.* **2016**, *28*, 691–699.
- (11) Gladfelter, W. L. *Chem. Mater.* **1993**, *5*, 1372–1388.
- (12) Mackus, A. J. M.; Bol, A. A.; Kessels, W. M. M. *Nanoscale* **2014**, *6*, 10941–10960.
- (13) Puurunen, R. L. *Chem. Vap. Deposition* **2014**, *20*, 332–344.
- (14) Parsons, G. N.; George, S. M.; Knez, M. *MRS Bull.* **2011**, *36*, 865–871.
- (15) Suntola, T.; Hyvärinen, J. *Annu. Rev. Mater. Res.* **1985**.
- (16) Alvaro, E.; Yanguas-Gil, A. *PLoS One* **2018**, *13*, 1–19.
- (17) Haukka, S. *ECS Trans.* **2007**, *3*, 15–26.
- (18) Puurunen, R. L. *J. Appl. Phys.* **2005**, *97*, 121301.
- (19) Hair, M. L.; Hertl, W. *J. Phys. Chem.* **1970**, *74*, 91–94.
- (20) Profijt, H. B.; Potts, S. E.; van de Sanden, M. C. M.; Kessels, W. M. M. *J. Vac. Sci. Technol. A* **2011**, *29*, 050801.
- (21) Rossnagel, S. M.; Sherman, A.; Turner, F. *J. Vac. Sci. Technol. B* **2000**, *18*, 2016–2020.

- (22) Kim, H.; Rossnagel, S. M. *J. Vac. Sci. Technol. A* **2002**, *20*, 802–808.
- (23) Kim, H.; Rossnagel, S. M. *Thin Solid Films* **2003**, *441*, 311–316.
- (24) Li, W.-M. *Chem. Vap. Deposition* **2013**, *19*, 82–103.
- (25) Alon, U. *Mol. Cell* **2009**, *35*, 726–728.
- (26) Miikkulainen, V.; Leskelä, M.; Ritala, M.; Puurunen, R. L. *J. Appl. Phys.* **2013**, *113*, 021301.
- (27) Knisley, T. J.; Kalutarage, L. C.; Winter, C. H. *Coord. Chem. Rev.* **2013**, *257*, 3222–3231.
- (28) Bahlawane, N.; Kohse-Höinghaus, K.; Premkumar, P. A.; Lenoble, D. *Chem. Sci.* **2012**, *3*, 929–941.
- (29) Elliott, S. D.; Dey, G.; Maimaiti, Y. *J. Chem. Phys.* **2017**, *146*, 052822.
- (30) Aaltonen, T.; Ritala, M.; Tung, Y.-L.; Chi, Y.; Arstila, K.; Meinander, K.; Leskelä, M. *J. Mater. Res.* **2004**, *19*, 3353–3358.
- (31) Ritala, M.; Leskelä, M.; Rauhala, E.; Haussalo, P. *J. Electrochem. Soc.* **1987**, *70*, 322–324.
- (32) Ritala, M.; Kalsi, P.; Riihelä, D. *Chem. Mater.* **1999**, *11*, 1712–1718.
- (33) Juppo, M.; Vehkamäki, M.; Ritala, M.; Leskelä, M. *J. Vac. Sci. Technol. A* **1998**, *16*, 2845–2850.
- (34) Utriainen, M.; Kröger-Laukkanen, M.; Johansson, L. S.; Niinistö, L. *Appl. Surf. Sci.* **2000**, *157*, 151–158.
- (35) Lim, B. S.; Rahtu, A.; Gordon, R. G. *Nat. Mater.* **2003**, *2*, 749–754.
- (36) Klaus, J. W.; Ferro, S. J.; George, S. M. *Thin Solid Films* **2000**, *360*, 145–153.
- (37) Grubbs, R. K.; Steinmetz, N. J.; George, S. M. *J. Vac. Sci. Technol. B* **2004**, *22*, 1811–1821.

- (38) Fabreguette, F. H.; Sechrist, Z. A.; Elam, J. W.; George, S. M. *Thin Solid Films* **2005**, *488*, 103–110.
- (39) Luoh, T.; Su, C. T.; Yang, T. H.; Chen, K. C.; Lu, C. Y. *Microelectron. Eng.* **2008**, *85*, 1739–1747.
- (40) Kalanyan, B.; Losego, M. D.; Oldham, C. J.; Parsons, G. N. *Chem. Vap. Deposition* **2013**, *19*, 161–166.
- (41) Seghete, D.; Rayner, G. B.; Cavanagh, A. S.; Anderson, V. R.; George, S. M. *Chem. Mater.* **2011**, *23*, 1668–1678.
- (42) Lemonds, A. M.; White, J. M.; Ekerdt, J. G. *Surf. Sci.* **2003**, *538*, 191–203.
- (43) Lemonds, A. M.; Bolom, T.; Ahearn, W. J.; Gay, D. C.; White, J. M.; Ekerdt, J. G. *Thin Solid Films* **2005**, *488*, 9–14.
- (44) Liu, X.; Wu, Y. D.; Cai, H.; Yang, Y.; Chen, T.; Vallet, C. E.; Zuhr, R. A.; Beach, D. B.; Peng, Z. H.; Wu, Z.; Concolino, T. E.; Rheingold, A. L.; Xue, Z. *J. Am. Chem. Soc.* **2001**, *123*, 8011–8021.
- (45) Schwarzkopf, P.; Kieffer, R. *Refractory Hard Metals*; Macmillan Co.: New York, 1953.
- (46) Levy, R. B.; Boudart, M. *Science* **1973**, *181*, 547–549.
- (47) Hwu, H. H.; Chen, J. G. *Chem. Rev.* **2005**, *105*, 185–212.
- (48) Dai, T.; Li, C.; Li, L.; Zhao, Z. K.; Zhang, B.; Cong, Y.; Wang, A. *Angew. Chem. Int. Ed.* **2018**, *57*, 1808–1812.
- (49) Högberg, H.; Tägtström, P.; Lu, J.; Jansson, U. *Thin Solid Films* **1996**, *272*, 116–123.
- (50) Beadle, K. A.; Gupta, R.; Mathew, A.; Chen, J. G.; Willis, B. G. *Thin Solid Films* **2008**, *516*, 3847–3854.
- (51) Sun, Y. M.; Lee, S. Y.; Lemonds, A. M.; Engbrecht, E. R.; Veldman, S.; Lozano, J.;

- White, J. M.; Ekerdt, J. G.; Emesh, I.; Pfeifer, K. *Thin Solid Films* **2001**, *397*, 109–115.
- (52) Xue, Z.; Caulton, K. G.; Chisholm, M. H. *Chem. Mater.* **1991**, *3*, 384–386.
- (53) Jipa, I.; Heinemann, F. W.; Schneider, A.; Popovska, N.; Siddiqi, M. A.; Siddiqui, R. A.; Atakan, B.; Marbach, H.; Papp, C.; Steinrück, H. P.; Zenneck, U. *Chem. Vap. Deposition* **2010**, *16*, 239–247.
- (54) Blakeney, K. J.; Winter, C. H. *J. Vac. Sci. Technol. A* **2018**, *36*, 01A104.
- (55) Kafizas, A.; Carmalt, C. J.; Parkin, I. P. *Coord. Chem. Rev.* **2013**, *257*, 2073–2119.
- (56) Winter, C. H.; Sheridan, P. H.; Lewkebandara, T. S.; Heeg, M. J. *J. Am. Chem. Soc.* **1992**, *114*, 1095–1097.
- (57) Dey, S.; Yu, K.-H.; Consiglio, S.; Tapily, K.; Hakamata, T.; Wajda, C. S.; Leusink, G. J.; Jordan-Sweet, J.; Lavoie, C.; Muir, D.; Moreno, B.; Diebold, A. C. *J. Vac. Sci. Technol. A* **2017**, *35*, 03E109.
- (58) Ritala, M.; Leskelä, M.; Dekker, J.-P.; Mutsaers, C.; Soininen, P. J.; Skarp, J. *Chem. Vap. Deposition* **1999**, *5*, 7–9.
- (59) Elam, J. W.; Schuisky, M.; Ferguson, J. D.; George, S. M. *Thin Solid Films* **2003**, *436*, 145–156.
- (60) Lima, L. P. B.; Dekkers, H. F. W.; Lisoni, J. G.; Diniz, J. A.; Van Elshocht, S.; De Gendt, S. *J. Appl. Phys.* **2014**, *115*, 074504.
- (61) Juppo, M.; Alén, P.; Ritala, M.; Leskelä, M. *Chem. Vap. Deposition* **2001**, *7*, 211–217.
- (62) Lee, Y. J.; Kang, S.-W. *Electrochem. Solid-State Lett.* **2003**, *6*, C70–C72.
- (63) Girolami, G. S.; Jensen, J. A.; Pollina, D. M.; Allocca, C. M.; Kaloyeros, A. E.; Williams, W. S. *J. Am. Chem. Soc.* **1987**, *109*, 1579–1580.
- (64) Cheon, J.; Dubois, L. H.; Girolami, G. S. *J. Am. Chem. Soc.* **1997**, *119*, 6814–6820.

- (65) Xiang, J.; Li, T.; Zhang, Y.; Wang, X.; Gao, J.; Cui, H.; Yin, H.; Li, J.; Wang, W.; Ding, Y.; Xu, C.; Zhao, C. *ECS J. Solid State Sci. Technol.* **2015**, *4*, 441–444.
- (66) Wei, C.; Fin Lin, J.; Jiang, T. H.; Ai, C. F. *Thin Solid Films* **2001**, *381*, 94–103.
- (67) Bull, S. J.; Bhat, D. G.; Staia, M. H. *Surf. Coatings Technol.* **2003**, *163–164*, 507–514.
- (68) Carmalt, C. J.; Newport, A. C.; O'Neill, S. A.; Parkin, I. P.; White, A. J. P.; Williams, D. *J. Inorg. Chem.* **2005**, *44*, 615–619.
- (69) Jeon, S.; Park, S. *J. Electrochem. Soc.* **2010**, *157*, H930–H933.
- (70) Blakeney, K. J.; Martin, P. D.; Winter, C. H. *submitted*.
- (71) Lee, B. H.; Hwang, J. K.; Nam, J. W.; Lee, S. U.; Kim, J. T.; Koo, S.-M.; Baunemann, A.; Fischer, R. A.; Sung, M. M. *Angew. Chem. Int. Ed.* **2009**, *48*, 4536–4539.
- (72) Vidjayacoumar, B.; Emslie, D. J. H.; Blackwell, J. M.; Clendenning, S. B.; Britten, J. F. *Chem. Mater.* **2010**, *22*, 4854–4866.
- (73) Vidjayacoumar, B.; Emslie, D. J. H.; Clendenning, S. B.; Blackwell, J. M.; Britten, J. F.; Rheingold, A. *Chem. Mater.* **2010**, *22*, 4844–4853.
- (74) Knisley, T. J.; Ariyasena, T. C.; Sajavaara, T.; Saly, M. J.; Winter, C. H. *Chem. Mater.* **2011**, *23*, 4417–4419.
- (75) Dey, G.; Elliott, S. D. *RSC Adv.* **2014**, *4*, 34448.
- (76) Kalutarage, L. C.; Clendenning, S. B.; Winter, C. H. *Chem. Mater.* **2014**, *26*, 3731–3738.
- (77) Kalutarage, L. C.; Clendenning, S. B.; Winter, C. H. *ECS Trans.* **2014**, *64*, 147–157.
- (78) Dhakal, D.; Assim, K.; Lang, H.; Bruener, P.; Grehl, T.; Georgi, C.; Waechtler, T.; Ecke, R.; Schulz, S. E.; Gessner, T. *J. Vac. Sci. Technol. A* **2016**, *34*, 01A111.
- (79) Väyrynen, K.; Mizohata, K.; Räisänen, J.; Peeters, D.; Devi, A.; Ritala, M.; Leskelä, M. *Chem. Mater.* **2017**, *29*, 6502–6510.



- (80) Hagen, D. J.; Connolly, J.; Povey, I. M.; Rushworth, S.; Pemble, M. E. *Adv. Mater. Interfaces* **2017**, *4*, 1700274.
- (81) Knisley, T. J.; Saly, M. J.; Heeg, M. J.; Roberts, J. L.; Winter, C. H. *Organometallics* **2011**, *30*, 5010–5017.
- (82) Klesko, J. P.; Kerrigan, M. M.; Winter, C. H. *Chem. Mater.* **2016**, *28*, 700–703.
- (83) Kerrigan, M. M.; Klesko, J. P.; Winter, C. H. *Chem. Mater.* **2017**, *29*, 7458–7466.
- (84) Kerrigan, M. M.; Klesko, J. P.; Rupich, S. M.; Dezelah, C. L.; Kanjolia, R. K.; Chabal, Y. J.; Winter, C. H. *J. Chem. Phys.* **2017**, *146*, 052813.
- (85) Kerrigan, M. M.; Klesko, J. P.; Blakeney, K. J.; Winter, C. H. *ACS Appl. Mater. Interfaces* **2018**, *10*, 14200–14208.
- (86) Sarr, M.; Bahlawane, N.; Arl, D.; Dossot, M.; McRae, E.; Lenoble, D. *J. Phys. Chem. C* **2014**, *118*, 23385–23392.
- (87) Klesko, J. P.; Thrush, C. M.; Winter, C. H. *Chem. Mater.* **2015**, *27*, 4918–4921.
- (88) Kaim, W. *J. Am. Chem. Soc.* **1983**, *105*, 707–713.
- (89) Tsurugi, H.; Tanahashi, H.; Nishiyama, H.; Fegler, W.; Saito, T.; Sauer, A.; Okuda, J.; Mashima, K. *J. Am. Chem. Soc.* **2013**, *135*, 5986–5989.
- (90) Yurino, T.; Ueda, Y.; Shimizu, Y.; Tanaka, S.; Nishiyama, H.; Tsurugi, H.; Sato, K.; Mashima, K. *Angew. Chem. Int. Ed.* **2015**, *54*, 14437–14441.
- (91) Saito, T.; Nishiyama, H.; Tanahashi, H.; Kawakita, K.; Tsurugi, H.; Mashima, K. *J. Am. Chem. Soc.* **2014**, *136*, 5161–5170.
- (92) Arteaga-Müller, R.; Tsurugi, H.; Saito, T.; Yanagawa, M.; Oda, S.; Mashima, K. *J. Am. Chem. Soc.* **2009**, *131*, 5370–5371.
- (93) Tsurugi, H.; Saito, T.; Tanahashi, H.; Arnold, J.; Mashima, K. *J. Am. Chem. Soc.* **2011**,

- 18673–18683.
- (94) *CRC Handbook of Chemistry and Physics*; Rumble, J. R., Ed.; 98th ed.; CRC Press/Taylor & Francis: Boca Raton, FL, 2018.
- (95) Knight, M. W.; King, N. S.; Liu, L.; Everitt, H. O.; Nordlander, P.; Halas, N. J. *ACS Nano* **2014**, *8*, 834–840.
- (96) Berner, M. K.; Zarko, V. E.; Talawar, M. B. *Combust. Explos. Shock Waves* **2013**, *49*, 625–647.
- (97) Adams, D. P. *Thin Solid Films* **2015**, *576*, 98–128.
- (98) Marín, L.; Gao, Y.; Vallet, M.; Abdallah, I.; Warot-Fonrose, B.; Tenailleau, C.; Lucero, A. T.; Kim, J.; Esteve, A.; Chabal, Y. J.; Rossi, C. *Langmuir* **2017**, *33*, 11086–11093.
- (99) Luo, B.; Gladfelter W. L. In *Chemical Vapour Deposition: Precursors, Processes and Applications*; Jones, A. C., Hitchman, M. L., Eds.; RSC Publishing: Cambridge, 2009; pp 320–356.
- (100) Levy, R. A.; Hill, M. J. *Electrochem. Soc.* **1984**, *131*, 2175–2182.
- (101) Green, M. L.; Levy, R. A.; Nuzzo, R. G.; Coleman, E. *Thin Solid Films* **1984**, *114*, 367–377.
- (102) Kondoh, E.; Ohta, T. *J. Vac. Sci. Technol. A* **1995**, *13*, 2863–2871.
- (103) Tanaka, K.; Yanashima, H.; Yako, T.; Kamio, K.; Sugai, K.; Kishida, S. *Appl. Surf. Sci.* **2001**, *171*, 71–81.
- (104) Gladfelter, W. L.; Boyd, D. C.; Jensen, K. F. *Chem. Mater.* **1989**, *1*, 339–343.
- (105) Gross, M. E.; Cheung, K. P.; Fleming, C. G.; Kovalchick, J.; Heimbrook, L. A. *J. Vac. Sci. Technol. A* **1991**, *9*, 57–64.
- (106) Liu, Y.; Overzet, L. J.; Goeckner, M. J. *Thin Solid Films* **2006**, *510*, 48–54.

- (107) Glass, J. A.; Kher, S. S.; Spencer, J. T. *Chem. Mater.* **1992**, *4*, 530–538.
- (108) Noya, A.; Sasaki, K. *Jpn. J. Appl. Phys.* **1991**, *30*, 624–627.
- (109) Prud'Homme, N.; Duguet, T.; Samélor, D.; Senocq, F.; Vahlas, C. *Appl. Surf. Sci.* **2013**, *283*, 788–793.
- (110) Xu, Q.; Chen, L. *ECS J. Solid State Sci. Technol.* **2014**, *3*, P60–P74.
- (111) Huang, R. P.; Tsai, T. C.; Lin, W.; Huang, H. F.; Tsai, M. C.; Hsu, H. K.; Hsu, C. M.; Lin, J. F.; Yang, C. L.; Wu, J. Y. *Microelectron. Eng.* **2013**, *106*, 56–62.
- (112) Hsien, Y. H.; Hsu, H. K.; Tsai, T. C.; Lin, W.; Huang, R. P.; Chen, C. H.; Yang, C. L.; Wu, J. Y. *Microelectron. Eng.* **2012**, *92*, 19–23.
- (113) Ragnarsson, L. A.; Chew, S. A.; Dekkers, H.; Luque, M. T.; Parvais, B.; De Keersgieter, A.; Devriendt, K.; Van Ammel, A.; Schram, T.; Yoshida, N.; Phatak, A.; Han, K.; Colombeau, B.; Brand, A.; Horiguchi, N.; Thean, A. V. Y. *Proc. Symp. VLSI Technol.* **2014**, 56–57.
- (114) Lee, Y. J.; Kang, S.-W. *Electrochem. Solid-State Lett.* **2002**, *5*, C91–C93.
- (115) Lee, Y. J.; Kang, S.-W. *J. Vac. Sci. Technol. A* **2002**, *20*, 1983–1988.
- (116) Hoffman, B. M.; Lukoyanov, D.; Yang, Z. Y.; Dean, D. R.; Seefeldt, L. C. *Chem. Rev.* **2014**, *114*, 4041–4062.
- (117) Lukoyanov, D.; Yang, Z. Y.; Khadka, N.; Dean, D. R.; Seefeldt, L. C.; Hoffman, B. M. *J. Am. Chem. Soc.* **2015**, *137*, 3610–3615.
- (118) Lukoyanov, D.; Khadka, N.; Yang, Z. Y.; Dean, D. R.; Seefeldt, L. C.; Hoffman, B. M. *J. Am. Chem. Soc.* **2016**, *138*, 10674–10683.
- (119) Harris, D. F.; Lukoyanov, D. A.; Shaw, S.; Compton, P.; Tokmina-Lukaszewska, M.; Bothner, B.; Kelleher, N.; Dean, D. R.; Hoffman, B. M.; Seefeldt, L. C. *Biochemistry*

- 2018**, 57, 701–710.
- (120) Shima, T.; Hou, Z. *Top Organomet Chem* **2017**, 60, 23–44.
- (121) Shima, T.; Hu, S.; Luo, G.; Kang, X.; Luo, Y.; Hou, Z. *Science* **2013**, 340, 1549–1552.
- (122) Hartwig, J. F. In *Organotransition Metal Chemistry*; University Science Books: Mill Valley, CA, 2010; pp. 122–146.
- (123) Harder, S. *Chem. Commun.* **2012**, 48, 11165–11177.
- (124) Yang, Z.; Zhong, M.; Ma, X.; Nijesh, K.; De, S.; Parameswaran, P.; Roesky, H. W. *J. Am. Chem. Soc.* **2016**, 138, 2548–2551.
- (125) Butler, M. J.; Crimmin, M. R. *Chem. Commun.* **2017**, 53, 1348–1365.
- (126) Li, W.; Ma, X.; Walawalkar, M. G.; Yang, Z.; Roesky, H. W. *Coord. Chem. Rev.* **2017**, 350, 14–29.
- (127) De Koning, A. J.; Boersma, J.; Van Der Kerk, G. J. M. *J. Organomet. Chem.* **1980**, 195, 1–12.
- (128) De Koning, A. J.; Boersma, J.; Van Der Kerk, G. J. M. *J. Organomet. Chem.* **1980**, 186, 159–172.
- (129) De Koning, A. J.; Boersma, J.; Van Der Kerk, G. J. M. *J. Organomet. Chem.* **1980**, 186, 173–184.
- (130) De Koning, A. J.; Budzelaar, P. H. M.; Van Aarssen, B. G. K.; Boersma, J.; Van Der Kerk, G. J. M. *J. Organomet. Chem.* **1981**, 217, C1–C4.
- (131) Rit, A.; Spaniol, T. P.; Maron, L.; Okuda, J. *Angew. Chem. Int. Ed.* **2013**, 52, 4664–4667.
- (132) Wiegand, A. K.; Rit, A.; Okuda, J. *Coord. Chem. Rev.* **2016**, 314, 71–82.
- (133) Mukherjee, D.; Okuda, J. *Angew. Chem. Int. Ed.* **2018**, 57, 1458–1473.
- (134) Bonyhady, S. J.; Collis, D.; Frenking, G.; Holzmann, N.; Jones, C.; Stasch, A. *Nat. Chem.*

- 2010**, 2, 865–869.
- (135) Arrowsmith, M.; Hill, M. S.; MacDougall, D. J.; Mahon, M. F. *Angew. Chem. Int. Ed.* **2009**, 48, 4013–4016.
- (136) Gardiner, M. G.; Raston, C. L. *Coord. Chem. Rev.* **1997**, 166, 1–34.
- (137) Jegier, J. A.; Gladfelter, W. L. *Coord. Chem. Rev.* **2000**, 206–207, 631–650.
- (138) Ruff, J. K.; Hawthorne, M. F. *J. Am. Chem. Soc.* **1960**, 82, 2141–2144.
- (139) Woong Jang, T.; Moon, W.; Tae Baek, J.; Tae Ahn, B. *Thin Solid Films* **1998**, 333, 137–141.
- (140) Gross, M. E.; Fleming, C. G.; Cheung, K. P.; Heimbrook, L. A. *J. Appl. Phys.* **1991**, 69, 2589–2592.
- (141) Atwood, J. L.; Butz, K. W.; Gardiner, M. G.; Jones, C.; Koutsantonis, G. A.; Raston, C. L.; Robinson, K. D. *Inorg. Chem.* **1993**, 32, 3482–3487.
- (142) Beachley, O. T.; Racette, K. C. *Inorg. Chem.* **1976**, 15, 2110–2115.
- (143) McMahon, C. N.; Francis, J. A.; Bott, S. G.; Barron, A. R. *J. Chem. Soc., Dalton Trans.* **1999**, 15, 67–72.
- (144) Choi, H.; Hwang, S. *Chem. Mater.* **1998**, 10, 2323–2325.
- (145) Gall, D. *J. Appl. Phys.* **2016**, 119, 085101.
- (146) Lagudu, U. R. K.; Chockalingam, A. M.; Babu, S. V. *ECS J. Solid State Sci. Technol.* **2013**, 2, Q77–Q82.
- (147) Chan, G. H.; Zhao, J.; Schatz, G. C.; Duyne, R. P. Van. *J. Phys. Chem. C* **2008**, 112, 13958–13963.
- (148) Knight, M. W.; Liu, L.; Wang, Y.; Brown, L.; Mukherjee, S.; King, N. S.; Everitt, H. O.; Nordlander, P.; Halas, N. J. *Nano Lett.* **2012**, 12, 6000–6004.

- (149) Taguchi, A.; Saito, Y.; Watanabe, K.; Yijian, S.; Kawata, S. *Appl. Phys. Lett.* **2012**, *101*, 081110.
- (150) McMahon, J. M.; Schatz, G. C.; Gray, S. K. *Phys. Chem. Chem. Phys.* **2013**, *15*, 5415–5423.
- (151) Sobhani, A.; Manjavacas, A.; Cao, Y.; McClain, M. J.; García De Abajo, F. J.; Nordlander, P.; Halas, N. J. *Nano Lett.* **2015**, *15*, 6946–6951.
- (152) Seayad, A. M.; Antonelli, D. M. *Adv. Mater.* **2004**, *16*, 765–777.
- (153) Fichtner, M. *Adv. Eng. Mater.* **2005**, *7*, 443–455.
- (154) Sakintuna, B.; Lamari-Darkrim, F.; Hirscher, M. *Int. J. Hydrogen Energy* **2007**, *32*, 1121–1140.
- (155) Luo, B.; Gladfelter, W. L. In *Chemical Vapour Deposition: Precursors, Processes and Applications*; Jones, A. C.; Hitchman, M. L., Eds.; RSC Publishing, 2009; pp. 320–356.
- (156) Ludviksson, A.; Nooney, M.; Bruno, R.; Bailey, A.; Kodas, T. T.; Hampden-Smith, M. J. *Chem. Vap. Deposition* **1998**, *4*, 129–132.
- (157) Aldridge, S.; Downs, A. J. *Chem. Rev.* **2001**, *101*, 3305–3365.
- (158) Wang, G.; Xu, Q.; Yang, T.; Luo, J.; Xiang, J.; Xu, J.; Xu, G.; Li, C.; Li, J.; Yan, J.; Zhao, C.; Chen, D.; Ye, T. *ECS Trans.* **2013**, *58*, 317–324.
- (159) Kim, D. H.; Kim, B. Y. *Korean J. Chem. Eng.* **2000**, *17*, 449–454.
- (160) Liu, Y.; Overzet, L.; Goeckner, M. *Thin Solid Films* **2007**, *515*, 6730–6736.
- (161) Crist, B. V. *Handbooks of Monochromatic XPS Spectra - The Elements and Native Oxides, Volume 1 in PDF*; XPS International LLC: Mountain View, CA, USA, 1999.
- (162) Schmidt, D. L.; Roberts, C. B.; Reigler, P. F. *Inorg. Synth.* **1973**, *14*, 47–52.
- (163) Hatanpää, T.; Ritala, M.; Leskelä, M. *Coord. Chem. Rev.* **2013**, *257*, 3297–3322.

- (164) Emslie, D. J. H.; Chadha, P.; Price, J. S. *Coord. Chem. Rev.* **2013**, *257*, 3282–3296.
- (165) Van Bui, H.; Grillo, F.; van Ommen, J. R. *Chem. Commun.* **2017**, *53*, 45–71.
- (166) Yoshitake, M. *J. Vac. Sci. Technol. A* **2014**, *32*, 061403.
- (167) Kalutarage, L. C.; Martin, P. D.; Heeg, M. J.; Winter, C. H. *J. Am. Chem. Soc.* **2013**, *135*, 12588–12591.
- (168) Mäkelä, M.; Hatanpää, T.; Mizohata, K.; Meinander, K.; Niinistö, J.; Räisänen, J.; Ritala, M.; Leskelä, M. *Chem. Mater.* **2017**, *29*, 2040–2045.
- (169) Mäkelä, M.; Hatanpää, T.; Ritala, M.; Leskelä, M.; Mizohata, K.; Meinander, K.; Räisänen, J. *J. Vac. Sci. Technol. A* **2017**, *35*, 01B112.
- (170) Blakeney, K. J.; Winter, C. H. *Chem. Mater.* **2018**, *30*, 1844–1848.
- (171) Carpene, E.; Schaaf, P.; Han, M.; Lieb, K. P.; Shinn, M. *Appl. Surf. Sci.* **2002**, *186*, 195–199.
- (172) Stricker, A.; Luithardt, W.; Benndorf, C. *Diam. Relat. Mater.* **1999**, *8*, 500–503.
- (173) Barry, S. T.; Gordon, R. *Mat. Res. Soc. Symp. Proc.* **2000**, *606*, 83–89.
- (174) Park, K.-H.; Marshall, W. J. *J. Am. Chem. Soc.* **2005**, *127*, 9330–9331.
- (175) McDonnell, S.; Longo, R. C.; Seitz, O.; Ballard, J. B.; Mordi, G.; Dick, D.; Owen, J. H. G.; Randall, J. N.; Kim, J.; Chabal, Y. J.; Cho, K.; Wallace, R. M. *J. Phys. Chem. C* **2013**, *117*, 20250–20259.
- (176) Greczynski, G.; Petrov, I.; Greene, J. E.; Hultman, L. *J. Vac. Sci. Technol. A* **2015**, *33*, 05E101.
- (177) Lemonds, A. M.; Kershen, K.; Bennett, J.; Pfeifer, K.; Sun, Y.-M.; White, J. M.; Ekerdt, J. G. *J. Mater. Res.* **2002**, *17*, 1320–1328.
- (178) Esteve, J.; Zambrano, G.; Rincon, C.; Martinez, E.; Galindo, H.; Prieto, P. *Thin Solid*

- Films* **2000**, 373, 282–286.
- (179) Wang, S. J.; Tsai, H. Y.; Sun, S. C.; Shiao, M. H. *J. Electrochem. Soc.* **2001**, 148, G500–G506.
- (180) Romanus, H.; Cimalla, V.; Schaefer, J. A.; Spieß, L.; Ecke, G.; Pezoldt, J. *Thin Solid Films* **2000**, 359, 146–149.
- (181) Weigert, E. C.; Humbert, M. P.; Mellinger, Z. J.; Ren, Q.; Beebe, Jr., T. P.; Bao, L.; Chen, J. G. *J. Vac. Sci. Technol. A* **2008**, 26, 23.
- (182) Kim, D. H.; Kim, Y. J.; Song, Y. S.; Lee, B. T.; Kim, J. H.; Suh, S.; Gordon, R. J. *Electrochem. Soc.* **2003**, 150, C740–C744.
- (183) Kim, J. B.; Jang, B.; Lee, H. J.; Han, W. S.; Lee, D. J.; Lee, H. B. R.; Hong, T. E.; Kim, S. H. *Mater. Lett.* **2016**, 168, 218–222.
- (184) Härkönen, K.; Doczy, M.; Lang, T.; Baxter, N. E. U.S. patent 0208994, October 21, 2004.
- (185) Klug, J. A.; Proslie, T.; Elam, J. W.; Cook, R. E.; Hiller, J. M.; Claus, H.; Becker, N. G.; Pellin, M. J. *J. Phys. Chem. C* **2011**, 115, 25063–25071.
- (186) Lee, A.; Fuchigami, N.; Pisharoty, D.; Hong, Z.; Haywood, E.; Joshi, A.; Mujumdar, S.; Bodke, A.; Karlsson, O.; Kim, H.; Choi, K.; Besser, P. *J. Vac. Sci. Technol. A* **2014**, 32, 01A118.
- (187) Jourdan, A.; Morel, B. *J. Fluor. Chem.* **2001**, 107, 255–264.
- (188) Lemaire, P. C.; Parsons, G. N. *Chem. Mater.* **2017**, 29, 6653–6665.
- (189) Kim, S.-H.; Kim, J.-K.; Kwak, N.; Sohn, H.; Kim, J.; Jung, S.-H.; Hong, M.-R.; Lee, S. H.; Collins, J. *Electrochem. Solid-State Lett.* **2006**, 9, C54.
- (190) Klaus, J. W.; Ferro, S. J.; George, S. M. *J. Electrochem. Soc.* **2000**, 147, 1175–1181.
- (191) Kim, S.-H.; Oh, S. S.; Kim, H.-M.; Kang, D.-H.; Kim, K.-B.; Li, W.-M.; Haukka, S.;



- Tuominen, M. *J. Electrochem. Soc.* **2004**, *151*, C272–C282.
- (192) Sundqvist, J. “BALD Engineering,”  
<http://www.blog.baldengineering.com/2016/08/entegris-launch-fluorine-free-tungsten.html> (accessed Jun 20, 2017).
- (193) Puurunen, R. L.; Lindblad, M.; Root, A.; Outi I. Krause, A. *Phys. Chem. Chem. Phys.* **2001**, *3*, 1093–1102.
- (194) Yamashita, S.; Watanuki, K.; Ishii, H.; Shiba, Y.; Kitano, M.; Shirai, Y.; Sugawa, S.; Ohmi, T. *J. Electrochem. Soc.* **2011**, *158*, 93–96.
- (195) Kim, T.; Zaera, F. *J. Phys. Chem. C* **2011**, *115*, 8240–8247.
- (196) Xie, Q.; Jiang, Y.; Detavernier, C.; Meirhaeghe, R. L. Van; Qu, X. *2006 8th International Conference on Solid-State and Integrated Circuit Technology Proceedings* **2006**, *87*, 2535.
- (197) Xie, Q.; Jiang, Y. L.; De Keyser, K.; Detavernier, C.; Deduytsche, D.; Ru, G. P.; Qu, X. P.; Tu, K. N. *Microelectron. Eng.* **2010**, *87*, 2535–2539.
- (198) Lee, S. Y.; Ju, B.; Kim, Y. T. *Jpn. J. Appl. Phys.* **2018**, *57*, 04FC01.
- (199) Kim, J. B.; Kim, S.-H.; Han, W. S.; Lee, D.-J. *J. Vac. Sci. Technol. A* **2016**, *34*, 41504.
- (200) *Atomic Layer Deposition for Semiconductors*; Hwang, C. S., Ed.; Springer: New York, 2014.
- (201) Lu, J.; Elam, J. W.; Stair, P. C. *Acc. Chem. Res.* **2013**, *46*, 1806–1815.
- (202) Kern, W. *J. Electrochem. Soc.* **1990**, *137*, 1887–1892.
- (203) Cordfunke, E. H. P.; Konings, R. J. M. *J. Chem. Thermodyn.* **1992**, *24*, 329–331.
- (204) Palko, A. A.; Ryon, A. D.; Kuhn, D. W. *J. Phys. Chem.* **1958**, *62*, 319–322.
- (205) Abad, M. D.; Sánchez-López, J. C.; Cusnir, N.; Sanjines, R. *J. Appl. Phys.* **2009**, *105*,

033510.

- (206) Gouy-Pailler, P.; Pauleau, Y. *J. Vac. Sci. Technol. A* **1993**, *11*, 96–102.
- (207) Arduengo, A. J.; Dias, H. V. R.; Harlow, R. L.; Kline, M. *J. Am. Chem. Soc.* **1992**, *114*, 5530–5534.
- (208) Hopkinson, M. N.; Richter, C.; Schedler, M.; Glorius, F. *Nature* **2014**, *510*, 485–496.
- (209) Fliedel, C.; Schnee, G.; Avilés, T.; Dagorne, S. *Coord. Chem. Rev.* **2014**, *275*, 63–86.
- (210) Arduengo, A. J.; Dias, H. V. R.; Calabrese, J. C.; Davidson, F. *J. Am. Chem. Soc.* **1992**, *114*, 9724–9725.
- (211) Francis, M. D.; Hibbs, D. E.; Hursthouse, M. B.; Smithies, N. A.; Jones, C. *J. Chem. Soc. Dalton Trans.* **1998**, 3249–3254.
- (212) Schmidt, D.; Berthel, J. H. J.; Pietsch, S.; Radius, U. *Angew. Chem. Int. Ed.* **2012**, *51*, 8881–8885.
- (213) Iversen, K. J.; Wilson, D. J. D.; Dutton, J. L. *Dalton Trans.* **2013**, *42*, 11035–11038.
- (214) Wang, T.; Stephan, D. W. *Chem. Eur. J.* **2014**, *20*, 3036–3039.
- (215) Iversen, K. J.; Wilson, D. J. D.; Dutton, J. L. *Dalton Trans.* **2015**, *44*, 3318–3325.
- (216) Würtemberger-Pietsch, S.; Radius, U.; Marder, T. B. *Dalton Trans.* **2016**, *45*, 5880–5895.
- (217) Anker, M. D.; Colebatch, A. L.; Iversen, K. J.; Wilson, D. J. D.; Dutton, J. L.; García, L.; Hill, M. S.; Liptrot, D. J.; Mahon, M. F. *Organometallics* **2017**, *36*, 1173–1178.
- (218) Schneider, H.; Hock, A.; Bertermann, R.; Radius, U. *Chem. Eur. J.* **2017**, *23*, 12387–12398.
- (219) Blakeney, K. J.; Ward, C. L.; Winter, C. H. *ECS Trans.* **2018**, in press.
- (220) Cole, M. L.; Hibbs, D. E.; Jones, C.; Junk, P. C.; Smithies, N. A. *Inorg. Chim. Acta* **2005**, *358*, 102–108.

- (221) Arentsen, K.; Caddick, S.; Cloke, F. G. N. *Tetrahedron* **2005**, *61*, 9710–9715.
- (222) Coyle, J. P.; Sirianni, E. R.; Korobkov, I.; Yap, G. P. A.; Dey, G.; Barry, S. T. *Organometallics* **2017**, *36*, 2800–2810.
- (223) Sun, R.; Liu, J.; Yang, S.; Chen, M.; Sun, N.; Chen, H.; Xie, X.; You, X.; Li, S.; Liu, Y. *Chem. Commun.* **2015**, *51*, 6426–6429.
- (224) Brown, A. C.; Altman, A. B.; Lohrey, T. D.; Hohloch, S.; Arnold, J. *Chem. Sci.* **2017**, *8*, 5153–5160.

**ABSTRACT****SYNTHESIS OF VOLATILE AND THERMALLY STABLE ALUMINUM HYDRIDE COMPLEXES AND THEIR USE IN ATOMIC LAYER DEPOSITION OF METAL THIN FILMS**

by

**KYLE JORDAN BLAKENEY****December 2018****Advisor:** Dr. Charles H. Winter**Major:** Chemistry (Inorganic)**Degree:** Doctor of Philosophy

The research discussed in this dissertation spans both synthetic inorganic and nanomaterials chemistry. Aluminum hydride complexes were synthesized and characterized which are highly volatile and thermally stable and their potential as reducing agents for ALD of electropositive metal and metal-containing films was evaluated. A major discovery presented herein is the deposition of aluminum metal films by thermal ALD using an aluminum dihydride complex supported by a bulky, yet simple, amido-amine ligand (Chapter 2). Aluminum is the most electropositive element deposited by purely thermal ALD to date and represents a significant breakthrough for this field. This process may have important industrial applications and the aluminum hydride reducing agents should enable a variety of novel ALD processes for difficult metals and elements. The deposition of titanium metal films was attempted using the aluminum hydride reducing agents (Chapter 3). Rather than pure titanium films, highly thermodynamically stable and conductive titanium carbonitride ( $\text{TiC}_x\text{N}_y$ ) films were deposited instead. Chapter 4 explored the ubiquitous ALD precursor trimethylaluminum ( $\text{AlMe}_3$ ) as a potential reducing agent and high quality tungsten carbide films were deposited using  $\text{AlMe}_3$  and  $\text{WCl}_6$ . Tungsten-rich tungsten carbide films were deposited using  $\text{WCl}_6$  and an aluminum

hydride reducing agent instead of  $\text{AlMe}_3$  (Chapter 5). While exploring the chemistry and properties of N-heterocyclic carbene aluminum hydride complexes, a structurally unusual dialane complex was synthesized which displayed good volatility and thermal stability and this novel complex was also used to deposit aluminum metal by a thermal ALD process (Chapter 6).

## AUTOBIOGRAPHICAL STATEMENT

KYLE JORDAN BLAKENEY

Ph.D., Inorganic Chemistry, Wayne State University, Detroit, Michigan (2014-2018)

Advisor: Professor Charles H. Winter

B.S., Chemistry, Iowa State University, Ames, Iowa (2009-2013)

Advisor: Professor Javier Vela

### PUBLICATIONS

---

1. "Axial Composition Gradients and Phase Segregation Regulate the Aspect Ratio of  $\text{Cu}_2\text{ZnSnS}_4$  Nanorods," M. J. Thompson, T. P. A. Ruberu, **K. J. Blakeney**, K. V. Torres, P. S. Dilsaver, J. Vela, *J. Phys. Chem. Lett.* **2013**, *4*, 3918–3923.
2. " $\text{Cu}_2\text{ZnSnS}_4$  Nanorods Doped with Tetrahedral, High Spin Transition Metal Ions:  $\text{Mn}^{2+}$ ,  $\text{Co}^{2+}$ ,  $\text{Ni}^{2+}$ ," M. J. Thompson, **K. J. Blakeney**, S. D. Cady, M. D. Reichert, J. Del Pilar-Albaladejo, S. T. White, J. Vela, *Chem. Mater.* **2016**, *28*, 1668–1677.
3. "Thermal Atomic Layer Deposition of Tungsten Carbide Films from  $\text{WCl}_6$  and  $\text{AlMe}_3$ ," **K. J. Blakeney** and C. H. Winter, *J. Vac. Sci. Technol. A* **2018**, *35*, 01A104.
4. "Atomic Layer Deposition of Aluminum Metal Films Using a Thermally Stable Aluminum Hydride Reducing Agent," **K. J. Blakeney** and C. H. Winter, *Chem. Mater.* **2018**, *30*, 1844–1848.
5. "Low Temperature, Selective Atomic Layer Deposition of Nickel Metal Thin Films," M. M. Kerrigan, J. P. Klesko, **K. J. Blakeney**, C. H. Winter, *ACS Appl. Mat. Int.* **2018**, *10*, 14200–14208.
6. "Atomic Layer Deposition of Tungsten-Rich Tungsten Carbide Films using  $\text{WCl}_6$  and  $\text{AlH}_2(\text{tBuNCH}_2\text{CH}_2\text{NMe}_2)$  as Precursors," **K. J. Blakeney**, C. L. Ward, and C. H. Winter, *ECS Trans.* **2018**, in press.
7. "Aluminum Dihydride Complexes and Their Unexpected Application in the Atomic Layer Deposition of Titanium Carbonitride Films," **K. J. Blakeney**, P. D. Martin, and C. H. Winter, *Dalton Trans.* **2018**, in press, DOI: 10.1039/C8DT02508H.
8. "A Volatile Dialane Complex from Ring-Expansion of an N-Heterocyclic Carbene and its Use in Atomic Layer Deposition of Aluminum Metal Films," **K. J. Blakeney**, P. D. Martin, and C. H. Winter, *submitted*.

### SELECTED PRESENTATIONS

---

- July 2016. Low Temperature Thermal Atomic Layer Deposition of Metallic Tantalum Films Using a New Organic Reducing Co-Reagent. *Selected for "Highlights of 2016" Plenary Session.* 16<sup>th</sup> International Conference on Atomic Layer Deposition, Dublin, Ireland. (Oral Presentation)
- July 2017. Atomic Layer Deposition of Tungsten Carbide Thin Films. ACS Central Regional Meeting, Detroit, Michigan. (Oral Presentation)
- July 2018. Thermal Atomic Layer Deposition of Aluminum Metal: Precursor Chemistry and Inherent Selectivity. *Finalist for Best Student Submission.* 18<sup>th</sup> International Conference on Atomic Layer Deposition, Incheon, South Korea. (Oral Presentation)